

HERON is jointly edited by:
 STEVIN-LABORATORY of the
 faculty of Civil Engineering,
 Delft University of Technology,
 Delft, The Netherlands
 and
 TNO BUILDING AND
 CONSTRUCTION RESEARCH.
 Rijswijk (ZH), The Netherlands
 HERON contains contributions
 based mainly on research work
 performed in these laboratories
 on strength of materials, structures
 and materials science.

ISSN 0046-7316

EDITORIAL BOARD:

A. C. W. M. Vrouwenvelder,
editor in chief
 R. de Borst
 J. G. M. van Mier
 R. Polder
 J. Wardenier

Secretary:

J. G. M. van Mier
 Stevinweg 1
 P.O. Box 5048
 2600 GA Delft, The Netherlands
 Tel. 0031-15-784578
 Fax 0031-15-611465
 Telex 38151 BUTUD

Contents

THE FATIGUE BEHAVIOUR OF T- AND X-JOINT MADE OF SQUARE HOLLOW SECTIONS

A. M. van Wingerde

Mechanics & Structures, Stevin Laboratory
 Civil Engineering, Delft University of Technology,
 The Netherlands

Abstract	3
Notation	4
1 Introduction	7
1.1 Hollow sections and their use in practice .	7
1.2 Aim of the investigation	8
1.3 Overview of the research carried out	10
2 Fatigue behaviour and analysis	14
2.1 Background on fatigue behaviour	14
2.2 Definitions regarding fatigue	16
2.3 Methods of assessing the fatigue behaviour	20
2.4 Discussion on the definition of the hot	
spot stress	27
2.5 Definitions and assessment of the hot	
spot stress used in this work	30
2.6 Survey of existing research on the fatigue	
behaviour of square hollow section joints .	32
2.7 Survey of some relevant design codes	36
2.8 Survey of techniques used for	
improvement of the fatigue behaviour ...	43
3 Experimental research	48
3.1 Introduction	48
3.2 Setup of experiments	49
3.3 Test results	62
4 Numerical research	71
4.1 Introduction	71
4.2 FE elements used	74
4.3 Development of the FE model	77
4.4 Comparison of the FE model with the	
experiments	80
4.5 Results of the comparison between FE	
analyses and experiments	83
5 Parametric study	84
5.1 Geometries and load cases considered ...	84

5.2	Comparison of T- en X-joints	87
5.3	Influence of axial load on the chord	99
5.4	Comparison of SNCFs and SCFs	101
5.5	Background to regression analyses	103
5.6	Establishment of parametric functions for loading on the brace	105
5.7	Establishment of parametric functions for leading on the chord	106
5.8	Results of the parametric study	107
6	Influence of corner radii and weld on the SCF	113
6.1	Introduction	113
6.2	Setup of the numerical work	114
6.3	Influence of the corner radii on the SCF	116
6.4	Influence of the weld on the SCF	120
6.5	Conclusions on the range of validity of the parametric formulae	122
7	Establishment of $S_{rh,s}$-N_f lines and thickness effect	124
7.1	Establishment of the $S_{rh,s}$ - N_f line based on experimental data	124
7.2	Establishment of the thickness effect ...	125
7.3	Establishment of the $S_{rh,s}$ - N_f line based on the parametric formulae	129
7.4	Comparison between parametric formulae and experimental results	132
7.5	Classification of the $S_{rh,s}$ - N_f line according to Eurocode 3, document 9.03	133
7.6	Comparison of $S_{rh,s}$ - N_f lines using linear and quadratic extrapolation	135
7.7	Comparison with parametric formulae derived by Soh	138
8	Design recommendations	142
8.1	Proposed design rules	142
8.2	Comparison with existing design rules ..	150
8.3	Design examples	151
9	Conclusions	155
9.1	General conclusions	155
9.2	Recommendations for future work	158
10	References	161
10.1	Reports on the research projects carried out	161
10.2	Other publications	166
	Samenvatting (Dutch abstract)	181
	Curriculum vitae	182

ABSTRACT

This work presents the results of experimental and numerical research on the fatigue behaviour of T- and X-joints between square hollow sections of which the brace is welded to the face of the chord, without any additional stiffeners. The work has been carried out in the framework of the CIDECT programme 7K "Fatigue behaviour of uniplanar joints", and an earlier ECSC programme "Fatigue strength of welded unstiffened RHS joints in latticed structures and Vierendeel girders" (CECA Convention nr. 7210-SA/111). Furthermore, experimental results of the CIDECT programme 7H "The low cycle fatigue behaviour of axially loaded T-joints between rectangular hollow sections" have been used in this work.

The aim of the research programmes is to establish a better design method for the fatigue strength of joints in square hollow sections, based on the hot spot stress method. The results are to be proposed for inclusion in Eurocode 3.

In the experimental investigation, the strain concentration factors are measured at various locations of the joint for comparison with results of the numerical investigations and $S_{r,h.s.}$ - N_f curves are determined.

The numerical work provides SCF values at weld toes for a range of parametric variations in the joint dimensions. These results form the basis for a set of parametric formulae. These formulae allow the determination of the SCF values at the weld toes of the brace and chord, depending on the non-dimensional parameters (β , 2γ and τ).

The results of tests and formulae are used to check the final validity of the formulae in combination with the $S_{r,h.s.}$ - N_f lines.

KEY WORDS

Fatigue, Square Hollow Section, Hot Spot Stress, Stress (strain) concentration factor

ACKNOWLEDGEMENTS

The donation of Hoogovens Buizen B.V. during my Ph.D. study is very much appreciated. Thanks are also due to CIDECT, Staalcentrum and Mannesmannröhren-Werke A.G. for their financial support for the research programmes and to Van Leeuwen buizen, Zwijndrecht and Oving-Diepenveen-Struyken BV, Barendrecht for their donation of hollow sections.

Thanks are due to mr. C.H.M. de Koning, mr. A. Verheul, mr. B. Stuivenberg and mr. K.C.A. Jungschläger for the experimental work necessary to produce the fatigue design curves.

Furthermore I wish to thank my family, friends and colleagues for all the support and friendship I have received during my promotion.

SYMBOLS

A	Cross sectional area of member considered.
E	Young's modulus of elasticity.
F	Axial load on a member.
I	Moment of inertia of member considered.
M	In-plane bending moment on a member.
N_i	Number of cycles to failure under constant amplitude load from the $S_{f,h.s.}-N_f$ curve, corresponding to stress range $S_{f,h.s.i}$.
N_{ini}	Number of cycles to crack initiation.
N_f	Number of cycles to failure.
R	Stress ratio between maximum and minimum nominal stress in a cycle for constant amplitude loading $\sigma_{min}/\sigma_{max}$.
$S_{f,h.s.}$	Hot spot stress range = $SCF \cdot \sigma_f = SCF \cdot (\sigma_{max} - \sigma_{min})$.
W	Elastic section modulus of member considered.
a	Weld throat thickness.
b	External width of member considered.
h	External height of member considered (for square sections: $h=b$).
l	Length of member considered between points of contraflexure or simple supports.
n_i	The number of cycles of stress ranges $S_{f,h.s.i}$ in the design life
r_{01}	Measured projected length of the curved corners of the chord on the face of the chord connected to the brace, used as outside radius of chord in numerical analyses for actual dimensions.
r_{02}	Measured projected length of the curved corners of the chord parallel to the brace axis, used as outside radius of chord in numerical analyses for actual dimensions.
r_{11}	Measured projected length of the curved corners of the brace used as outside radius of brace in numerical analyses for actual dimensions.
$t_{01} \dots t_{06}$	Measured wall thicknesses of the chord at various locations.
$t_{11} \dots t_{13}$	Measured wall thicknesses of the brace at various locations.
t	Wall thickness of member considered.
w	Weld dimension parallel to member considered.
α	Chord length to half width ratio $2 l_o/b_o$.
β	Brace to chord width ratio b_i/b_o .
2γ	Width to wall thickness ratio of the chord b_o/t_o .
ϵ_e	Yield strain of the member considered.
ϵ_r	Nominal strain range (strain range according to beam theory).
ϵ_u	Ultimate elongation of the member considered.
σ	Standard deviation.
σ_c	Detail category (classification) according to EC3.
σ_e	Yield stress of the member considered.
σ_r	Nominal stress range (stress range according to beam theory).
σ_u	Ultimate stress of the member considered.
σ_{max}	Maximum nominal stress in a constant amplitude loading cycle.
σ_{min}	Minimum nominal stress in a constant amplitude loading cycle.
τ	Brace to chord wall thickness ratio t_i/t_o .

INDICES

0	chord
1	brace
a	axial stress
m	in-plane bending stress

NOTATION

API	American Petroleum Institute
AWS	American Welding Society
CHS	Circular hollow section.
CIDECT	Comité International pour le Développement et l'Étude de la Construction Tubulaire.
DEn	Department of Energy (UK).
EC3	Eurocode No. 3.
ECSC	European Coal and Steel Community.
FE	Finite Element.
IIW	International Institute of Welding.
RHS	Rectangular hollow section.
SAE	Society of Automotive Engineers
SCF	Stress concentration factor.
SNCF	Strain concentration factor.

1 INTRODUCTION

1.1 *Hollow sections and their use in practice*

Hollow sections are a major structural element in nature. The reasons for this are obvious: they offer a good ratio between weight and resistance of longitudinal and lateral forces from all directions and have relatively low drag coefficients which is important in resisting wind or water flows. Also they allow the internal space to be used for transport and other functions, shielded from the outside world by the hollow section which offers an optimal ratio between cross section and perimeter.

Structural hollow sections for use in steel structures offer very similar advantages over open structural elements, such as I-Beams:

- Circular hollow sections are the structural elements best suited for withstanding wind- and wave loadings, as they have a low drag coefficient. This has made these sections the obvious choice for the design of offshore jackets.
- They also have a large strength and stiffness, independent of the direction of the force. This is useful for withstanding lateral forces from all directions.
- Although the maximum moment of inertia is smaller than that of an I-beam of the same weight per length, the minimum moment of inertia is larger. This is important in designing members in compression (columns).
- The large resistance of closed sections against torsion prevents lateral buckling of beams. The torsional resistance together with the semi-rigid welded end connections in trusses allows for an effective buckling length of the braces between 0.50 and 0.75 times of the system length. This enhances the resistance against buckling even further.
- The closed sections have a better ratio between cross section and exposed area than open sections. This means that protection of closed sections against corrosion can be cheaper and the savings in coating systems also attribute to a reduced strain on the environment. Corrosion protection is also enhanced by the 'cleaner' connections where dirt cannot easily accumulate and the absence of sharp corners which might give rise to a less optimal coating.

- The relatively small outer area also gives a larger inherent fire resistance. This resistance can be improved by filling the sections with concrete, possibly in combination with intumescent coating. Another way of improving the fire resistance is the use of water inside the sections of the structure, allowing the water to flow through the structure. When a fire breaks out, the heat will start a convection flow of the water, providing an effective cooling of the structure.
- The interior of the sections can be used for transport of liquids, electrical wires, heating or ventilation.
- The smooth shape of the sections and joints is appealing to architects.

The rectangular hollow sections have higher drag coefficients and are therefore less suited than circular sections for withstanding large wind or wave loadings. Their properties are not completely independent of the cross sectional axes as for circular hollow sections. The ratio between cross sectional area (weight, costs) or outer area (corrosion protection) on the one hand and section modulus (strength) on the other hand is about the same as for circular hollow sections. However, the connections between rectangular hollow sections are simpler and fabricated more economically, since the preparations at the joints are in most cases essentially straight cuts, rather than complex shapes. Also connections with other structural or non-structural elements are more easily made.

1.2 *Aim of the investigation*

Although rectangular hollow structural sections have some very favourable qualities, initially their use in practice has been hampered because of a lack of design recommendations. For the static strength of uniplanar structures made of structural hollow sections (SHS), this problem has been overcome. Design recommendations can be found in the IIW [69], the API [31], the AWS [32], EC3 [53, 97], CIDECT [115], Dutta [52], Wardenier [112], Reusink et al. [91, 92] and Packer et al. [84]. Also, the fatigue behaviour of uniplanar circular hollow sections is now well studied, resulting in parametric formulae describing the relation between joint geometry and fatigue behaviour, such as those by Efthymiou [54, 55], UEG (originally Wordsworth and Smedley) [108], Kuang et al. [71] and Gibstein [60].

However, except for the ECSC-CIDECT programme "Fatigue strength of welded unstiffened R.H.S. joints in latticed structures and Vierendeel girders" and the CIDECT research programme "Fatigue behaviour of uniplanar joints" both described in this work, only a few investigations have been carried out on the fatigue behaviour of rectangular hollow section joints. These investigations are purely numerical, carried out by Soh et al. [100, 102] or contain only N- and K-joints, such as the work reported by van Dooren et al. [20], Noordhoek et al. [82, 83] and Frater [59]. Other investigations were carried out by Ferreira [57] on very small specimens (both brace and chord 40 mm width, 2 mm wall thickness).

Therefore, the present EC3 fatigue design recommendations for joints between rectangular hollow sections are based upon the "classification method" (see Chapter 2), where the joints are primarily classified into groups with nearly the same fatigue resistance. The geometrical stress concentration has indirectly been taken into account by giving different $S_{h.s.}$ - N_f lines for different types of joints.

The research programmes by the ECSC and CIDECT aim to provide fatigue design recommendations for structures consisting of unstiffened welded joints between rectangular hollow sections. These design recommendations are based upon the so-called hot spot stress method, which aims to include the effects of the overall joint geometry on the stress distribution and hence on the fatigue behaviour of the joint (see Chapter 2). The chosen approach for T- and X-joints is based on determining the geometrical hot spot stress along a few established lines, by means of an extrapolation method which aims to exclude the local influence of the weld. The aim of these research projects is to develop a design method for T- and X-joints loaded by axial forces or in-plane bending moments on chord and brace with a wide range of validity and a good balance between accuracy and complexity in use.

Both experimental and numerical work are covered. The experiments (described in Chapter 3) serve to determine the fatigue life of a given joint geometry and are used as a calibration for the geometrical stress and strain concentration factors (SCF and SNCF) determined by the finite element analyses (see Chapter 4). Furthermore, the influence of the thickness effect and stress ratio has been determined. On the other hand, the numerical work is carried out for a wider range of geometries, to enable the determination of the influence of various geometrical parameters and for obtaining a detailed view of strain (or stress) distributions in the joints. It is then possible to derive parametric formulae on this basis (see Chapter 5).

With the establishment of parametric formulae which give the SCFs as a function of the joint geometry and loading, the hot spot stress or strain can be determined at a number of fixed positions (see Chapter 2.5). The total hot spot stress range in case of combined axial forces and in-plane bending moments on both brace and chord can be determined for these positions by multiplying the relevant nominal stress by the appropriate SCF. By means of an appropriate $S_{h.s.}-N_f$ line the fatigue life can now be determined. This procedure is illustrated in Figure 49 (see Chapter 8.1).

1.3 *Overview of the research carried out*

The ECSC research programme "Fatigue strength of welded unstiffened R.H.S. joints in latticed structures and Vierendeel girders" on rectangular hollow sections, also sponsored by CIDECT has been carried out in Germany and the Netherlands, with four participants, namely, Mannesmannröhren-Werke A.G., Düsseldorf, the University of Karlsruhe, the Delft University of Technology and TNO Building and Construction Research in Rijswijk. The work in the Netherlands concentrated on T- and X- joints, whereas K-joints were studied by the University of Karlsruhe.

To extend the range of the parametric formulae, a follow-up study was started in the framework of the CIDECT research programme 7K "Fatigue Behaviour of Uniplanar Joints" [5]. The participating partners are: Mannesmannröhren-Werke A.G., Düsseldorf, Verenigde Buizenfabrieken, Oosterhout, TNO Building and Construction Research, Rijswijk and the Delft University of Technology.

This thesis concentrates on T- and X-joints.

It describes the method of approach for the research, as well as noteworthy problems that are encountered.

The research programmes consist of 5 steps:

- Experimental testing of some representative joints (see Chapter 3) for the determination of the strain gradients and the fatigue strength.
- Numerical simulations of the experiments to calibrate the FE model (see Chapter 4).
- FE Analysis of a large number of joints as a basis for parametric formulae, for all load cases considered and covering the geometrical variations found in practice (described in Chapter 5).

- Establishment of the parametric formulae, based on regression analysis of the SCFs found from the FE analyses (also in Chapter 5).
- Establishment of appropriate $S_{r_{h.s.}}-N_f$ lines, based on the experiments or on experiments combined with the SCFs found from the parametric formulae (see Chapter 7).

Details of the programme of work on T-, X- and K-joints are given in the sub-reports of the ECSC-CIDECT project [6] to [16] (T- and X-joints) and [21] to [28] (K-joints). The main results are summarized in [1] to [4]. Experiments carried out in the additional CIDECT research programme 7K "Fatigue behaviour of uniplanar joints" are described in [19]. The main results of this CIDECT programme are summarized in [5]. Furthermore, results of CIDECT programme 7H "The low cycle fatigue behaviour of axially loaded T-joints between rectangular hollow sections" have been used [17].

Experimental work

Table 1 gives an overview of the number of experiments carried out per type of joint and per type of loading as well as the responsible organisation and the research programme for which they were carried out. Also the number of Runouts, Overloads, Weld failures, specimens where welding started and ended at the Corners, Untested joints and K-joints of which the overlapping brace was loaded in Tension specimens, is mentioned. These tests were excluded for determination of $S_{r_{h.s.}}-N_f$ lines (see Chapter 7). The specimens where the SNCFs were Not measured have been used only for 'numerically' determined $S_{r_{h.s.}}-N_f$ lines (N_f , σ_r from experiments, SCF from parametric formulae). The number of tests usable for the $S_{r_{h.s.}}-N_f$ lines is also given in Table 1. Chapter 3 contains details about the set up and results of the experimental work.

Numerical work

The numerical work started by calibrating the SNCFs of the FE model with the experiments and continued with a parametric study on the SCFs for axially loaded T- and X-joints, and T- and X-joints loaded by a bending moment on the brace [1, 3, 4]. This was done for the geometries summarized in Table 8. See Chapter 4 for more details on the numerical work.

Analysing the T-joints loaded by a bending moment on the chord for the complete range of geometries allows elimination of the bending component in the chord of T-joints, so that one set of parametric formulae can be used for X- and T-joints loaded on the brace [118].

In order to check whether the parametric formulae for bending moment in the chord of T-joints would also be valid for an axial force on the chord, 5 T-joints are analysed by the FE method, applying an axial force on the chord. As even for more critical load cases the difference between X- and T-joints is small (see Chapter 5), the formulae for loads on the chord are also applicable to X-joints, so that the range of application of the parametric formulae is then completed.

The resulting parametric formulae relate the SCF to the geometric parameters β , 2γ and τ . The geometries investigated have all butt welds ($w_0=t_1/2$, $w_1=t_1+2$) and corner radii that vary from 1 to 2 times the wall thickness of the member, dependent on the width of the member. The influence of the corner radii and weld dimensions and weld type is therefore investigated separately (see Chapter 6). As a result, the range of validity of the parametric formulae can be extended.

Analysis of results

The $S_{f.h.s.}$ - N_f lines, based entirely on experiments or with N_f taken from experiments and $S_{f.h.s.}$ taken from the parametric formulae, form a basis for the fatigue design of T- and X-joints in square hollow sections. The research has also established a thickness correction factor [120]. In case the parametric formulae are used, this implies checking both members, which is illustrated in the design example in Chapter 8. A comparison of the $S_{f.h.s.}$ - N_f lines (see Chapter 7) reveals the reduction of scatter which can be obtained by applying the thickness correction.

For inclusion in EC3, a classification according to EC3, Document 9.03 is necessary (see Chapter 7). The class in EC3 is the stress corresponding to a fatigue life of $2 \cdot 10^6$ cycles. The classification, based on the hot spot stress obtained from experiments or parametric formulae is established.

As a result of this study, design recommendations are proposed (see Chapter 8), consisting of a set of parametric formulae, usable for uniplanar X- and T-joints made of square hollow sections, loaded by in-plane bending moments or axial forces on their members. The formulae are also applicable for various corner radii (for instance cold formed square hollow sections, which generally have larger corner radii than hot finished sections) and various weld shapes.

Table 1. Overview of experiments carried out														
No. of Exp	Type of Joint	Type of Loading on the Brace	Prog.	Institute responsible for Work	Remarks ¹							Ref.	Valid Tests ²	
					R	O	W	N	C	T	U		E	N
16	T-joint	Axial Force	ECSC	Delft Un. of Technology	1	-	3	-	-	-	-	[20]	12	12
8	T-joint	Axial Force	CIDECT 7H	Delft Un. of Technology	-	1	-	-	-	-	-	[25]	7	7
4	T-joint	I.P.B. Moment	CIDECT 7K	Delft Un. of Technology	-	-	-	-	-	-	-	[27]	4	4
14	X-joint	Axial Force	ECSC	TNO Building & C. Research	1	2	-	-	-	-	1	[15]	10	10
27	X-joint	I.P.B. Moment	ECSC	Universität Karlsruhe	3	-	11	22	23	-	-	[19]	1	1
24	K-joint (gap)	Axial ³ Force	ECSC	Universität Karlsruhe	1	-	2	20	-	-	-	[30]	4	21
12	K-joint (overlap)	Axial ³ Force	ECSC	Universität Karlsruhe	1	-	-	8	-	12	-	[34]	-	-

¹ Runout: the specimen had not (completely) failed at the end of the test.

Overload: the specimen had accidentally been loaded by a high load.

Weld Failure: the weld itself failed, rather than the sections.

Not measured: at Karlsruhe the SCFs were only measured for 1 specimen per series.

Corner weld start/stop: welding commenced and finished at the corners, resulting in degraded fatigue behaviour.

Tension on the overlapping brace, rather than the through brace, which decreases the fatigue strength.

Untested: 1 X-joint proved too strong for the test setup and was therefore not tested.

² Experimentally determined $S_{f,h.s.}$ - N_f lines (hot spot strains from measurements).

All joints with remarks under 1 have been excluded from the analysis.

Numerically determined $S_{f,h.s.}$ - N_f lines (measured N_f , σ_{nom} , SCF from parametric formulae)

Joints with remarks under 1 have been excluded from the analysis, except for joints where the SCF was not measured.

The $S_{f,h.s.}$ - N_f lines in this work are exclusively based upon work carried out on T- and X-joints.

³ For the K-joints, also some bending moment is introduced.

2 FATIGUE BEHAVIOUR AND ANALYSIS

2.1 Background on fatigue behaviour

A dominant factor affecting fatigue under cyclic or fluctuating loads is the localized peak stress (or peak strain) range which can be defined as the nominal stress (strain) times a stress (strain) concentration factor. Under fluctuating stresses or strains induced at these concentration points, progressive localized permanent damage can occur, called fatigue. This may culminate in cracks or complete failure after a sufficient number of fluctuations. For statically loaded joints with sufficient deformation capacity, the stress or strain concentration is of minor importance due to stress redistribution by local yielding.

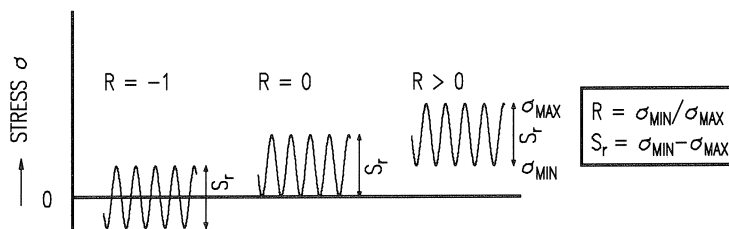


Figure 1. Stress range S_r and stress ratio R .

The fatigue behaviour is usually investigated on the basis of constant amplitude loading tests (see Figure 1), and is primarily dependent upon:

- The nominal stress range $\sigma_r = \sigma_{\max} - \sigma_{\min}$. The nominal stress range is the stress range derived in a member from simple beam theory. It therefore represents a situation excluding the effects of geometrical discontinuities which cause stress concentrations.
 σ_{\max} or σ_{\min} are the maximum and minimum nominal stress in a constant amplitude cycle.
- The geometry of the joint, determining the geometrical stress concentration.
- The wall thickness of the member considered. The fatigue strength tends to decrease with increasing wall thickness. This effect is called the size effect or thickness effect.
- The stress ratio $R = \sigma_{\min} / \sigma_{\max}$ is generally of minor importance, due to the uncertain relation between the local minimum and maximum stresses and the external nominal stresses, which is caused by residual stresses due to fabrication, by stress redistribution caused by local yielding and by other usually unknown stress components, such as those caused by uneven settlement of the foundation.

R may have some influence on small thicknesses, or for post weld heat treated specimens (see Chapter 2.8).

- Environmental effects could aggravate the situation (corrosion fatigue) and would then have to be taken into account.
- The material may also influence the fatigue behaviour, especially in the low cycle region, or in case of fatigue improvement techniques (see Chapter 2.8). However, in most applications the influence of the strength of the material on the fatigue behaviour of welded components is small and not taken into account in the design guidelines.

The relation between stress or strain and the number of cycles to failure is generally given in $S_{h.s.}$ - N_f (Wöhler) diagrams in which the stress- or strain range is given on the vertical axis and the number of cycles to failure on the horizontal axis, both on a logarithmic scale as illustrated in Figure 2. The number of cycles to failure decreases with increasing stress range and wall thickness.

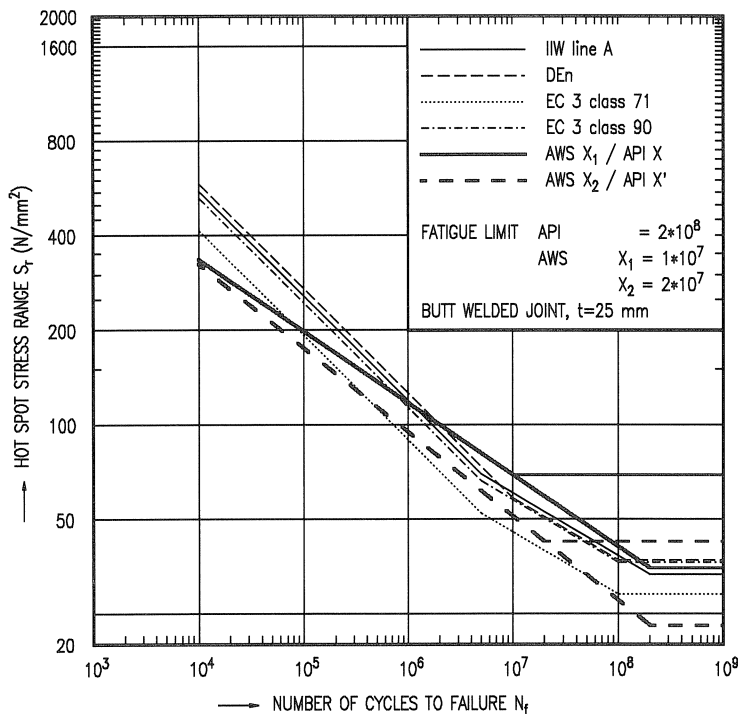


Figure 2. $S_{h.s.}$ - N_f lines for hollow section joints ($t=25$ mm).

In practice, constant amplitude loading is seldom present. Therefore, cumulative damage rules are used to describe the behaviour under spectrum loading. A popular rule, which is no worse than other known rules [106] is the Palmgren-Miner's rule, where fatigue damage accumulates linearly with the number of cycles at a particular load level:

$$\sum \frac{n_i}{N_i} \leq 1 \quad (2-1)$$

where n_i =number of cycles at load level i

N_i =number of cycles to failure at this load level i .

This programme concentrates on the influence of the joint geometry on the fatigue life.

2.2 Definitions regarding fatigue

The weld toes in welded joints have preformed notches and therefore positions of weakness where fatigue cracks are most likely to occur. Attention is therefore primarily focused on fatigue of welded joints. The International Institute of Welding (IIW SC-XV-E) has provided recommendations in which certain definitions in relation to the fatigue design procedure for hollow section joints are listed [68].

These are given below with small adaptations and some additional information:

- "branch" is replaced by "brace".
- "these" recommendations is replaced by "the IIW" recommendations.

More important are the comments in the case of the hot spot stress and the stress concentration factor, as well as the additional information on the definition of fatigue.

Fatigue

When fluctuating loads are applied to a material they may induce local stresses and strains which are sufficient to induce localised micro structural changes resulting in the development of cracks. This process is known as fatigue. The cracks, fatigue cracks, can grow to a size sufficient to cause failure.

In the IIW definition, fatigue is defined from a constructional point of view. The underlying mechanism is a repeated movement of the steel at the crystal interfaces at a microscopic level. However, more advanced fatigue assessment methods try to take more stress raising components into account, such as the local notch strain approach (see Chapter 2.3).

Fatigue life

The fatigue life is generally specified as the number of cycles N of stress or strain of a specified character, that a given joint sustains, before failure of a specified nature occurs:

- In the IIW recommendations a crack through the wall is considered as failure.
- In the European Offshore programme [33, 50], four failure modes are considered:
 - N_1 : 15% change in strain, measured "near" the crack initiation point.
 - N_2 : first "visible" crack.
 - N_3 : through thickness crack
 - N_4 : end of test (complete loss of strength).
- For the present work, a crack extending over a length of the brace width (in the brace) or the brace width plus twice the projected length of the weld in the chord face (in the chord) is considered as fatigue failure.

Nominal stress

The nominal stress is specified as the maximum stress in a cross section calculated on the actual cross section by simple elastic theory, without taking into account the effect of geometrical discontinuities due to the joint configuration on the stress.

Stress range

The stress range σ_r is defined as the algebraic difference between the maximum and minimum stresses in a stress cycle (see Figure 1). The nominal stress range is based on the nominal stresses while the hot spot stress range is based on hot spot stresses.

Stress ratio R

The stress ratio R is defined as the ratio between the minimum and maximum stresses for constant amplitude loading taking account of the sign of the stress. Tension is taken as positive and compression as negative. See Figure 1.

Hot spot stress, geometric stress

General definition

The hot spot stress (range) is the stress range that occurs at the hot spot, which is defined as the point where the maximum stress range according to a certain definition occurs (generally at the toe of the weld).

IIW Definition

The stress range to be used for fatigue design of hollow section joints is the range of the "hot spot" stress. The "hot spot" is defined as the point along the weld toe where the extrapolated principal stress has its maximum value. The extrapolation must be carried out from the region outside the influence of the effects of the weld geometry and discontinuities at the weld toe, but close enough to fall inside the zone of the stress gradient caused by the global geometrical effects. The extrapolation is to be carried out on the brace (cut and welded member) side and the chord (continuous member) side of each weld (see Figure 3). In some simple connections the "hot spot" stress can be determined by considering only the stress normal to the weld toe since the orientation of the maximum principal stress is in these cases normal or almost normal to the weld toe.

Comments on the IIW definition

The IIW bases its definition of the hot spot stress range on extrapolated principal stress values, where local stress concentrations are excluded (see Figure 3). The EC3 [53] refers to this as the "geometric stress", whereas Niemi [81] terms it a "structural stress" or "shell stress". There are several different definitions of the hot spot stress. A discussion on the hot spot stress definition is given in Chapter 2.4.

Stress concentration factor

The stress concentration factor SCF is defined as the geometrical hot spot stress divided by the nominal stress in an attached brace. In joints with more than one brace each brace has to be considered. Generally, stress concentration factors are calculated for the chord and brace.

Comments to the IIW definition

This definition, like that used in many other design recommendations always treats the stress concentration as a factor on the nominal stress in the brace. In general, the chord is loaded as well, causing additional hot spot stress. Therefore, this has to be taken into consideration. A more general definition, also used in this work would be : The stress concentration factor SCF is defined as the (part of the total) hot spot stress divided by the nominal stress which causes this (part of) the hot spot stress. The total hot spot stress is then a function of all nominal stresses in all members of the joint and their stress concentration factors. See Chapter 2.5 where the hot spot stress definition used in this work is presented.

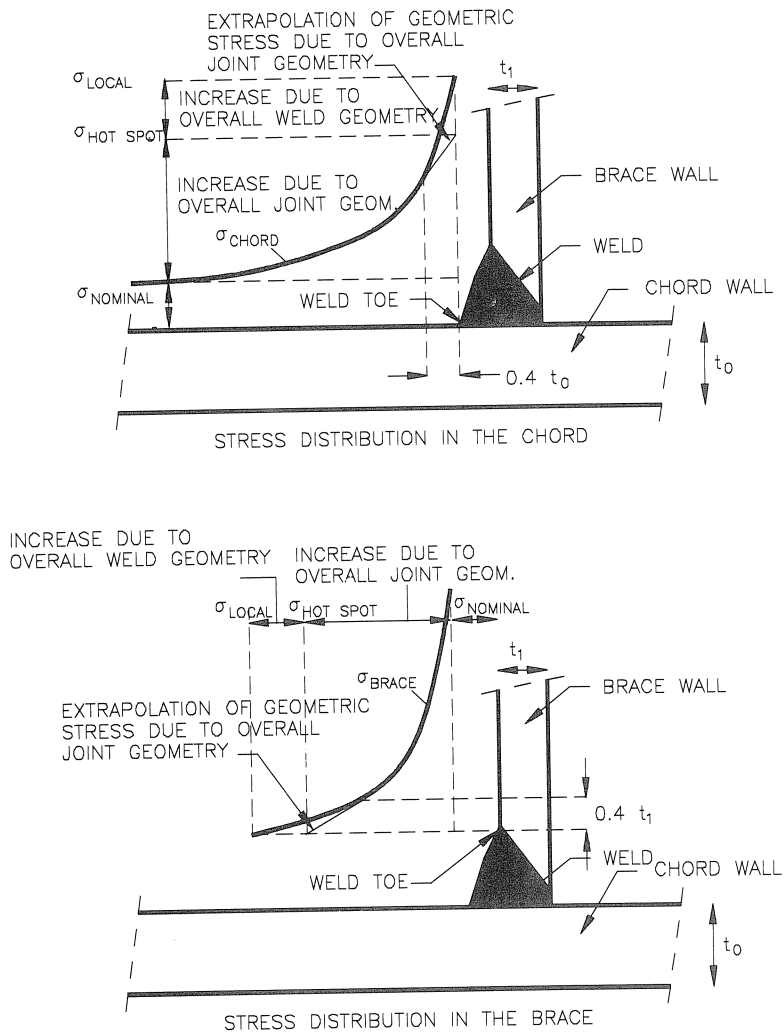


Figure 3. Hot spot stress definition in hollow section joints.

Other terms related to fatigue, not defined by IIW

$S_{rh.s}$ - N_f curve

An $S_{rh.s}$ - N_f curve or Wöhler line gives the relationship between the (hot spot) stress range and the number of cycles to failure. Conventionally, the (hot spot) stress range is plotted on the vertical axis and the number of cycles on the horizontal axis, using logarithmic scales for both axes.

The $S_{rh.s}$ - N_f curves given by the IIW for square hollow section joints have been derived from a statistical analysis of the relevant hot spot stresses and number of cycles to failure and represent lives which are less than the mean life by two standard deviations. Based upon the philosophy of the hot spot stress range method, the curves should also be applicable to rectangular hollow sections.

Fatigue strength

The fatigue strength of a specimen is the stress range that this specimen can resist for a specified number of cycles (for instance $2 \cdot 10^6$ cycles).

2.3 *Methods of assessing the fatigue behaviour*

The fatigue assessment of hollow section joints would ideally require a very accurate determination of the stress distribution in the joint as the results are extremely sensitive to small changes in the geometry. Apart from requiring a very large computer capacity, it is usually not possible to measure the exact geometry of the weld and joint to the level required. Hence a large scatter in results is commonly accepted for the fatigue behaviour. The aim of the fatigue assessment method is to establish a good balance between complexity and accuracy in the prediction of the fatigue strength. Various research projects have come up with several fundamentally different ways of assessing the fatigue behaviour of hollow sections joints, at various levels of complexity and accuracy.

Stress analysis based assessment methods

The most common fatigue assessment methods are based upon an approach of the stress distribution at the weld toe to different degrees of accuracy. These approaches, based on nominal stress (classification method), hot spot stress, local notch stresses or fracture mechanics are grouped together, since they can be regarded as refinements of one another.

The nominal stress range σ_r is the stress range in the member determined from beam theory, without taking the stress discontinuity due to the presence of the joint into account. The actual stress causing the fatigue cracking is build up as follows from the nominal stress (see also Figure 3):

- Stress raisers from the global geometry of the joint. The stress resulting from these stress raisers, accounted for in stress concentration factors is usually referred to as the geometric hot spot stress in EC3 [53], the structural stress by Petershagen [87], σ_G by Marshall [77, 79] or simply the hot spot stress IIW [68]. These stress raising effects are incorporated in most parametric formulae for the determination of the fatigue strength. Usually, this is presented in a non-dimensional way by using terms such as β , 2γ , τ and α .
- Another factor that might have to be included in the parametric formulae as it influences the hot spot stress is the size of the weld. Especially for joints between square hollow sections, this factor can have a significant influence on the hot spot stress (see Chapter 6). Extrapolation to the weld toe from $0.4t$ (see Chapter 2.4) would include this factor and hence the influence of the size of the weld might be considered part of the geometrical hot spot stress.
- More localised stress raisers, caused by the overall shape of the weld which influences the stresses very locally and are typically non-linearly distributed over the plate thickness. The AWS [32] includes some local stress raisers by providing different $S_{h.s.}-N_f$ lines, depending on the profile of the weld (see also Chapter 2.7, where the AWS is discussed and Chapter 2.8 where fatigue improvement techniques are discussed). These factors might be included by multiplying the hot spot stress that includes the effects of the global joint geometry by a factor denoted as K_f by Marshall [76] or K_{tw} by Iida [67]. Marshall refers to this stress as σ_L .
- Another influence is the local stress raising influence of the shape of the weld toe, especially the angle between weld toe and parent material and the radius of the weld toe. This influence is claimed to overrule the influence of the overall shape of the weld [44]. In contrast to the AWS, the DEn design guidelines place an emphasis on the shape of the weld toe rather than the complete weld profile, by allowing 30% higher stress for ground weld toes (remedial use only).

Inclusion in the analysis could again be presented as a multiplication factor, perhaps in combination with the previous influence to establish one "weld shape factor". However, measurement of these factors is difficult and the level of quality assurance in fabrication that is necessary to ensure the specifications would hamper these factors from being included in today's practical fatigue design.

- Notch peak stresses, caused by the condition of the weld toe, including factors like undercut and lack of fusion. These stress raisers may vary widely along the weld and are strongly dependent on the skill of the welder and the welding method used. It is not feasible to give explicit correction factors for these influences so that the current practice of demanding a minimum quality of the weld toe would have to be maintained. Including these factors in the analysis could improve the accuracy of the fatigue analysis.
- Microscopic stress raisers, caused by the granular structure of the steel. It is not normally feasible to take these stress raisers into account.

From a FE point of view, the nominal stress can typically be determined by beam elements, the global hot spot stress requires shell elements (with preferably solid elements at the weld for a clear definition of the weld toe, see Chapter 4). The localised stresses require solid elements for a 3D representation or shell elements to represent a cross section.

Although it is tempting to assess ever more local stresses, a probably more important aspect to include in the fatigue assessment would be the stress gradient, which might well prove to be as important as the local stresses.

Fatigue analysis based on the nominal stress (classification method)

This method is based on the so-called nominal stress, which is determined from beam theory: $\sigma_{\text{nom}} = F/A + M/W$. The geometry of the joint with its inherent stress distribution is taken into account by grouping joints with a similar behaviour into a single fatigue class. This approach is currently included in EC3 [53]. This method is very straightforward in use: just the type of joint will give information about the fatigue strength. In EC3, the class of a specimen is related to the stress level which a specimen can sustain for 2 million cycles. The S-N line of that class then gives the relationship between the stress and the number of cycles to failure. A major disadvantage of this method is the inherent conservativeness: joints with a large range of fatigue strengths are grouped together. For safety, the lowest fatigue strength should determine the class of the whole group (see also Chapter 2.7, remarks on the EC3 classification).

For X- and T-joints between square hollow sections, the stress concentration factor varies from about 2 to 30, depending upon the geometry of the joint (see Figure 32). Either many classes have to be defined, or a conservative approach would have to be adopted, or correction factors on the class should be given (such as multiplying the class by τ). When a certain joint has different classes for in-plane bending and axial load on the brace, the class has to be calculated on the basis of the ratio of the load cases. The concept is most useful when not enough data is available to establish a hot spot approach, or for details for which the fatigue behaviour is less influenced by the geometry.

Fatigue analysis based on the hot spot method

In the hot spot stress approach, the fatigue life is not directly related to the nominal stress, but through the so called hot spot stress, which is the maximum geometrical stress occurring in the joint where the cracks are usually initiated. In the case of welded joints between hollow sections, this generally occurs at the toe of the weld. The stresses and strains near the joint are not uniformly distributed, due to the stiffness variation. In the case of rectangular hollow sections, the stresses tend to be highest near the corners of the brace.

In the past twenty years, many international investigations have been carried out on circular hollow section joints, leading to $S_{f.h.s.}$ - N_f curves, together with a number of parametric formulae for determining the stress concentration factors (SCFs) for various types of joints. As an example, Figure 2 shows the $S_{f.h.s.}$ - N_f curves recommended by the various design guidelines. In principle, the advantage of the hot spot stress method is that all kinds of joints are related to the same $S_{f.h.s.}$ - N_f curves by the stress concentration factors, which depend on the global joint geometry. Usually, they can be determined by parametric formulae. However, if parametric formulae do not exist, or the parameters are outside the range of validity of the formulae, expensive numerical analyses or measurements on experiments have to be carried out.

Numerical analyses have the distinct advantage of giving the exact positions, directions and magnitudes of high stresses and the patterns of stress distribution in the entire zone of the specific joint being considered, based upon the amount of refinement put into the modelling. However, the modelling cannot give the actual peak stress at the weld toe, due to inherent difficulties in representing the singularity at the notch formed between weld and parent metal [44]. However, since only "geometric stress" is used to define the SCF (see Figure 3), this information is not necessary.

Factors not covered by the geometrical hot spot stress method are:

- The stress field around the hot spot such as the stress gradient.
- Global geometry of the weld, especially the leg length.
- The condition of the weld toe, for instance the toe radius and the influence of weld toe improvement techniques (see Chapter 2.8).

In spite of the restrictions mentioned above, the hot spot stress (or strain) method has proven to be the most commonly used approach for fatigue design of circular hollow section joints.

The local notch stress approach

This method needs information on the stress or strain distribution in the vicinity of the weld, which is usually obtained by means of an FE analysis as used for the hot spot method. The influence of the notch and the notch stress can be obtained from a FE analysis of a small region in the vicinity of the weld, using a fine 2D (shell) or 3D (solid) mesh. As a result, additional stress concentration factors can be established, to be multiplied with the SCFs of the hot spot method. In this way, correction factors for different weld types might be established.

The results of the local stress or strain concept seem to be more consistent, as they cover yet another source of scatter in fatigue behaviour. There are however, disadvantages of this method, which so far prohibited use of these method in design recommendations, other than the simple correction for the weld shape used in the AWS , API and EC3 codes:

- The determination of the effect of local stress raisers in a uniform way for inclusion in design guidelines is still a problem.
- The influence of the weld shape, especially the leg length also changes the hot spot stress as noted by de Back [34] and van Wingerde [85, 119] since the weld toe is moved away from the highest stress range.
- To take full advantage of this method, the weld profile must be controlled. Usually, this is very difficult and hence expensive, so that other techniques might be preferred to enhance the fatigue behaviour. (see Chapter 2.8).

In a Japanese investigation by Yoshida and Iida [123], the notch peak stress raisers had been virtually eliminated in the ground weld toes. In this case the basic $S_{th.s.}-N_f$ line for smooth material could be used.

Fracture Mechanics approach

This approach is based on Paris' law that governs the fatigue crack growth rate:

$$\frac{da}{dN} = C (\Delta K_{(\pi/2)})^m \text{ in thickness direction and}$$

$$\frac{dc}{dN} = C (F_c \Delta K_{(0)})^m \text{ in the direction of the length of the crack.}$$

Here:

da/dN crack depth extension per load cycle.

dc/dN half crack length extension per load cycle.

ΔK the stress intensity factor in the direction ($\pi/2$ in depth direction or $0 //$ surface).

C, m material constants

F_c reduction factor for crack growth at the surface [46].

In principle this method can accurately predict the fatigue behaviour of a joint and is only dependent upon material constants and the stress intensity factor. However, the stress intensity factors are usually lacking in the case of welded joints between structural hollow sections due to the geometry with its inherent complex stress distribution.

The fracture mechanics model can be incorporated in a FE model of the complete joint. This would normally require a very extensive 3D element mesh with crack tip elements. One alternative is the use of the hot spot stress from FE analyses or from strain gauges as the nominal stress in a plate with a welded attachment plate, which is used to model a part of the weld with chord wall and brace wall of a joint. This method can obtain reasonable predictions of the fatigue life of a joint as was shown by van Straalen [105].

Another alternative is the line spring method as applied by de Lange [73]. The basic procedure of the method is as follows:

- Derive the compliance characteristics of the crack as a function of the crack depth and material properties only. As a first approach (only considering the cracking mode I), this can be done by referencing to a crack in a simple edge-cracked plain strain specimen subject to tension and bending.
- Couple the crack zone to the surrounding structure enforcing compatibility conditions and solve the resulting boundary value problem for the applied loads.

The size of the initial defects has to be estimated. The estimation of these initial defects governs the fatigue strength found. However, for joints where cracks are already detected, this method is valuable in predicting the remaining fatigue life of the joint. In this case, the actual weld dimensions are known, and the extra effort that this method requires over lower level analyses might well be offset by avoiding costly repairs. Also, this method is a useful tool in research and can explain some aspects of the fatigue behaviour, such as (a part of) the thickness effect.

Other fatigue behaviour assessment methods

These methods differ fundamentally from the methods describe above. Although their application is very limited at this time, they are mentioned for the sake of completeness and because of future application.

Frequency measurement

Analysis based upon vibrations in which the member is hit by an impulse in the direction of the nominal force for which stress concentration factors are to be established, see Kahoutek [70]. The rigidity of the test specimens used was measured by analysing the dynamic behaviour, especially the natural frequencies. These rigidities were then plotted against the SCF as determined by Kuang [71] and Lloyds and DNV. If enough data is found, the SCF and rigidity might be related to each other. The method cannot give much indication about the actual distribution of the stiffness around the joint as it only gives one value per joint and must therefore be classified as indicative rather than practical when it comes to determination of the SCF.

Comparison with the static strength

Comparison with the static strength of the joint. This method is proposed for use by the Architectural Institute of Japan [72], although mainly in the low cycle area. There are certainly a number of similarities between the static and fatigue strength of a joint, such as the generally unfavourable behaviour for $\beta=0.4$ to 0.7 . However, the static strength tends to be almost proportional to the yield stress of the material, whereas the fatigue behaviour is normally hardly effected (except for improvement techniques, see Chapter 2.8). Also, the fatigue behaviour is strongly influenced by factors like local stress concentrations in the corner of the joint and the weld quality which would not affect the static behaviour of the joint so much. Nevertheless, if the static strength of a joint is known, this method might be useful for a quick reference to determine whether a more elaborate check on the fatigue strength of a joint is necessary.

2.4 Discussion on the definition of the hot spot stress

Although the hot spot method is used in many design guidelines, the definition of the hot spot stress is still under debate. Various design guidelines do not address this matter explicitly although the result can vary considerably, depending on the way the hot spot stress or strain is determined. It is clear that the different definitions used for the hot spot stress tend to cloud comparisons between various test results, research results such as parametric formulae and design recommendations. The IIW has started an initiative to reach a common definition for the hot spot stress, see Niemi [81].

Stress or strain based definition

Although in this work and in most design recommendations the terms hot spot stress and stress concentration factor are used, in many cases these are really based on strains. Strains have two advantages over stresses:

- They can be measured easily by individual strain gauges (unless principal strains are to be determined), whereas stresses would require strain gauge rosettes to measure various strain components.
- From a theoretical point of view, strains are more logical, since low cycle fatigue tests with strains far exceeding the yield strain do not show any difference in behaviour as could be the case for stress based phenomena [17].

However, as design recommendations are geared toward stresses, the results are usually presented as stresses. As a result, $S_{h.s.}-N_f$ lines showing "stresses" far exceeding the yield or even ultimate stress are presented (see Chapter 7). The nominal stress and strain ranges can be easily converted: $\sigma_f = E \cdot \epsilon_f$.

In the numerical analysis, both hot spot strains and hot spot stresses have been determined, resulting in SNCFs and SCFs respectively. Chapter 5 contains a comparison between SNCFs and SCFs for quadratical extrapolation of strains or stresses of T-joints loaded by an in-plane bending moment on the brace. The ratio between SCF and SNCF varies considerably: $SCF = c \cdot SNCF$ or $\sigma_{h.s.} = c \cdot E \cdot \epsilon_{h.s.}$, where "c" varies between 0.6 and 1.4. For the European Offshore programme, van Delft [47] found a mean value of 1.15 for c for circular hollow section joints. Frater [59] found a ratio of 1.091 to 1.146 for RHS K-joints.

Type of stress (strain) to be used

Which stress is to be used: principal stress or a stress perpendicular to the weld toe. The IIW, DEN (T-curve definition) and EC3 definitions all use principal stresses, but IIW states that these stresses are usually perpendicular to the weld toe in the case of simple connections. The AWS and API use the hot spot stress perpendicular to the weld toe. Principal stresses can be tens of percents higher than stress perpendicular to the weld toe [94]. Closer to the weld the stresses are diverted perpendicular to the weld by the stiffening influence of weld and attached wall [79]. Therefore, the ratio $\frac{\sigma_{\text{principal}}}{\sigma_{\text{perpendicular}}}$

decreases closer to the weld. For the extrapolation this means that $SCF_{\text{principal}}$ is often lower than $SCF_{\text{perpendicular}}$ since the principal stresses tend to increase less sharply towards the weld toe [94]. As only stress components perpendicular to the weld are enlarged by stress concentrations caused by the global weld shape and the wall of the adjacent member, the author favours a definition based upon stresses perpendicular to the weld. This view is supported by the direction of crack growth, which is usually mainly along the toe of the weld, especially at the initial stages of the crack. Furthermore, strains perpendicular to the weld toe can be measured by simple strain gauges instead of strain gauge rosettes and extrapolation of principal strains or stresses would require extrapolation of all components, which is rather cumbersome. Also, the direction of the principle stress would be different for different load cases, prohibiting superposition of load cases.

Positions where the hot spot stresses are determined

Some parametric formulae are only provided for the highest values of the stress concentration factors for a particular single load action. However, for combined loading, both the location and value of the stress concentration factors have to be determined, to allow superposition. The appropriate determination of the hot spot stress can only be obtained from those sets of parametric formulae which give sufficient information at several locations. As may be observed in Chapter 2.5, a number of locations are considered in the present work.

Type of extrapolation

Since the local stress concentrations due to weld geometry and irregularities at the weld toe cannot easily be determined and as these stress concentrations are heavily dependent upon fabrication, they are not to be taken into account in the hot spot method. This is a major source of scatter in fatigue test results. The influence of the local weld notch strains is excluded by carrying out an extrapolation procedure from outside this region (see Chapter 2.5). The hot spot stresses or strains arrived at in this manner are divided by the nominal stress or strain to arrive at the stress concentration

factor (SCF) or strain concentration factor (SNCF). At first, working group III of the ECSC proposed a linear extrapolation to the weld for joints between circular hollow sections. Later on, the stress distribution was found to be non-linear in some cases. As a consequence, the IIW recommendations [68] no longer specify any method of extrapolation.

In this work, two extrapolation methods, described in Chapter 2.5 (linear and quadratic) have been used for the determination of the hot spot stress. The difference between linear and quadratic extrapolation can be up to 40%, as is shown in Chapter 7.6, where the two extrapolation methods are compared to each other. For joints in rectangular hollow sections, the geometric strain can be strongly non-linear and therefore the quadratic extrapolation method should give more realistic values for the $S(N)CF$ at the weld toe. This is supported by comparing the $S_{h.s.}-N_f$ curves based on test results, corrected for the thickness effect, see Figures 42 and 43 in Chapter 7.

Another advantage of the quadratic extrapolation is a better agreement between characteristic S_f-N_f lines based on experiments and those based on parametric formulae. This allows the same classification according to EC3, document 9.03 without any correction factors on the parametric formulae being necessary. This classification is carried out in Chapter 7.5 and presented in Table 23. Therefore, although the quadratic extrapolation is slightly more difficult to carry out and more sensitive to small changes in the data points, this extrapolation method is preferred.

Limits for the extrapolation

Not only the type of extrapolation is important, but also the distance from where the extrapolation to the toe should be carried out. Working group III of the ECSC originally used a value of $0.2\sqrt{rt}$ (with r the radius and t the wall thickness of the brace considered) for the closest point to the weld for extrapolation. Later on, as the influence of r on the position of the extrapolation was considered doubtful, a value of $0.4 t$ was adopted by Gurney [61] and van Delft [44] with a minimum of 4 mm. This value was also used for this work. In the research projects presented in this paper, the second strain gauge (or data point from numerical analysis) is taken to be $0.6 t$ further away for linear extrapolation and $1.0 t$ further away for quadratic extrapolation, but this point tends to be less critical. The SAE [99] uses strain gauges of 6 mm length straddling the weld toe for a local stress (including some local influences from the weld). Yoshita and Iida went even more local by applying 0.6 mm strain gauges. Note that the use of absolute values like 4 mm from the weld toe, or strain gauges of 6 mm length influence the thickness effect obtained: for larger wall thicknesses, the strain gauges tend to be more in the local stress zone and hence obtain higher strains. These effects tend to mitigate the thickness effect (see also Marshall [79]).

2.5 Definitions and assessment of the hot spot stress used in this work

Positions where the hot spot stresses are determined

The stress concentration factor SCF is defined as the (part of the total) hot spot stress divided by the nominal stress which causes this (part of) the hot spot stress. The total hot spot stress is then a function of all nominal stresses in all members of the joint multiplied by their stress concentration factors. In case only axial forces and in-plane bending moments are considered, the total hot spot stress can be determined by:

$$S_{r_{h.s.}} = \sigma_{r_{m1}} \cdot SCF_{m1} + \sigma_{r_{a1}} \cdot SCF_{a1} + \sigma_{r_{m0}} \cdot SCF_{m0} + \sigma_{r_{a0}} \cdot SCF_{a0} \quad (2-2)$$

In this formula:

$\sigma_{r_{m1}}$ The nominal in-plane bending stress range in the brace.

$\sigma_{r_{a1}}$ The nominal axial stress range in the brace.

$\sigma_{r_{m0}}$ The nominal in-plane bending stress range in the chord.

$\sigma_{r_{a0}}$ The nominal axial stress range in the chord.

SCF_{m1} , SCF_{a1} , SCF_{m0} and SCF_{a0} are the corresponding stress concentration factors.

In case of axially loaded T-joints, the hot spot stresses are caused by the induced bending moment in the chord $\sigma_{r_{m0}}$ as well as by the axial force on the brace $\sigma_{r_{a1}}$ (see Chapter 5.3). This concept deviates from many popular definitions: the IIW design recommendations [68] and the API [31] divide the total hot spot stress by the nominal stress in the brace to arrive at the stress concentration factor.

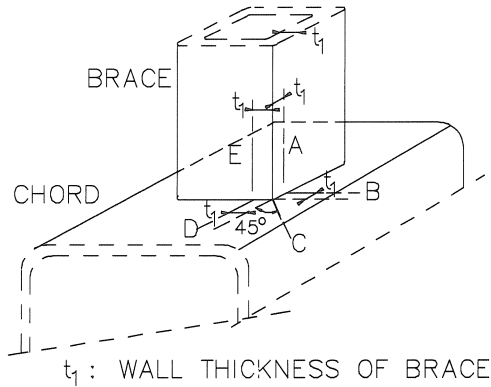


Figure 4. Position of lines A to E.

To be able to determine the total hot spot stress according to Equation 2-2, allowing superposition of load cases that consist of forces and in-plane bending moments on chord and brace, it is necessary to establish fixed positions where the SCFs are determined. The stresses are considered along five lines A to E on the chord and brace (see Figure 4), which have been found to give highest stresses [6].

As a consequence, the hot spot stresses found may underestimate the 'true' hot spot stress if the direction of the principal stresses deviates from these lines, especially if the stress concentration is less pronounced. Here, the stresses at other positions or in other directions or at the inside of the members may be higher. Therefore, a minimum value of 2.0 is specified for SCF_{al} and SCF_{ml} in the proposed design recommendations, see Chapter 8.

Extrapolation to the weld toe

For the extrapolation of the hot spot stress at the weld toe, two methods have been used in this research programme (see Figure 5).

Both methods start by fitting a curve through all available data points (by hand or numerically).

Linear extrapolation

Two points on the curve determined from all data points are used for the extrapolation: the first is 0.4 t from the weld toe, with a minimum of 4 mm. The second point is taken to be 0.6 t further from the weld toe.

Quadratic extrapolation

The first point is again 0.4 t from the weld toe, with a minimum of 4 mm. The second point on the curve used for the quadratic extrapolation is taken 1.0 t further from the weld toe.

The quadratic extrapolation is carried out through:

- The first and second point on the curve based upon all data points.
- All data points between the first and second point on the curve (for $t > 10$ mm, this means from 0.4 t to 1.4 t from the weld toe)

In this case, the curve passing through all data points supplies two additional data points as a basis for the extrapolation.

By means of the least squares method, a quadratic curve is fitted through all these points, obtaining the quadratic SCF.

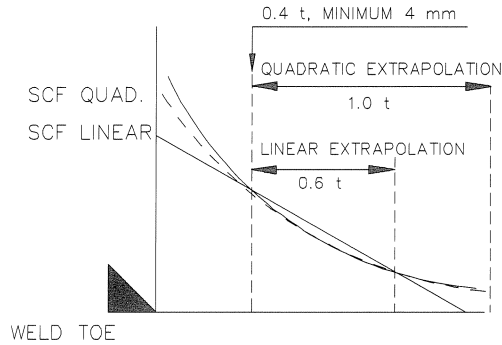


Figure 5. Method of extrapolation to the weld toe.

2.6 Survey of existing research on the fatigue behaviour of square hollow section joints

Work concerning the SCFs of tubular joints

The research on the fatigue behaviour of uniplanar tubular joints has resulted in usable parametric equations, such as those derived by Kuang [71], Wordsworth, later modified by the UEG [108] and by Smedley [98], Gibstein [60] and Efthymiou [54, 55]. The work of Efthymiou is based on FE analysis with solid elements for 150 geometries with various load cases, resulting in a sound basis for parametric equations, with a wide range of validity. Comparison with experimental results by van Delft [45], Fessler [58], and Smedley [98] showed good agreement. Efthymiou supplies correction factors for short chords and determines all SCFs at fixed positions (chord crown and saddle as well as brace crown and saddle) to allow for superposition of load cases.

This idea of superposition is extended by supplying so-called influence formulae which relate the SCFs of all members in crown and saddle to an unbalanced load on a member, allowing every possible load combination. The same method could be used for the analysis of multiplanar joints. The disadvantage of having to calculate many SCFs in case of combined loads on various members is offset by the fact that any given combination of load cases can be analysed by using the parametric formulae, without loss of accuracy.

Note that the set up of the research as described in Chapter 2.5 in this work follows a similar philosophy, as does the ongoing work at the Delft University of Technology on multiplanar joints [94].

Work carried out for earlier ECSC research [82, 83]

This work contains tests on K- (134 specimens), KT- (16 specimens) and N-joints (67 specimens) from various laboratories in Paris, Liège, Nottingham, Karlsruhe and Delft. The results were presented as classification per type of joint. The influence of the steel grade was found to be negligible in most cases. Cold finished sections showed a slightly better fatigue behaviour than hot finished sections, but the difference was found to be small. The classification factors and τ influence found in this investigation (although slightly modified) form the basis for the present EC3 classification rules (see Chapter 2.7). The classification method was used as only limited information about SCFs was provided at the time of drafting.

Work carried out for K-joints in Karlsruhe [2, 21 to 28, 75]

In the scope of the same research programmes presented here for T- and X-joints, work was also carried out for K-joints with gap or overlap and loaded by axial forces or in-plane bending moments. A large number of tests were carried out (see Table 1). By means of the FE method a wider range of parameters was studied, including interactions between various geometric parameters.

However, there are a few comments to the work:

- Series of tests were carried out with the same nominal dimensions. Per series of tests, the SNCFs were measured for one joint only. Applying this SNCF for the other joints in the series introduces an extra scatter in the $S_{t,h.s.}$ - N_f lines, since the different fatigue behaviour of various test specimens with the same nominal geometry may partly be caused by different SNCFs.
- The overlapped joints were loaded with the overlapping brace in tension. This is known to decrease the fatigue strength and for this reason is usually avoided.
- By basing the nominal stress purely on the axial stress in the brace, rather than including the bending stresses caused by eccentricities and stiffness distribution around the brace, the SCFs are valid for this ratio between bending moments and axial forces only.
- The numerical analyses were used to obtain only maximum SCFs in brace and chord, rather than at fixed positions. This prohibits a superposition of load cases.

Work on K-joints, carried out in Delft [20]

Numerical work was carried out for only twelve K-joints with gap, hence the resulting formulae must be classified as preliminary. Only one experiment was carried out for SCF measurements, without fatigue testing. However, it contains valuable information on the interpretation of the SCFs found by modelling the weld with shell elements, rather than solid elements and on the influence of the secondary bending moments in K-joints on the SCF, which were experimentally verified by variation of the end support conditions of the chord, to introduce bending moments.

Work carried out at the Nanyang Technological Institute (Singapore) [100 to 104]

This research contains a numerical investigation of the SCFs of K-, T- and Y-joints made of RHS braces and chords or RHS braces and CHS chords [101, 103]. Comparisons with SCFs for circular hollow section joints are made. Also, a study on the SCFs of joints made of square hollow sections for T-, K- and Y-joints, including out-of-plane bending moments, is carried out. A comparison of the SCF formulae for K-joints [100] with experiments carried out for a Canadian investigation [59] showed a generally better agreement than the preliminary formulae established in Delft [20] and the formulae of Karlsruhe [2]. However, the Delft formulae were used outside its range of validity and the measurements in the gap area of one joint were not made at the correct position as there was no room to fit the strain gauges, thereby underestimating the SCF. The formulae for T-joints will be compared with the results of this work in Chapter 7.

There are also some comments to this work:

- The investigation is purely based upon numerical investigations and no comparison with experimental results was made yet. No $S_{r_{h.s.}}-N_f$ lines were established.
- The omission of the weld modelling in the FE analyses might result in relatively large errors, depending on the geometry of the joint.
- The research is carried out by starting from one geometry and then varying one parameter only, to determine the influence of that parameter. Then the same procedure is repeated for the other parameters. This procedure ignores the important interaction between the various geometric parameters such as shown in the formulae of Efthymiou for tubular joints [55] and the present work.
- No joints with $\beta=1.0$ were studied, limiting the range of validity of the formulae considerably.

Work carried out by the University of Coimbra and Lisbon (Portugal) [57]

The experiments consisted of T- and Y-joints made of RHS 40x40x2 mm, hence the practical application may be limited. Also, no different geometries were tested so that no parametric formulae were established. Instead the investigation concentrated on the influence of the shape of the weld and the use of FE models and an assumed 3D crack propagation law.

The influence of the thickness (size) effect on fatigue behaviour

In many publications the influence of the size effect on the fatigue behaviour has been investigated.

The size effect is also recognized in the design recommendations (see Chapter 2.7).

The thickness effect is attributed to three origins:

- Geometrical thickness effects arise from the stress gradient at the notch root, which is less steep for larger thicknesses even if geometric scaling is maintained in full (for instance the radius of the weld toe). This means that the crystals at the crack tip are subjected to larger loadings. This effect can be partly investigated by means of fracture mechanics.
Compare two specimens, one being twice as large as the other in all aspects. Paris' law : $\frac{da}{dN} = C (\Delta K_{(\pi/2)})^m$ (see Chapter 2.3), in which $\Delta K \sim a$ and $m \approx 3$ results in a $\sqrt{2^m} \approx 2^{1.5}$ faster crack growth for the larger specimen. Since the construction is only 2 times larger, failure (for instance a through thickness crack) occurs 40% faster in the larger specimen. This thickness effect alone would account for a thickness effect of $N_f \sim t^{-0.5}$. For a slope of 1:3 in the $S_{th.s.} - N_f$ line, the thickness effect on stress basis is $t^{-0.17}$.
Usually, the geometry is not completely scaled as for instance the radius of the weld toe is not increased as much as the wall thickness, so that the stress magnification factor increases stronger with increasing thickness [64], resulting in a larger thickness effect.
- The statistical thickness effect is caused by the fact that in a larger volume of material, the chance of a large defect increases. As fatigue is a weakest link driven mechanism, the fatigue strength will generally decrease with the size of the detail considered.
- The technological thickness effect results from differences in production parameters. The grain structure is coarser, the yield strength is lower, the residual stresses are higher, the probability of hydrogen cracking increases and the toughness decreases.

The thickness effect is the result of fairly complex factors, which is the reason why results obtained by various researchers differ considerably. Haagenzen [64] and Marshall [76] claim that the size effect is larger for joints with a higher stress gradient K_t . Indeed, in the current investigation with generally high SNCFs, a large thickness effect is found (see Chapter 7).

For an ongoing research project at Delft [94], lower SCFs were found and also a smaller thickness effect. Berge [37], Sablok [96] and Booth [40] report that the thickness effect is independent of the weld profile, post weld heat treatment or random loading. Berge [37] notices a sometimes larger thickness effect for tubular joints (with typically higher SCFs) than for welded plates. Sablok [96] finds about the same thickness effect for plates and tubular structures, also independent of the environment (air, sea, sea and cathodic protection). Van Delft finds a thickness effect of $t^{-0.075 \log_{10}(N)}$ for tubular joints, based on a statistical analysis of European fatigue test data. There seems to be evidence indicating that there might be a relationship between the thickness effect and the SCF, as indeed might be expected from fracture mechanics analyses.

2.7 *Survey of some relevant design codes*

From the results of the research projects, conclusions can be drawn regarding the various existing design recommendations. The developments of fatigue research on tubular joints are reflected in the different design guidelines, which are based on a wide variety of philosophies and contain many uncertainties in definitions, fairly "open" guidelines on how the hot spot stress should be determined and even gross inconsistencies.

Many design guidelines do not specify which parametric equations (which can also vary by a factor of 2 in stress as found by the UEG [109]) to use for the determination of the SCF. This is especially surprising in view of the many different definitions of the hot spot stress with inclusion of different effects (see Chapter 2.4). If for instance the local stress is included in a set of parametric formulae, the accompanying $S_{h.s.}-N_f$ lines should be higher than when only the geometrical stress concentrations are considered. If a quadratic extrapolation is used, again the hot spot stresses found are higher than for linear extrapolation.

The author believes that unless the formulae to be used for the SCFs are specified or exact specifications of the kind of hot spot stress to be used are made, the very exact specifications on $S_{h.s.}-N_f$ lines to be used are pointless. Similar objections exist against allowing the designer to base designs on stress concentration factors "obtained from parametric formulae within their domains of validity, a finite element analysis or an experimental model" such as in the EC3 [53] and many other design recommendations allow unless explicit specification on the background to the $S_{h.s.}-N_f$ lines is provided. Similar conclusions are drawn by an investigation by the UEG [109]. Of course, for joints not covered by the design recommendations, the usual freedom should be allowed to the designer.

International Institute of Welding [68]

This institute, especially committee XV-E, is strongly committed to establish internationally accepted design guidelines for the fatigue design of joints between structural hollow sections. The hot spot stress definition is based upon extrapolation of principal stresses and contains specific thickness corrections down to 4 mm wall thickness, as well as (simple) parametric equations for joints between square hollow sections and a hot spot stress definition.

Parametric formulae for the determination of stress concentration factors are given for uniplanar T-, Y-, X-, K- and N-joints made from circular hollow sections loaded by axial force or in-plane or out-of-plane bending moments, as well as for uniplanar K- and N-joints made from square hollow sections loaded by axial force or in-plane bending moments. These formulae are fairly provisional as at the time of drafting only limited evidence was available. For square hollow section joints, only the influence of τ is taken into account. The influence of improved weld profiles is not taken into account.

The design curve A applies in general to all types of joints independent of the stress ratio R. The characteristic (95% survival) fatigue strength is given in relation to the wall thickness t of the member under consideration. The curves are therefore modified for the actual thickness of the relevant member (brace or chord) being considered in the figures.

The reference line for the IIW is given for a wall thickness of 22 mm. Between 10^4 and $5 \cdot 10^6$, the line has a slope of 1:3. After $5 \cdot 10^6$, the $S_{r_{h.s.}}-N_f$ line has a slope of 1:5 until $N=2 \cdot 10^8$, beyond which the $S_{r_{h.s.}}-N_f$ line runs horizontally (fatigue limit).

The thickness correction for wall thicknesses between 4 and 22 mm is rather complicated:

- For $N=10^4$, all $S_{r_{h.s.}}$ for $t=4$ to 22 mm are the same.
- For $N=5 \cdot 10^6$, the corresponding hot spot stress range can be calculated from the reference $S_{r_{h.s.}}-N_f$ line using Equation 2-3, based on Gurney [62].

$$S_r = S_{r_{22}} \left(\frac{22}{t} \right)^{0.25} \quad (2-3)$$

- After $N=5 \cdot 10^6$, the $S_{r_{h.s.}}-N_f$ lines are parallel to the reference $S_{r_{h.s.}}-N_f$ line at a slope of 1:5, until $N=2 \cdot 10^8$ beyond which the $S_{r_{h.s.}}-N_f$ lines run horizontally.

For thicknesses greater than 22 mm, the $S_{r_{h.s.}}-N_f$ line for 22 mm has to be reduced according to Equation 2-3 for all values of N , so that these $S_{r_{h.s.}}-N_f$ lines are parallel to the reference $S_{r_{h.s.}}-N_f$ line. The reference $S_{r_{h.s.}}-N_f$ line is taken from the existing DEn $S_{r_{h.s.}}-N_f$ line (1984), together with the thickness correction for $t \geq 22$ mm. However, the thickness correction below 22 mm is added by IIW and the slope of 1:5 starts at $5 \cdot 10^6$ instead of 10^7 in the DEn design recommendations.

Department of Energy Guidelines [48]

The hot spot stress definition of the DEN is based upon extrapolation of principal stresses. Linear extrapolation is used by the DEN for T- and X-joints. For Y- and K-joints, a nonlinear extrapolation is recommended. No bonuses are given for controlled overall weld profiles. However, grinding the weld toe is stated to give at least 30% improvement on the fatigue strength of a joint.

Curve T' (Thorpe [107], Reynolds [93] to be included in the currently proposed revision of the DEN design guidelines)

This design curve is based on a wide database, containing over 400 data points and is currently proposed for inclusion in the revised DEN design guidelines for offshore installations, using $t=16$ mm as the reference line, unlike the current DEN design guideline, which is based on $t=22$ mm. The slope of the line is 1:3 for $N_f=10^4$ to 10^7 , after which the slope becomes 1:5 until 10^8 , which is the fatigue limit. The line with slope 1:3 may be extended in the low cycle range, with hot spot stress ranges up to $2\sigma_e$. The results of low cycle fatigue tests [17], where hot spot stress ranges of up to $5\sigma_e$ occurred, fit in quite well in the $S_{h.s.}-N_f$ lines. Therefore the limit to $2\sigma_e$ does not seem necessary, at least in the case of joints between (square) hollow sections (see Chapter 7).

For wall thicknesses larger than 16 mm, a thickness correction is applied for the whole $S_{h.s.}-N_f$ line, resulting in parallel $S_{h.s.}-N_f$ lines. The thickness correction is then given in Equation 2-4.

$$S_x = S_{x,t} \left(\frac{16}{t} \right)^{0.3} \quad (2-4)$$

Inclusion of thinner walled specimens, below 16 mm, would yield a larger thickness correction exponent, but this was attributed to the disproportionate large welds for these thicknesses. But a similar wall thickness effect was shown by van Delft [45] and Iida [67] (in case of bending moments). This is also in accordance with the larger thickness effect found for the present research. However, in the proposed revision for the DEN design recommendations, no thickness effect below 16 mm is taken into account, due to a lack of reliable data and the fact that the DEN guidelines tend to concentrate on offshore applications. A comparison between Figures 40 and 42 (see Chapter 7) which present the experimental results of this work shows that this is very conservative for smaller wall thicknesses. The DEN will also specify which parametric equations for tubular joints are to be used in conjunction with the $S_{h.s.}-N_f$ line specified (for instance the Eftymiou equations [54]).

Euro Code 3 [53]

The hot spot stress called geometric stress in the draft version of the EC3 follows the same definition as the IIW code [68]. However, EC3 restricts the thickness effect to 25 mm and above. Instead of specifying $S_{r,h.s.}$ - N_f lines, the EC3 specifies classes, which represents $S_{r,h.s.}$ at $N_f=5 \cdot 10^6$ of the detail. The corresponding $S_{r,h.s.}$ - N_f line starts at 10^4 cycles, $(5.84 \cdot \sigma_c)$, runs at a slope of 1:3 until $5 \cdot 10^6$ cycles $(0.737 \cdot \sigma_c)$, and then at 1:5 until the fatigue limit at 10^8 cycles $(0.405 \cdot \sigma_c)$. EC3 currently uses both the classification and the hot spot stress method. Classes are also given for joints between rectangular hollow sections. No parametric formulae are specified by EC3.

For the hot spot stress concept ($t \leq 25$ mm) the relevant classes are:

class 90: butt welded joints with controlled weld profile.

class 71: butt welded joints.

class 36: fillet welded joints.

A comparison between classification method and hot spot method reveals some serious inconsistencies in the EC3. For instance, for fillet welded K-joints with gap and $\tau=1.0$, class 36 is to be used for the classification method, based on nominal stress ($t \leq 12.5$ mm). For the hot spot method, class 36 is also to be used, whereas the nominal stress is to be multiplied by the SCF. So based on nominal stresses the class of the hot spot method is $36/SCF$.

Experiments carried out at the University of Toronto [59] found SCFs of up to 6.0. These experiments were within the range of validity (only the tests at Toronto had fillet welds for a brace wall thickness of 12.5 mm, whereas EC3 restricts the classification method for fillet welded joints to a maximum of 8 mm wall thickness). This results in a factor of 6 difference in stress for the classification method versus the hot spot stress method.

In case of other joint geometries the differences might even be larger. At the University of Karlsruhe, test K20S34 [24] SNCFs well over 10 were measured, for a fillet welded K-joint which was fully within the range of validity. These measurements did not take the secondary bending moments due to eccentricities and uneven stiffness distribution around the joint into account. Would this effect have been taken into account for the nominal strains, with the nominal bending strain being about 50% of the nominal axial strain, a SNCF of about 6 would have been found. Applying the hot spot method would again result in a factor of 6 difference in stress between the classification method and the hot spot method.

The classification method is probably unconservative in some cases. For instance several test specimens of series K20S34 [24] (chord 100x100x4 mm, brace 40x40x4 mm, gap 43.4 mm), within the range of validity of the EC3 classification method would exhibit a class based on nominal stress of under 40 (including a factor 1.5 on the nominal stress, to account for secondary bending stress). Applying the thickness correction derived in Chapter 7 at $N_f=2 \cdot 10^6$ for a joint that is twice as large in all aspects (still within the range of validity), the class would be about 25, so class 36 can be unconservative.

The classification method is restricted to wall thicknesses below 12.5 mm and the $S_{th.s.}-N_f$ lines for the classification method have a slope of 1:5 for $N_f < 10^8$, making them slightly more conservative in the low cycle range. But this does not clear the inconsistency between the hot spot method and the classification method (with the classification method being less conservative). It is clear and also confirmed by the present investigation that the hot spot stress classification of 36 is not correct for hollow section joints. Also, the favourable thickness effect, which has been implicitly included for the classification method, should be taken into account for the hot spot method.

The newest draft of the EC3 allows class 36 for fillet welds unless it can be proven that a higher class can be used. In Chapter 7, the results of this investigation are classified according to EC3, resulting in class 90 (for $t=16$ mm), for both fillet and butt welds without controlled weld profile, so that the designer can safely use this class. Class 90, in good agreement with most $S_{th.s.}-N_f$ lines of the existing recommendations, is now proposed for inclusion in EC3, together with a favourable thickness correction for wall thicknesses below 25 mm.

Structural Welding Code (American Welding Society [32], Marshall [78, 79])

The hot-spot strain definition given for structures made of hollow sections states that the hot spot strain is "The cyclic total range of strain which would be measured at the point of highest stress concentration in a welded connection. When measuring hot-spot strain, the strain gauge should be sufficiently small to avoid averaging high and low strains in the regions of steep gradients." No extrapolation is to be carried out, nothing is said about the parametric formulae to be used, and only simple SCF equations are given.

A difference with most other codes is a strong emphasis on the overall weld profile, also discussed in Chapter 2.8.

The effect of the plate thickness is to be compensated by improving the weld profile from a standard flat weld profile for brace wall thicknesses smaller than 10 mm to concave smooth profile welds which have to be fully ground for large brace wall thicknesses (Marshall [77]). In this way, the basic $S_{h.s.}-N_f$ line (X_1) is also valid for larger wall thicknesses. In case the weld profile requirements for the wall thickness of the brace are not met a lower $S_{h.s.}-N_f$ line (X_2) is to be used. In the commentary, a correction of $t/t_{limit}^{-0.25}$ is suggested for sharp notched welds and brace wall thicknesses exceeding the limits given for X_2 in the code.

The equations of the lines X_1 and X_2 are not given in the AWS code. No detailed parametric equations are given to determine the hot spot stress. Instead, "prototype measurements" or analysis according to the "best available theory" are suggested.

Recommended Practice for Planning, Designing and Constructing Fixed Offshore Platforms (American Petroleum Institute [31])

The API design recommendations closely resemble the AWS regulations. The hot spot strain is taken as the strain "measured by a strain gauge element adjacent to and perpendicular to the toe of the weld, after stable strain cycles have been achieved". Therefore no extrapolation is carried out, and the thickness effect is mitigated by the fact that for larger sizes the strain gauge tends to pick up a larger portion of the local strains, resulting in higher strains. In this way, the measured SCF becomes thickness dependent. The formulae for the SCFs of tubular joints are very simple, based on Kellogg's formulas.

Instead of the AWS $S_{h.s.}-N_f$ lines X_1 and X_2 , the API uses the notation X (=AWS X_1) and X' (=AWS X_2), where X may be applied when the weld profile is improved (the toe smoothly merging with the adjoining base material). The fatigue limit is taken to be $2 \cdot 10^8$ cycles, in contrast to the AWS, where the fatigue limit is taken as 10^7 for X_1 and $2 \cdot 10^7$ for X_2 . Also, no thickness correction factors are included, although a simplified version of the AWS thickness correction is now proposed for inclusion in the API [80]. Stress concentration factors may be derived from FE analysis, model tests or empirical equations.

Comparison between the $S_{h.s.}-N_f$ lines of the design recommendations

In order to compare the various $S_{h.s.}-N_f$ lines, a wall thickness of the member under consideration of 25 mm (the reference thickness of EC3) and a butt weld is considered applying the thickness corrections in the design recommendations.

EC3 : class 71/90 (depending on weld profile)

DEn : $114 \cdot (16/25)^{0.3} = 100$

IIW : $106 \cdot (22/25)^{0.25} = 95$

AWS/API: 79/100 (depending on both weld profile and wall thickness)

See also Figure 2, where the various $S_{h.s.}-N_f$ lines are plotted.

It is encouraging that the variation between the various $S_{h.s.}-N_f$ lines at $2 \cdot 10^6$ cycles is relatively modest ($\pm 15\%$ on the basis of stress). However, the American $S_{h.s.}-N_f$ lines have a different slope and the AWS has also a comparatively optimistic fatigue limit, resulting in the fatigue limit of AWS line X_1 being a factor 2 higher on stress basis than that of any other $S_{h.s.}-N_f$ line.

As for the $S_{h.s.}-N_f$ line definition: the EC3 manages to describe the complete $S_{h.s.}-N_f$ line with only one parameter (the class), which is quite useful for the designer and easy to incorporate in computer software. On the other hand, the AWS does not give any numerical information on the $S_{h.s.}-N_f$ lines, forcing the designer to measure from the graphs.

The influence of the thickness (size) effect in the design recommendations

Previous research [3, 120] has established a thickness correction factor of $(16/t)^{0.11 \log_{10} N_f}$ (which is limited to $N_f \leq 5 \cdot 10^6$, see Chapter 8) in which t is the wall thickness of the member that fails. In case the parametric formulae are used, this implies checking both members. In the present draft versions of EC3 and DEn, the thickness correction is only applicable for wall thickness over 25 and 16 mm respectively, resulting in prohibitively conservative designs for small wall thicknesses. The API omits the thickness effect by specifying an improved weld profile for larger wall thicknesses, in order to compensate for the thickness effect. The AWS also includes the influence of the weld profile, but for thicknesses exceeding the limit thickness the $S_{h.s.}-N_f$ lines are modified by a factor $t/t_{\text{limit}}^{-0.25}$.

2.8 *Survey of techniques used for improvement of the fatigue behaviour*

The use of high strength steel decreases the ratio between the amount of material required and the static strength of the structure. However, the fatigue performance is not (or hardly) influenced by the steel grade. For larger wall thicknesses, the fatigue performance degrades even further. The use of improvement techniques is meant to enhance the fatigue strength, as reported by many researchers. Combining several techniques would even bring larger gains in fatigue performance. However, there are considerable disadvantages connected to the application of improvement techniques:

- The results are usually subject to considerable scatter and very sensitive to the skill of the operator, so quality control is critical.
- The number of experiments is limited and often solely based on plate tests or small scale specimens. It is expected that some improvement techniques will have less influence for larger thicknesses. Also, the fatigue behaviour of welded plates can not always be translated to that of hollow section joints. Some hollow section joint geometries are difficult to access, in which case application of improvement techniques might be less effective.
- Application of improvement techniques is often costly.
- Other locations and failure modes might govern the fatigue strength, for instance root failure, in which case further improvement at the toe is useless.
- Stress relief techniques are sensitive to the influence of stresses introduced during further stages of fabrication and erection.
- Some improvement techniques, such as weld profile control are dependent on the stress gradient of the connection [56].

Because of the uncertainties mentioned above, the discussed improvements in this paragraph are only an indication of the effectiveness of the improvement method considered. Most design guideline committees have been reluctant to attribute a higher fatigue strength to improved welds. Nevertheless, it is obvious that more research would enable a more widespread application of the improvement techniques.

Weld profile control

For this technique, the welder should control the overall weld shape and the transition from weld to base material should be smooth. Especially the local angle and radius are considered important by de Back [33] and Elliot [56]. The main advantage of this method is that no extra technique is required for fatigue behaviour improvement.

The AWS acknowledges the effect of weld profile control by allowing a higher $S_{h.s.}-N_f$ line for those profiles that pass a disc test [32]. Recent tests in France [39] and Norway [63] indicate about 25% improvement in fatigue strength at long lives for plates with transverse fillet welds with controlled profile. For tubular joints, the results vary considerably: early UKOSPR and ECSC programmes did not reveal any significant influence of weld profile control. Later tests by Dijkstra and Noordhoek [50] revealed improvements of 150% on fatigue lives for the improved joints. Improved weld profiles tend to have the weld toe further away from the brace wall, resulting in lower spot stresses [56]. Reductions in SCF for improved welds of up to 25% are reported by Marshall and Elliot [56].

Another way to control the weld profile is the use of special electrodes as was done for Japanese tests on high strength steels with $\sigma_e=500$ to 800 MPa. The improvements in fatigue life were 50 to 85%, with the largest increase occurring for the highest strength steel. These electrodes might also be used for the finishing passes at the weld toe. At this moment, it is not known how the results are for non-horizontal positions.

Grinding

A rotary burr grinder or a disc grinder is used to remove slag intrusions and improve the transition from weld toe to basic material. It has to be extended to 0.5 mm below the bottom of any visible undercut, according to DEn [48]. This method is the only method allowed by European design guides for improving the fatigue strength and is only allowed for remedial measure in case the fatigue strength of a joint is found to be inadequate. A problem with grinding, especially disc grinding is that too much material may be removed. Also, it is very difficult to grind in confined areas. These effects cause a considerable scatter in fatigue behaviour improvement. At long lives, improvements ranging from 10 to 160% (the larger improvements being for high strength, quench tempered steels) are reported by Booth [41]. Another advantage is that by reducing the highest stresses in sea environments, also stress corrosion is reduced [38].

Weld toe remelting by TIG or plasma dressing

The weld toe is remelted, resulting in a smoother transition and removal of slag inclusions and undercuts, as well as residual stresses. TIG dressing is rather sensitive to operator skill. Improvements ranging from 10 to 100% are reported [64]. Plasma dressing has a larger heat input and a wider weld pool, thus making this method less sensitive to the skill of the operator. The results are generally better than for TIG dressing.

Post weld heat treatment

After welding, the specimens are heated to about 600°, in order to relieve the residual stresses. Van Delft [45] finds no influence for $R=0$. The only specimen with $R=-1$ and PWHT was found to be above the scatter band, suggesting a beneficial effect of PWHT.

Peening

Peening can be done by a hammer with a round tip of 6 to 14 mm radius, or a bundle of wires, used to plastically deform the material to about 0.6 mm depth. The equipment is usually pneumatically operated. The purpose is to remove the residual tensile stresses and introduce compressive stresses at the weld toe. Like most other improvement techniques, peening is believed to be most successful for high strength steel.

As an alternative, shot peening can be used: small shots in an air stream blast the material. The coverage is called 100% if all dimples at the surface just overlap. Normally 200% coverage is specified. Typically, peening results in a 30 to 100% increase in fatigue life, especially for high strength steel and $R=-1$. It can be expected that high loads in variable amplitude load conditions could decrease the performance gain, but tests do not confirm this.

Improvement techniques in the design guides

Various design recommendations reward a better weld profile by allowing a higher $S_{th.s.}-N_f$ line (see Chapter 2.7). The DEn norm allows a 30% higher fatigue strength if the toe of the weld is ground (only remedial use allowed). The EC3 goes from class 71 to 90 for a controlled weld profile. The AWS and API go from 80 N/mm² (at $N=2 \cdot 10^6$) to 100 N/mm² for an improved weld profile. Note that most design guidelines give a more or less constant improvement, independent of the yield stress and number of cycles to failure. This is in contradiction with the results of improvement techniques, which show a larger effect for longer lives (which should result in a less steep slope in the $S_{th.s.}-N_f$ line for improved welds) and high strength steels [64].

By suggesting that the wall thickness effect can more or less be compensated by an improved weld profile, the AWS and API attribute a very large influence to the weld profile. This influence has been heavily disputed by American versus European researchers.

Verification tests on the influence of the weld profile

To verify the influence of the weld profile tests were carried out in the USA [77]. Eighteen specimens were tested with $t=12.7$, 25.4 and 50.8 mm wall thickness and a weld profile as demanded by the AWS. Figure 6 shows the fatigue strength relative to the AWS $X_1 S_{r_{th.s.}} - N_f$ line, plotted against the chord wall thickness. The thin line connects the average results of all tests with $t=12.7$ and $t=50.8$ mm, the thin dashed line connects the average results minus 2 times the standard deviation of all tests with $t=12.7$ and $t=50.8$ mm (the results for $t=25.4$ mm were omitted to show the results in one straight line).

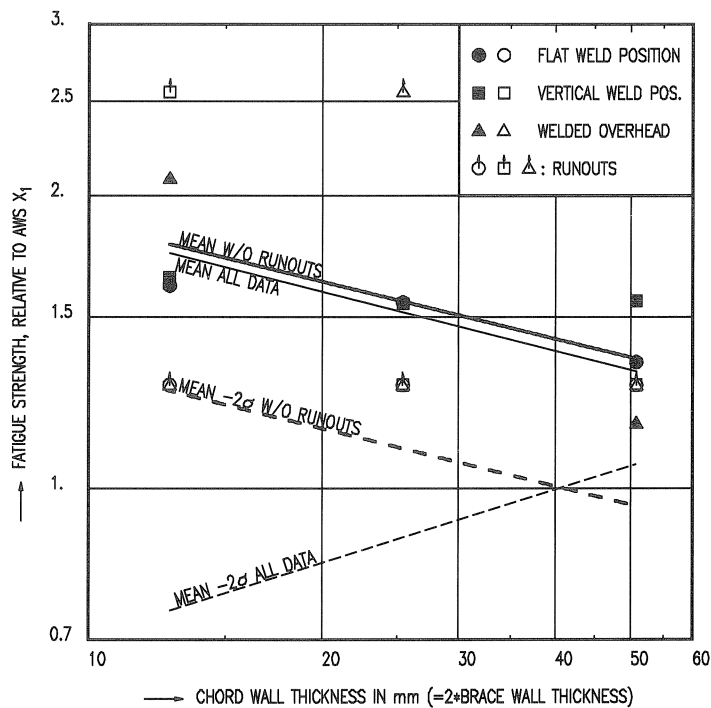


Figure 6. Evaluation of the Rice tests.

By observing the fatigue results it can be seen that the specimens with a smaller wall thickness on average showed a better fatigue behaviour. However, as the scatter is also considerably larger, the characteristic (mean minus 2 times the standard deviation) fatigue strength of thin walled specimens is no better than that of the thick walled specimens. As the designer has to use the characteristic strength, the AWS philosophy seems to be fully supported by the test results.

However, the test results shown include a large number of runouts, shown as open symbols with arrows pointing upwards. The runouts are test specimens which did not fail after $2 \cdot 10^7$ cycles. The conclusion must be that these specimens were tested at a stress level below their fatigue limit and are actually indeterminately better than shown in Figure 6. The exclusion of these results, which are especially low for the thin walled specimens is therefore necessary to obtain valid results. The thick line in Figure 6 connects the average results of the test results after exclusion of runouts with $t=12.7$ and $t=50.8$ mm, the dashed thick line connects the average results minus 2 times the standard deviation of the test results after exclusion of runouts with $t=12.7$ and $t=50.8$ mm.

In this way, a clear thickness effect of $t^{-0.2}$ is observed and claims on the influence of the weld profile do not seem to find any justification by the Rice tests any more.

Sablok [96] reports that the improved weld profiles can compensate for the thickness effect until $t=25$ mm. As a conclusion, it would be better not to couple the thickness effects and the effect of weld profile improvement as in the AWS, but to give independent influence factors.

3 EXPERIMENTAL RESEARCH

3.1 Introduction

The ECSC-CIDECT project [1, 11] which forms the basis of this work consisted of experiments on axially loaded X- and T-joints, as well as X-joints loaded by an in-plane bending moment.

These experiments consisted of:

- 27 X-joints loaded by an in-plane bending moment on the brace
- 14 X-joints with an axial force on the brace
- 16 T-joints with an axial force on the brace
- 24 K-joints (gap) with axial forces on the braces
(not used in this work)
- 12 K-joints (overlap) with axial forces on the braces
(not used in this work)

The experimental part of the additional CIDECT programme [19] consisted of:

- 4 T-joints loaded by an in-plane bending moment on the brace.

The results from CIDECT programme 7H "The low cycle fatigue behaviour of axially loaded T-joints between rectangular hollow sections" [17] were also used:

- 8 T-joints with an axial force on the brace

Other T-joints, loaded by random loading [18] were not used in this report.

Table 1 gives an overview of the experiments used in this work. It also contains the work carried out on K-joints for the ECSC-CIDECT project.

The primary reason for experimentation is to determine fatigue data for the joints from constant amplitude fatigue testing at two different stress ranges ($S_{r.h.s.}$), to use for classification according to EC3 (see Chapter 7) and to obtain reliable $S_{r.h.s.}-N_f$ (or $\epsilon_{r.h.s.}-N_f$) lines for square hollow section joints.

3.2 Set up of experiments

Material and welding method used for the test specimens

Hot finished hollow sections with steel grade Fe430D and Fe430B, in accordance with Euronorm 25-72, are used for the specimens.

All test specimens are welded with rutile electrodes (trade name OMNIA) in accordance with NEN 1062 (ERa 112), NBN F31-001 (E43-2R), ASME SFA-5.1 (EE6013), DIN 1913 (E43 22R(C)3), ISO 2560 (E432R12) and BS 639 (E43 22R). Fillet welds are provided at the joints for all brace wall thicknesses below 8 mm and butt welds for 8 mm and above. The fillet welds are carried out in 3 runs and the butt welds in 4 runs.

Figure 7 shows the welding details and welding sequences used for the test specimens. Note that for X-joints with a bending moment in the brace nearly all specimens (except the four specimens of series X1B) had a welding sequence starting and ending at the corners of the brace and not as for the rest of the specimens.

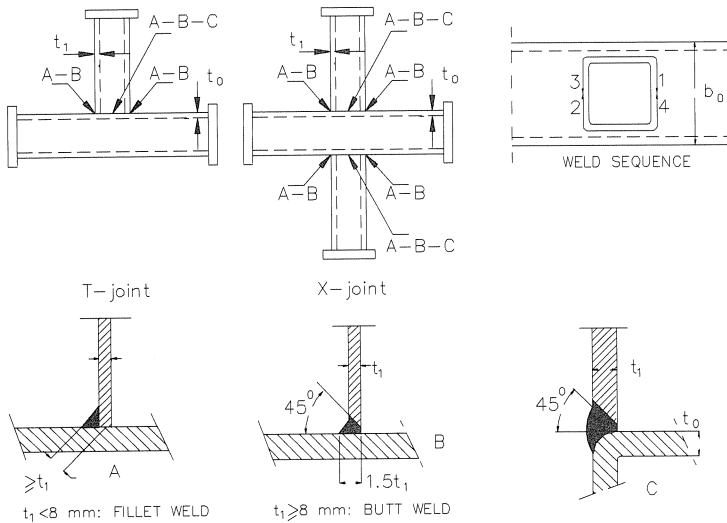


Figure 7. Recommended welding details and weld sequence.

Test set-up

Figure 8 shows the test rig used for X-joints that are loaded by axial force.

Figures 9 and 10 show the test rigs used for T-joints loaded by in-plane bending moment and axial force.

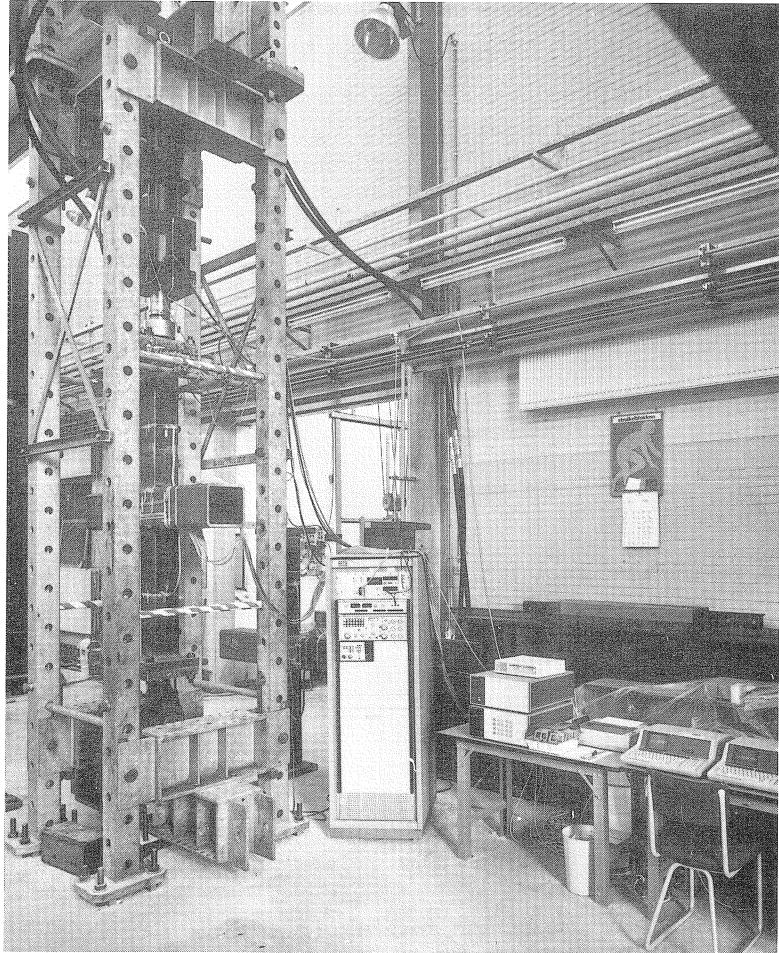


Figure 8. Test rig used for axially loaded X-joints.

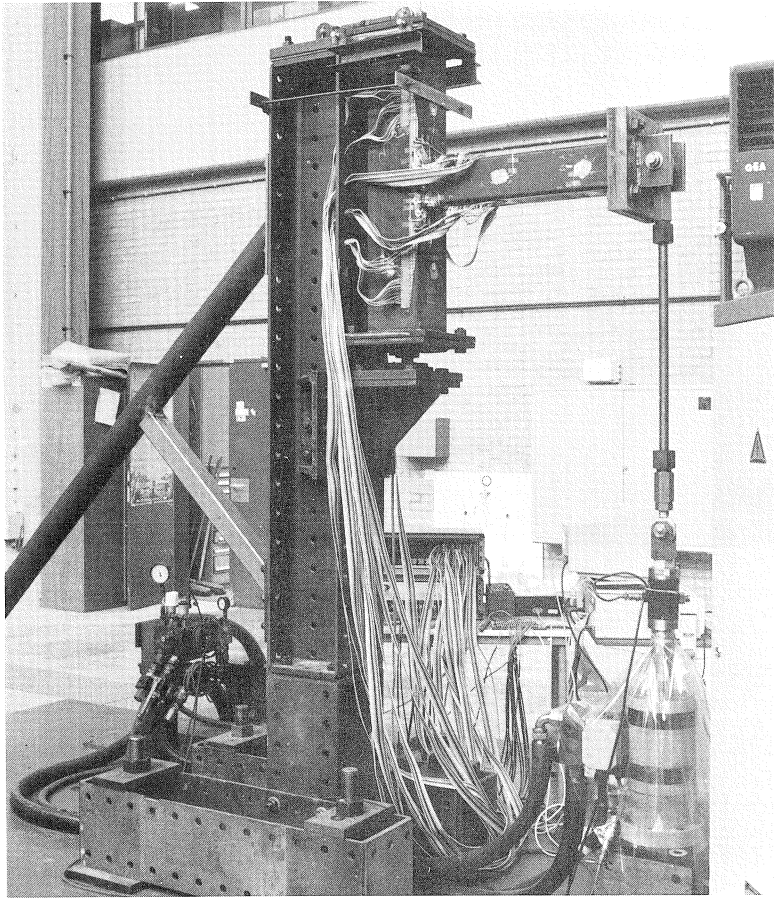


Figure 9. Test rig used for T-joints loaded by an in-plane bending moment.

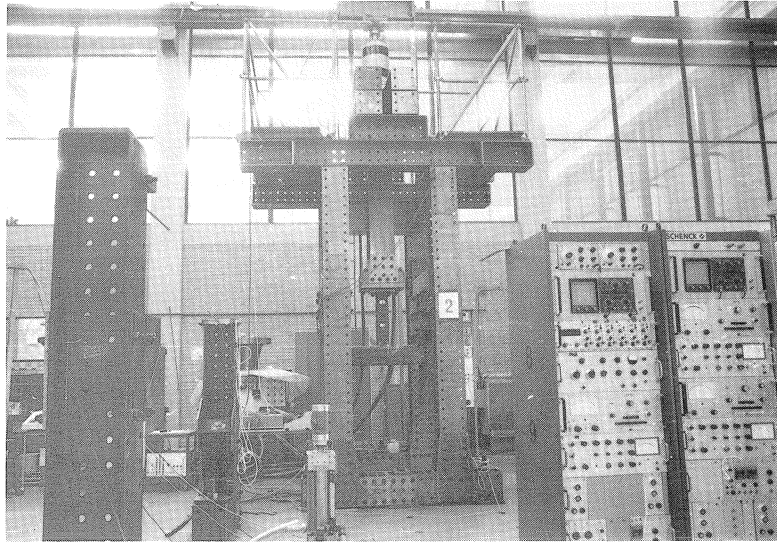


Figure 10. Test rig used for axially loaded T-joints.

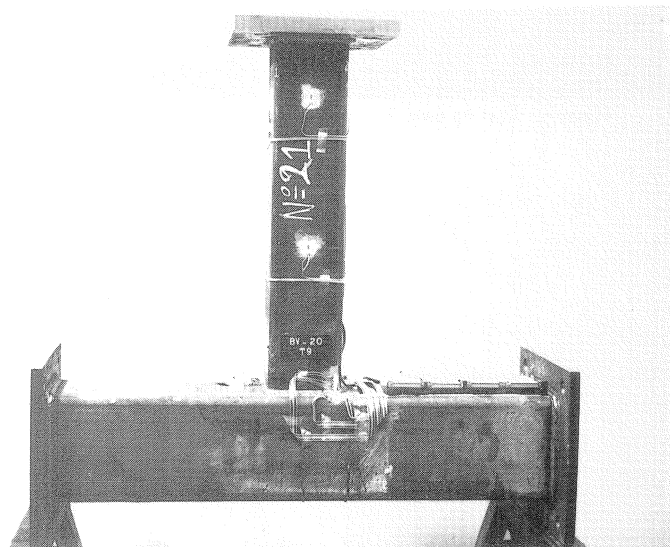


Figure 11. Test specimen T9.

Test specimens

The length of the members is chosen such that the strains to be measured were not influenced by the end conditions. The measurements had to take place at about 2 to 2.5 b from any end conditions. Therefore, the length of the chords was taken to be 2.5 b from the intersection of brace and chord, resulting in $l_0 = 6 \cdot b_0$. In the braces the nominal strains had to be measured at about 2.5 b_1 from the intersection of brace and chord and also 2.5 b_1 from the end plates, determining the length of the brace $l_1 = 5 \cdot b_1$. The geometry of the members and welds as well as material properties of the joints used for the experiments is summarized in Tables 2 (X-joints) and 3 (T-joints). A typical test specimen is shown in Figures 11 and 12.

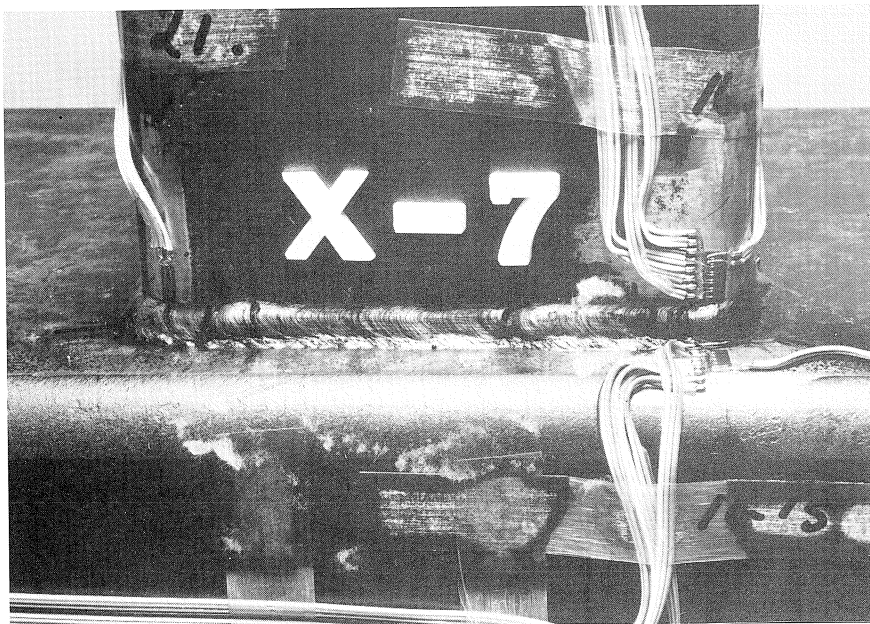


Figure 12. Detail of test specimen X7, showing the strain gauges.

Table 2. Measured dimensions and mechanical properties of X-joints (Delft)

test no.	measured dimensions of the test specimens		wall thickness in corner		projected length of radius		projected length of weld along		cross sectional area		yield ² stress		ultimate ³ stress		ultimate ³ elongation	
	chord	brace	chord	brace	chord	brace	chord	brace	chord	brace	chord	brace	chord	brace	chord	brace
	$b_0 \cdot b_0 \cdot t_0$	$b_1 \cdot h_1 \cdot x_1 \cdot t_1$	t_0	t_1	r_0	r_1	w_0	w_1	A_0	A_1	σ_{y0}	σ_{y1}	σ_{u0}	σ_{u1}	ϵ_{u0}	ϵ_{u1}
X-JOINTS LOADED BY AN AXIAL FORCE ON THE BRACE																
X1	101.0x101.0x 6.1	⁴ 70.0x 70.0x 4.2	7.57	5.25	6.24	4.04	5.30	4.25	2250	1099	341	284	467	372	35	40
X2	101.0x101.0x 6.1	⁴ 70.0x 70.0x 4.2					6.30	5.70								
X3	101.0x101.0x 6.1	⁴ 70.0x 70.0x 4.2					6.33	5.62								
X4	101.0x101.0x 6.1	⁴ 70.0x 70.0x 4.2					6.32	5.83								
X5	200.6x200.6x12.6	139.8x139.8x 7.8	15.03	9.48	15.04	10.15	4.98	9.75	9320	4032	324	285	466	421	33	40
X6	200.6x200.6x12.6	139.8x139.8x 7.8					5.84	10.20								
X7	200.6x200.6x12.6	139.8x139.8x 7.8					4.65	9.10								
X8	201.1x201.1x12.7	139.8x139.8x 7.8	14.60		15.50		4.79	9.88	9370		314		459		37	
X9	259.2x259.2x17.0	180.5x180.5x10.6	20.10	11.80	22.50	17.16	4.23	12.00	16085	7017	³ 241	295	403	486	28	31
X10	259.2x259.2x17.0	180.5x180.5x10.6					5.04	11.56								
X11	259.2x259.2x17.0	180.5x180.5x10.6					4.69	12.14								
X12	259.2x259.2x17.0	180.5x180.5x10.6					4.42	12.36								
X20	201.1x201.1x 8.0	⁴ 80.0x 80.0x 4.1	9.24	4.84	11.45	4.58	6.42	6.54	6005	1237	309	351	450	483	32	33
X38	199.7x199.7x16.2	201.1x201.1x 8.0	19.60	9.33	21.25	11.50	³ 5.25	10.13	12020	6005	336	309	510	450	34	32
							1.56	8.6/2.1								

All properties in N and mm (ϵ in %).

¹ The dimensions and mechanical properties were based on measured dimensions and the mechanical properties for each delivered tube length.

² The joints which were used for the calibration of the FE model were also measured near the joint.

³ Stub column tests.

⁴ Tensile tests (dp0).

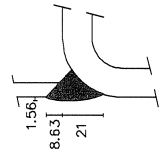
⁵ Test specimens with a nominal $t_1 < 8$ mm were fillet welded, the other specimens had a butt weld.

⁶ For specimens with $\beta = 1.0$, w_1 and w_0 were measured at the side of the brace but also at the front of the brace (this is always a butt weld).

⁷ The length of the weld // brace (upper-lower part) and t_1 brace (exclusive the wall thickness of the brace) respectively. (see figure below)

All X-joints loaded by an in-plane bending moment, with the exception of series X1B, were welded starting and ending in the corners, which is known to adversely affect the fatigue behaviour. Therefore the results must be interpreted with care.

The weld of specimens T22 to T24 was not measured, therefore the results of T21 were applied.



test no.	measured dimensions of the test specimens		wall thickness in corner		projected length of radius		projected length of weld along		cross sectional area		yield ² stress		ultimate ¹ stress		ultimate ³ elongation	
	chord	brace	chord	brace	chord	brace	chord	brace	chord	brace	chord	brace	chord	brace	chord	brace
	$b_0 \times b_0 \times t_0$	$b_1 \times h_1 \times t_1$	t_9	t_{13}	r_0	r_{11}	w_0	w_1	A_0	A_1	σ_{y_0}	σ_{y_1}	σ_{u_0}	σ_{u_1}	ε_{u_0}	ε_{u_1}
X-JOINTS LOADED BY AN IN-PLANE BENDING MOMENT ON THE BRACE																
⁶ X1Aa	100 x100 x 7.8	⁴ 100 x100 x 3.7	9.42	4.49	-	-	5	5	-	-	265	313	417	425	34.5	32.6
⁶ X1Ab	100 x100 x 7.8	⁴ 100 x100 x 3.7	-	-	-	-	-	-	-	-	-	-	-	-	-	-
⁶ X1Ac	100 x100 x 7.8	⁴ 100 x100 x 3.7	-	-	-	-	-	-	-	-	-	-	-	-	-	-
⁶ X1Ad	100 x100 x 7.8	⁴ 100 x100 x 3.7	-	-	-	-	-	-	-	-	-	-	-	-	-	-
⁶ X1Ba	100 x100 x 7.8	⁴ 100 x100 x 3.7	-	-	-	-	-	-	-	-	-	-	-	-	-	-
⁶ X1Bb	100 x100 x 7.8	⁴ 100 x100 x 3.7	-	-	-	-	-	-	-	-	-	-	-	-	-	-
⁶ X1Bc	100 x100 x 7.8	⁴ 100 x100 x 3.7	-	-	-	-	-	-	-	-	-	-	-	-	-	-
⁶ X1Bd	100 x100 x 7.8	⁴ 100 x100 x 3.7	-	-	-	-	-	-	-	-	-	-	-	-	-	-
⁶ X2a	100 x100 x 6.1	⁴ 100 x100 x 3.9	6.75	5.10	-	-	8	6	-	-	252	313	432	425	34.0	32.6
⁶ X2b	100 x100 x 6.1	⁴ 100 x100 x 3.9	-	-	-	-	-	-	-	-	-	-	-	-	-	-
⁶ X2c	100 x100 x 6.1	⁴ 100 x100 x 3.9	-	-	-	-	-	-	-	-	-	-	-	-	-	-
⁶ X2d	100 x100 x 6.1	⁴ 100 x100 x 3.9	-	-	-	-	-	-	-	-	-	-	-	-	-	-
⁶ X3a	100 x100 x 3.9	⁴ 100 x100 x 3.9	5.13	5.23	-	-	6	6	-	-	313	313	425	425	32.6	32.6
⁶ X3b	100 x100 x 3.9	⁴ 100 x100 x 3.9	-	-	-	-	-	-	-	-	-	-	-	-	-	-
⁶ X3c	100 x100 x 3.9	⁴ 100 x100 x 3.9	-	-	-	-	-	-	-	-	-	-	-	-	-	-
⁶ X3d	100 x100 x 3.9	⁴ 100 x100 x 3.9	-	-	-	-	-	-	-	-	-	-	-	-	-	-
⁶ X4a	100 x100 x 8.0	⁴ 70 x 70 x 3.7	9.42	3.95	-	-	6	6	-	-	265	272	417	423	34.5	33.2
⁶ X4b	100 x100 x 8.0	⁴ 70 x 70 x 3.7	-	-	-	-	-	-	-	-	-	-	-	-	-	-
⁶ X4c	100 x100 x 8.0	⁴ 70 x 70 x 3.7	-	-	-	-	-	-	-	-	-	-	-	-	-	-
⁶ X4d	100 x100 x 8.0	⁴ 70 x 70 x 3.7	-	-	-	-	-	-	-	-	-	-	-	-	-	-
⁶ X4e	100 x100 x 8.0	⁴ 70 x 70 x 3.7	-	-	-	-	-	-	-	-	-	-	-	-	-	-
⁶ X4f	100 x100 x 8.0	⁴ 70 x 70 x 3.7	-	-	-	-	-	-	-	-	-	-	-	-	-	-
⁶ X4g	100 x100 x 8.0	⁴ 70 x 70 x 3.7	-	-	-	-	-	-	-	-	-	-	-	-	-	-
⁶ X5a	100 x100 x 3.8	⁴ 70 x 70 x 3.6	5.20	3.89	-	-	5	5	-	-	313	272	425	423	32.6	33.2
⁶ X5b	100 x100 x 3.8	⁴ 70 x 70 x 3.6	-	-	-	-	-	-	-	-	-	-	-	-	-	-
⁶ X5c	100 x100 x 3.8	⁴ 70 x 70 x 3.6	-	-	-	-	-	-	-	-	-	-	-	-	-	-
⁶ X5d	100 x100 x 3.8	⁴ 70 x 70 x 3.6	-	-	-	-	-	-	-	-	-	-	-	-	-	-

Table 3. Measured dimensions and mechanical properties of T-joints (Delft)

test no.	measured dimensions of the test specimens		wall thickness in corner		projected length of corner radius		projected length of weld along		cross sectional area		yield ² stress		ultimate ³ stress		ultimate ³ elongation	
	chord	brace	chord	brace	chord	brace	chord	brace	chord	brace	chord	brace	chord	brace	chord	brace
	$b_0 \times b_0 \times t_0$	$b_1 \times h_1 \times t_1$	t_0	t_1	r_0	r_1	w_0	w_1	A_0	A_1	σ_y	σ_y	σ_u	σ_u	ϵ_u	ϵ_u
T-JOINTS LOADED BY AN AXIAL FORCE ON THE BRACE																
T1	200.7x200.7x12.8	⁴ 140.0x140.0x 5.0	14.9	6.0	15.44	5.98	6.60	6.30	9059	2595	333	310	467	437	35	42
T2	200.7x200.7x12.8	⁴ 140.0x140.0x 5.0					7.12	7.12								
T3	200.7x200.7x12.8	⁴ 140.0x140.0x 5.0					7.04	6.39								
T4	200.7x200.7x12.8	⁴ 140.0x140.0x 5.0					6.05	9.86								
T5	200.6x200.6x12.6	⁴ 140.0x140.0x 5.0	14.8		15.04		10.26	7.68	9320		324		466		33	
T6	199.7x199.7x12.7	⁴ 140.0x140.0x 5.0	15.0		15.31		8.93	7.24	9301		304		450		37	
T7	200.6x200.6x12.6	⁴ 140.0x140.0x 5.0	14.8		15.04		8.58	8.20	9320		324		466		33	
T8	200.7x200.7x12.6	⁴ 139.9x139.9x 5.0				5.85	8.31	8.42		2584	302		419			38
T9	200.6x200.6x12.7	⁴ 140.0x140.0x 7.6	14.9	8.9	15.24	10.11	5.91	9.50	9240	3939	314	296	462	431	33	31
T10	200.6x200.6x12.7	⁴ 140.0x140.0x 7.6					6.20	9.16								
T11	200.6x200.6x12.7	⁴ 140.0x140.0x 7.6					5.65	10.22								
T12	200.6x200.6x12.7	⁴ 140.0x140.0x 7.6					5.19	9.55								
T13	200.7x200.7x12.8	⁴ 140.0x140.0x 7.6			15.44		5.20	9.30	9059		333		467		35	
T14	200.6x200.6x12.7	⁴ 140.0x140.0x 7.6			15.24		6.14	9.33	9240		314		462		33	
T15	200.7x200.7x12.8	⁴ 140.0x140.0x 7.6			15.44		5.27	9.55	9059		333		467		35	
T16	200.6x200.6x12.7	⁴ 140.0x140.0x 7.6			15.24		5.53	10.14	9240		314		462		33	
T17	199.7x199.7x12.7	⁴ 139.9x139.9x 5.0	15.0	6.0	15.31	5.85	6.90	8.70	9301	2584	304	302	450	419	37	38
T18	199.7x199.7x12.7	⁴ 139.9x139.9x 5.0					7.15	9.90								
T19	200.6x200.6x12.7	⁴ 140 x140 x 5.0	14.9		15.24	5.98	6.54	8.72	9240	2595	314	310	462	437	33	42
T20	200.6x200.6x12.7	⁴ 140 x140 x 5.0					7.59	9.90								
T21	199.7x199.7x12.7	⁴ 140 x140 x 7.6	15.0	8.9	15.31	10.11	9.60	5.64	9301	3939	304	296	450	431	37	39
T22	199.7x199.7x12.7	⁴ 140 x140 x 7.6					⁷ 9.60	⁷ 9.60								
T23	199.7x199.7x12.7	⁴ 140 x140 x 7.6					⁷ 9.60	⁷ 9.60								
T24	199.7x199.7x12.7	⁴ 140 x140 x 7.6					⁷ 9.60	⁷ 9.60								
T-JOINTS LOADED BY AN IN-PLANE BENDING MOMENT ON THE BRACE																
T31	200.7x200.7x12.8	⁴ 140 x140 x 5.0	14.9	6.0	15.44	5.98	10.27	7.90	9059	2595	333	310	467	437	35	42
T32	200.7x200.7x12.8	⁴ 140 x140 x 5.0	14.9	6.0	15.44	5.98	6.19	6.23	9059	2595	333	310	467	437	35	42
T37	199.7x199.7x12.7	⁴ 140 x140 x 7.6	15.0	8.9	15.31	10.11	10.51	5.38	9301	3939	304	296	450	431	37	39
T38	199.7x199.7x12.7	⁴ 139.8x139.8x 7.8	15.0	9.4	15.31	10.15	9.15	5.50	9301	4032	304	285	450	421	37	40

Strain gauges locations

A detail of an instrumented test specimen is shown in Figure 12, whereas the location and numbering of strain gauges is shown as an example in Figure 13. For the X-joints with a bending moment in the brace, strain measurements were carried out for only one specimen per series. The SNCFs obtained in this way are used for all specimens of the series. In the case of specimen T1 and line D of all T-joint specimens, measurements were carried out at one corner only. Other T-joints tested had 5 strain gauges as a strip in one corner plus 1 strain gauge in one or three other corners, on which mean values or maximum values of the SNCF were based by simply scaling the determined values of SNCF to the ratios of the strains found at the same distance to the weld toe of the four corners.

Strain measurements

Prior to the fatigue testing of all joints, strains are measured at preselected measurement lines where peak strains are known to occur (see Figure 4). Strain gauge chains are placed at these locations to fall sufficiently within the extrapolation limits (see Chapter 2.5). By means of extrapolation of the measured values, the strain concentration factors (SNCF) at the weld toe on the chord and brace were determined. In most cases, 4 test specimens with the same geometry and dimensions are used for the fatigue tests, a pair at two different stress ranges ($S_{h.s.}$). Measurements of strain and determination of SNCF are also carried out for all these specimens. Where possible, the SNCF values per measurement line (experimental measurements) are recorded for 3 cases:

- At the corner where the first crack occurs during fatigue testing (SNCF_{crack loc.})
- At the corner where the maximum SNCF distribution occurs (SNCF_{max})
- For the average SNCF distribution at the corners (SNCF_{average}).

At an earlier stage [16, 90] a choice was made to use the experimental results obtained for crack location. However, the experimental results were not in all cases recorded at the corner where crack initiation occurred. Also, in the majority of cases, the crack location also gave the maximum values and where this was not the case, the difference was less than 10% in virtually all cases. Therefore, only maximum values are used and presented in this work. However, for calibration of the FE model, the average SNCFs at the corners of the joints were used, rather than the maximum SNCF, since the geometry of the numerical model used for calibration is also based upon average dimensions measured at all corners of the joint.

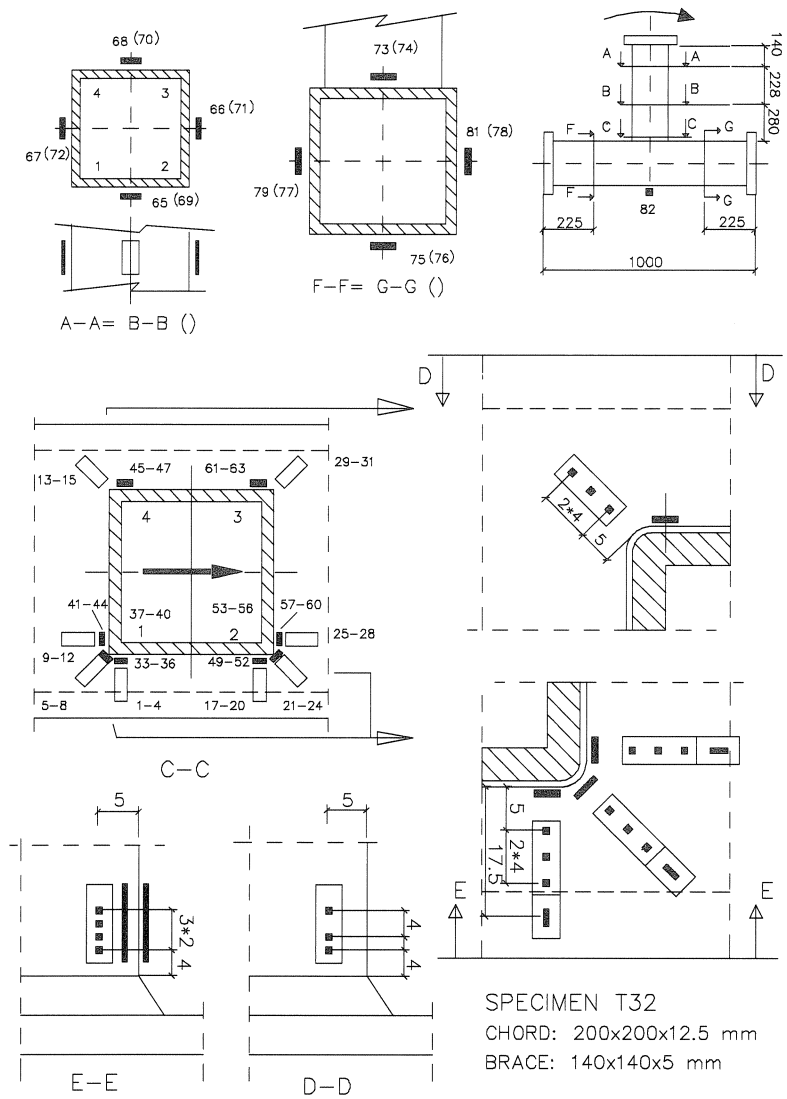


Figure 13. Location of strain gauges.

Selection of test series

Besides providing data for the establishment of $S_{th.s.}-N_f$ lines and a comparison for the numerical model, the test series were carefully selected to provide information on other subjects as well.

- The stress ratio (R) is generally chosen for all tests as $R = +0.1$. However, $R = +0.5$ is also used for some T-joints (see Table 4), in order to determine the influence of R .
- The influence of τ is studied by 2 series of axially loaded T-joints with the same β (0.7) and 2γ (16) but with $\tau=0.4$ and $\tau=0.64$ respectively. The two series are T1 to T8 with $t_1=5$ mm and fillet welds, and T9 to T16, which had $t_1=8$ mm and butt welds.
- The influence of the wall thickness (size) was studied for axially loaded X-joints. The axially loaded X-joints consist of three series with various dimensions for the chord and brace but the same non-dimensional parameters $2\gamma=16$, $\beta=0.7$ and $\tau=0.63$. In this way, the size effect ($b_0=100, 200$ and 260 mm for tests X1 to X4, X5 to X8 and X9 to X12 respectively) could be investigated. In this work, the size effect is determined by analysing all valid experimental data, as presented in Chapter 7.
- As all other axially loaded test specimens had a width ratio $\beta = 0.7$, it was decided at a later stage to add two axially loaded test specimens X20 and X38 with β (2γ) values of 0.4 (25) and 1.0 (12.5) respectively, providing a basis for comparison with the numerical work over a range of parameters in β and 2γ .
- For the X-joints with a bending moment in the brace, t_0 was varied for the series X1 to X3, thus varying both γ and τ simultaneously. The series X1 versus X4, and X3 versus X5 provide information about the influence of β (1.0 versus 0.7).
- Because all X-joints with a bending moment in the brace (except the four specimens of series X1B) had a welding sequence starting and ending at the corners of the brace, the effect of the weld sequence on the fatigue strength of the joints could also be studied.

Table 4. Summary of the test results and numerically determined SCFs used for the $S_{n.s.}$ - N_f lines (Delft)

no.	non-dim. parameters			R	ϵ_{nom} µm/m	N_{ini}	N_f	t_{cr} (mm)	SNCF ¹ measured		SCF ² formulae		Remarks (see below table)							
	β	2γ	τ						lin.	quad.	lin.	quad.	F	B	C	N	W	R	O	
AXIALLY LOADED X-JOINTS																				
X1	0.70	15.9	0.63	0.1	252	13000	105000	4.0	5.60	8.17	6.51	7.28	1	1	0	0	0	0	0	0
X2	0.70	15.9	0.63	0.1	252	2500	150000	4.0	7.30	9.00	6.51	7.28	1	1	0	0	0	0	0	0
X3	0.70	15.9	0.63	0.1	114	571000	9000000	4.0	6.84	8.87	6.51	7.28	1	1	0	0	0	1	0	0
X4	0.70	15.9	0.63	0.1	141	260000	3270000	4.0	6.00	8.47	6.51	7.28	1	1	0	0	0	0	0	0
X5	0.70	16.0	0.64	0.1	212	2500	280000	12.5	3.80	5.18	5.53	6.41	0	0	0	0	0	0	0	0
X6	0.70	16.0	0.64	0.1	212	30000	310000	12.5	3.00	4.11	5.53	6.41	0	0	0	0	0	0	0	0
X7	0.70	16.0	0.64	0.1	143	70000	665000	12.5	4.50	5.51	5.53	6.41	0	0	0	0	0	0	0	0
X8	0.70	16.0	0.64	0.1	143	140000	1400000	12.5	4.15	5.15	5.53	6.41	0	0	0	0	0	0	0	1
X9	0.70	16.3	0.63	0.1	257	5000	100000	16.0	3.05	4.60	5.67	6.58	0	0	0	0	0	0	0	0
X10	0.70	16.3	0.63	0.1	257	2500	90000	16.0	3.35	4.88	5.67	6.58	0	0	0	0	0	0	0	0
X11	0.70	16.3	0.63	0.1	140	25000	790000	16.0	3.90	5.19	5.67	6.58	0	0	0	0	0	0	1	0
X12	0.70	16.3	0.63	0.1	140	30000	330000	16.0	4.28	5.91	5.67	6.58	0	0	0	0	0	0	0	0
X20	0.40	25.0	0.50	0.1	277	2000	18300	8.0	13.00	14.80	17.32	18.48	1	0	0	0	0	0	0	0
X38 ³	1.00	12.5	0.50	-	-	-	-	-	-	-	-	-	0	-	0	1	-	-	-	-
AXIALLY LOADED T-JOINTS																				
T1	0.70	16.0	0.40	0.1	167	419000	2046000	5.0	6.47	6.92	6.56	7.33	1	1	0	0	1	0	0	0
T2	0.70	16.0	0.40	0.1	127	867000	4515000	5.0	6.35	6.94	6.56	7.33	1	1	0	0	1	0	0	0
T3	0.70	16.0	0.40	0.1	232	91000	457000	5.0	7.30	8.12	6.56	7.33	1	1	0	0	1	0	0	0
T4	0.70	16.0	0.40	0.1	128	1400000	9800000	12.5	2.64	2.61	4.93	5.74	1	0	0	0	0	1	0	0
T5	0.70	16.0	0.40	0.5	131	380000	2942000	5.0	7.69	9.26	6.56	7.33	1	1	0	0	0	0	0	0
T6	0.70	16.0	0.40	0.1	178	181000	686000	5.0	7.06	7.71	6.56	7.33	1	1	0	0	0	0	0	0
T7	0.70	16.0	0.40	0.5	181	76000	550000	5.0	6.48	7.09	6.56	7.33	1	1	0	0	0	0	0	0
T8	0.70	16.0	0.40	0.5	238	23000	209000	5.0	7.46	8.46	6.56	7.33	1	1	0	0	0	0	0	0
T9	0.70	16.0	0.64	0.1	275	25000	185000	12.5	4.49	5.51	7.39	8.57	0	0	0	0	0	0	0	0
T10	0.70	16.0	0.64	0.1	151	129000	1250000	12.5	4.43	5.67	7.39	8.57	0	0	0	0	0	0	0	0
T11	0.70	16.0	0.64	0.1	122	197000	2062000	12.5	4.31	5.51	7.39	8.57	0	0	0	0	0	0	0	0
T12	0.70	16.0	0.64	0.1	83	1211000	11630000	12.5	4.42	5.34	7.39	8.57	0	0	0	0	0	0	0	0
T13	0.70	16.0	0.64	0.5	154	185000	716000	12.5	4.26	5.49	7.39	8.57	0	0	0	0	0	0	0	0
T14	0.70	16.0	0.64	0.5	118	261000	2146000	12.5	4.15	5.87	7.39	8.57	0	0	0	0	0	0	0	0
T15	0.70	16.0	0.64	0.5	83	543000	5390000	12.5	5.17	6.49	7.39	8.57	0	0	0	0	0	0	0	0
T16	0.70	16.0	0.64	0.5	156	40000	838000	12.5	4.73	5.88	7.39	8.57	0	0	0	0	0	0	0	0
T17	0.70	16.0	0.40	0.1	861	300	1300	5.0	8.38	9.55	6.56	7.33	1	1	0	0	0	0	0	0
T18	0.70	16.0	0.40	0.1	709	300	3500	5.0	7.99	9.18	6.56	7.33	1	1	0	0	0	0	0	0
T19	0.70	16.0	0.40	0.5	525	900	7500	5.0	7.95	9.09	6.56	7.33	1	1	0	0	0	0	0	0
T20	0.70	16.0	0.40	0.5	485	2000	11000	5.0	7.82	8.77	6.56	7.33	1	1	0	0	0	0	0	0
T21	0.70	16.0	0.64	0.1	446	1000	74000	12.5	5.82	6.45	7.39	8.57	0	0	0	0	0	0	0	1
T22	0.70	16.0	0.64	0.1	560	1200	7000	12.5	5.73	7.08	7.39	8.57	0	0	0	0	0	0	0	0
T23	0.70	16.0	0.64	0.5	312	5600	47000	12.5	4.57	6.12	7.39	8.57	0	0	0	0	0	0	0	0
T24	0.70	16.0	0.64	0.5	357	3300	38000	12.5	4.92	5.71	7.39	8.57	0	0	0	0	0	0	0	0
T-JOINTS LOADED BY AN IN-PLANE BENDING MOMENT ON THE BRACE																				
T31	0.70	16.0	0.40	0.1	495	6000	71000	5.0	5.11	5.60	4.55	5.06	1	1	0	0	0	0	0	0
T32	0.70	16.0	0.40	0.1	370	40000	684000	5.0	3.95	4.24	4.55	5.06	1	1	0	0	0	0	0	0
T37	0.70	16.0	0.64	0.1	296	78000	648000	12.5	2.45	3.24	4.57	5.13	0	0	0	0	0	0	0	0
T38	0.70	16.0	0.64	0.1	203	158000	2201000	12.5	2.80	3.28	4.57	5.13	0	0	0	0	0	0	0	0

Table 4. Summary of the test results and numerically determined SCFs used for the $S_{h.s.}$ - N_f lines (Karlsruhe)																			
no.	non-dim. parameters			R	ϵ_{nom} $\mu\text{m/m}$	N_{ini}	N_f	t_{cr} (mm)	SNCF ¹ measured		SCF ² formulae		Remarks (see below table)						
	β	2γ	τ						lin.	quad.	lin.	quad.	F	B	C	N	W	R	O
X-JOINTS LOADED BY AN IN-PLANE BENDING MOMENT ON THE BRACE																			
⁴ X1Aa	1.00	12.5	0.50	0.1	557	-	134600	4.0	4.17	4.76	1.96	2.01	1	1	1	1	0	0	0
⁴ X1Ab	1.00	12.5	0.50	0.1	428	-	329600	4.0	4.17	4.76	1.96	2.01	1	1	1	1	0	0	0
⁴ X1Ac	1.00	12.5	0.50	0.1	343	-	735200	4.0	4.17	4.76	1.96	2.01	1	1	1	1	1	0	0
⁴ X1Ad	1.00	12.5	0.50	0.1	257	-	2960400	4.0	4.17	4.76	1.96	2.01	1	1	1	1	1	0	0
X1Ba	1.00	12.5	0.50	0.1	686	-	193600	4.0	4.17	4.76	1.96	2.01	1	1	0	1	1	0	0
X1Bb	1.00	12.5	0.50	0.1	428	-	1208000	4.0	4.17	4.76	1.96	2.01	1	1	0	0	0	0	0
X1Bc	1.00	12.5	0.50	0.1	514	-	2612500	4.0	4.17	4.76	1.96	2.01	1	1	0	1	1	0	0
X1Bd	1.00	12.5	0.50	0.1	300	-	10636400	4.0	4.17	4.76	1.96	2.01	1	1	0	1	0	1	0
⁴ X2a	1.00	15.9	0.63	0.1	557	-	92500	4.0	2.61	3.23	2.26	2.32	1	1	1	1	1	0	0
⁴ X2b	1.00	15.9	0.63	0.1	428	-	283300	4.0	2.61	3.23	2.26	2.32	1	1	1	1	0	0	0
⁴ X2c	1.00	15.9	0.63	0.1	300	-	1498800	4.0	2.61	3.23	2.26	2.32	1	1	1	1	1	0	0
⁴ X2d	1.00	15.9	0.63	0.1	257	-	1518300	4.0	2.61	3.23	2.26	2.32	1	1	1	0	1	0	0
⁴ X3a	1.00	25.0	1.00	0.1	557	-	95800	4.0	3.33	3.82	2.94	3.03	1	1	1	1	1	0	0
⁴ X3b	1.00	25.0	1.00	0.1	428	-	293700	4.0	3.33	3.82	2.94	3.03	1	1	1	1	1	0	0
⁴ X3c	1.00	25.0	1.00	0.1	343	-	503400	4.0	3.33	3.82	2.94	3.03	1	1	1	0	1	0	0
⁴ X3d	1.00	25.0	1.00	0.1	257	-	4556700	4.0	3.33	3.82	2.94	3.03	1	1	1	1	1	0	0
⁴ X4a	0.70	12.5	0.50	0.1	729	-	43900	4.0	2.33	2.71	3.44	3.79	1	1	1	0	0	0	0
⁴ X4b	0.70	12.5	0.50	0.1	428	-	238600	4.0	2.33	2.71	3.44	3.79	1	1	1	1	0	0	0
⁴ X4c	0.70	12.5	0.50	0.1	515	-	272500	4.0	2.33	2.71	3.44	3.79	1	1	1	1	0	0	0
⁴ X4d	0.70	12.5	0.50	0.1	386	-	607100	4.0	2.33	2.71	3.44	3.79	1	1	1	1	0	0	0
⁴ X4e	0.70	12.5	0.50	0.1	343	-	644800	4.0	2.33	2.71	3.44	3.79	1	1	1	1	0	0	0
⁴ X4f	0.70	12.5	0.50	0.1	300	-	2115200	4.0	2.33	2.71	3.44	3.79	1	1	1	1	0	1	0
⁴ X4g	0.70	12.5	0.50	0.1	257	-	2492600	4.0	2.33	2.71	3.44	3.79	1	1	1	1	0	1	0
⁴ X5a	0.70	25.0	1.00	0.1	214	-	167900	4.0	5.79	7.03	14.99	18.01	1	0	1	0	0	0	0
⁴ X5b	0.70	25.0	1.00	0.1	171	-	216400	4.0	5.79	7.03	14.99	18.01	1	0	1	1	0	0	0
⁴ X5c	0.70	25.0	1.00	0.1	129	-	379100	4.0	5.79	7.03	14.99	18.01	1	0	1	1	0	0	0
⁴ X5d	0.70	25.0	1.00	0.1	76	-	2651600	4.0	5.79	7.03	14.99	18.01	1	0	1	1	0	0	0

¹ The hot spot stress for the $S_{h.s.}$ - N_f lines was determined using $S_{h.s.} = 1.1 \cdot E \cdot \text{SNCF} \cdot \epsilon_{nom}$.

² SCF formula taken for the member that failed in the test.

³ Testing of joint X38 was abandoned since the test rig required repeated repair due to the large fatigue strength of the joint.

⁴ All X-joints loaded by an in-plane bending moment, with the exception of series X1B, were welded starting and ending in the corners, which is known to adversely effect the fatigue behaviour. Therefore the results must be interpreted with care.

Remarks

- F: 1 indicates a fillet weld (all joints with $t_f \geq 8$ mm were butt welded).
B: 1 indicates a brace failure.
C: 1 indicates that welded started and stopped at the corner, often resulting in worse fatigue performance.
N: 1 indicates that no hot spot strains were measured, SNCFs were taken from another specimen in the same series.
W: 1 indicates that the weld itself failed, rather than cracks starting at the weld toe.
R: 1 indicates that the test was stopped before the member had failed completely.
O: 1 indicates that the joint was accidentally overloaded, possible resulting in an improved fatigue performance.

3.3 Test results

Table 4 summarizes the test results for X- and T-joints. In this table, the number of cycles to crack initiation and failure, the nominal strain range, the maximum SNCFs in the member that failed provide adequate information for an evaluation of the test results. $S_{\epsilon_{h.s.}}-N_f$ lines (in fact converted $\epsilon_{h.s.}-N_f$ lines) and a wall thickness correction factor can be determined for the various test series from the results of the fatigue tests and the extrapolated hot spot strain ranges at the weld toes of chord and brace, see Chapter 7. A few other phenomena are covered below.

Sensitivity of SNCFs for small variations in the actual joint geometry

As expected, a scatter exists in the strain distribution along the measurement lines at identical locations and therefore in the SNCFs. In general, this scatter is influenced by small differences in corner radii and weld dimensions (both influences are also studied numerically in Chapter 6) and especially the tapering in wall thickness. The measured thicknesses were found to be ranging from values close to the nominal wall thickness in the middle of the flat parts to sometimes 30% larger thicknesses measured at the corners, so a strong impact on the measured SNCFs is to be expected. Note that the variation in corner radii is absent in circular hollow sections, whereas the variation in wall thickness of circular hollow sections is typically smaller than $\pm 10\%$. Also the variation in weld dimension is larger in the corners of the rectangular hollow sections. The scatter in fatigue strength of joints between rectangular hollow sections can therefore be expected to exceed the scatter for circular sections.

The SNCF values at the weld toe in brace and chord obtained from linear and quadratic extrapolation of the measurements are summarized in Table 5 for the X-joints and Table 6 for the T-joints. The measured SNCFs are sometimes as much as 50% different for different test specimens with the same nominal dimensions and load type. Together with the typical scatter associated with fatigue testing, a large scatter in fatigue strength is to be expected. Comparison between the SNCFs found from parametric formula and measurements such as carried out by Frater [59] should be made with these results in mind.

Weld failures

In the first T-joints tested weld failure was observed (which also occurred for some X-joints with a bending moment in the brace, see Table 4). Therefore, for subsequent specimens T4 to T8, the weld geometry was revised.

Influence of the stress ratio R

In previous investigations by Mang and Zirn [51], a considerable influence of the stress ratio R was observed for thin walled hollow section joints. This influence is also shown in Figures 14 and 15, where the numbers of cycles to failure are plotted against the nominal strains in the brace for axially loaded T-joints (all X-joints were tested for R=0.1 only). As can be observed in these figures, the fatigue strength based on nominal strains tends to be higher for R=0.1 than for R=0.5. When the numbers of cycles are plotted against the hot spot strains, as shown in Figures 16 and 17, the influence of R is no longer apparent. Due to the fact that somewhat higher SNCFs were observed for the tests with R=0.5, which was also found by Yura [66] for CHS X-joints, almost no influence is observed for the presentation based on $\epsilon_{t.h.s.}$.

Table 5. maximum SNCFs at the weld toe from measurements of X-joints (Delft)											
test no.	measured dimensions of the test specimens		SNCF linear extrapolation				SNCF quadratic extrapolation				
	chord	brace	chord		brace		chord			brace	
	$b_0xh_0xt_0^{-1}$	$b_1xh_1xt_1^{-1}$	B	C	D	A	E	B	C	D	A
X-JOINTS LOADED BY AN AXIAL FORCE ON THE BRACE											
X1	101.0x101.0x 6.1	² 70.0x 70.0x 4.2	1.65		5.60	2.28			8.17		
X2	101.0x101.0x 6.1	² 70.0x 70.0x 4.2			7.30				9.00		
X3	101.0x101.0x 6.1	² 70.0x 70.0x 4.2			6.84				8.87		
X4	101.0x101.0x 6.1	² 70.0x 70.0x 4.2			6.00				8.47		
X5	200.6x200.6x12.6	139.8x139.8x 7.8	3.80	2.95	1.13	7.32	5.18	4.56	1.53	8.98	
X6	200.6x200.6x12.6	139.8x139.8x 7.8	3.00		7.60	4.11			8.43		
X7	200.6x200.6x12.6	139.8x139.8x 7.8	4.50		6.40	5.51			6.65		
X8	201.1x201.1x12.7	139.8x139.8x 7.8	4.15		6.80	5.15			7.68		
X9	259.2x259.2x17.0	180.5x180.5x10.6	3.05	1.15		6.40	4.60	1.39		7.25	
X10	259.2x259.2x17.0	180.5x180.5x10.6	3.35		6.40	4.88			6.71		
X11	259.2x259.2x17.0	180.5x180.5x10.6	3.90		³ 6.40	5.19			³ 6.98		
X12	259.2x259.2x17.0	180.5x180.5x10.6	4.28		³ 6.40	5.91			³ 6.98		
X20	201.1x201.1x 8.0	² 80.0x 80.0x 4.1	13.00		8.00	14.80			11.40		
X38	199.7x199.7x16.2	201.1x201.1x 8.0	0.88	0.34	2.38	0.97			0.48	2.43	

All dimensions in mm.

¹ The dimensions and mechanical properties were based on measured dimensions and the mechanical properties for each delivered tube length. The joints which were used for the calibration of the FE model were also measured near the joint.

² Test specimens with a nominal $t_1 < 8$ mm were fillet welded, the other specimens had a butt weld.

³ Test specimens X11/X12 and T9/T11 were not measured in the brace, therefore the average of the SNCFs of X9/X10 and T10/T12 was used.

⁴ No strain gauges were used for the determination of the SNCF, instead the values of the measured specimen of each series were used.

⁵ All X-joints loaded by an in-plane bending moment, with the exception of series X1B, were welded starting and ending in the corners, which is known to adversely effect the fatigue behaviour. Therefore the results must be interpreted with care.

test no.	measured dimensions of the test specimens		SNCF linear extrapolation				SNCF quadratic extrapolation					
	chord	brace	chord			brace		chord			brace	
	b ₀ xh ₀ xt ₀	b ₁ xh ₁ xt ₁ ¹	B	C	D	A	E	B	C	D	A	E
X-JOINTS LOADED BY AN IN-PLANE BENDING MOMENT ON THE BRACE												
X1Aa ⁴⁵	100 x100 x 7.8	² 100 x100 x 3.7	0.90		0.52	1.59	4.17	1.04		0.69	2.31	4.76
X1Ab ⁴⁵	100 x100 x 7.8	² 100 x100 x 3.7										
X1Ac ⁴⁵	100 x100 x 7.8	² 100 x100 x 3.7										
X1Ad ⁴⁵	100 x100 x 7.8	² 100 x100 x 3.7										
X1Ba ⁴	100 x100 x 7.8	² 100 x100 x 3.7										
X1Bb	100 x100 x 7.8	² 100 x100 x 3.7										
X1Bc ⁴	100 x100 x 7.8	² 100 x100 x 3.7										
X1Bd ⁴	100 x100 x 7.8	² 100 x100 x 3.7										
X2a ⁴⁵	100 x100 x 6.1	² 100 x100 x 3.9	0.72		0.44	2.04	2.61	0.85		0.51	1.77	3.23
X2b ⁴⁵	100 x100 x 6.1	² 100 x100 x 3.9										
X2c ⁴⁵	100 x100 x 6.1	² 100 x100 x 3.9										
X2d ⁵	100 x100 x 6.1	² 100 x100 x 3.9										
X3a ⁴⁵	100 x100 x 3.9	² 100 x100 x 3.9	2.70		0.40	2.91	3.33	2.95		0.63	3.43	3.82
X3b ⁴⁵	100 x100 x 3.9	² 100 x100 x 3.9										
X3c ⁵	100 x100 x 3.9	² 100 x100 x 3.9										
X3d ⁴⁵	100 x100 x 3.9	² 100 x100 x 3.9										
X4a ⁵	100 x100 x 8.0	² 70 x 70 x 3.7			0.31	2.33	1.46			0.48	2.71	1.56
X4b ⁴⁵	100 x100 x 8.0	² 70 x 70 x 3.7										
X4c ⁴⁵	100 x100 x 8.0	² 70 x 70 x 3.7										
X4d ⁴⁵	100 x100 x 8.0	² 70 x 70 x 3.7										
X4e ⁴⁵	100 x100 x 8.0	² 70 x 70 x 3.7										
X4f ⁴⁵	100 x100 x 8.0	² 70 x 70 x 3.7										
X4g ⁴⁵	100 x100 x 8.0	² 70 x 70 x 3.7										
X5a ⁵	100 x100 x 3.8	² 70 x 70 x 3.6			5.79	7.59	3.65			7.03	11.12	5.64
X5b ⁴⁵	100 x100 x 3.8	² 70 x 70 x 3.6										
X5c ⁴⁵	100 x100 x 3.8	² 70 x 70 x 3.6										
X5d ⁴⁵	100 x100 x 3.8	² 70 x 70 x 3.6										

Table 6. maximum SNCFs at the weld toe from measurements of T-joints (Delft)											
test no.	measured dimensions of the test specimens		SNCF linear extrapolation				SNCF quadratic extrapolation				
	chord	brace	chord			brace		chord			brace
	$b_0 x h_0 x t_0$	$b_1 x h_1 x t_1$ ¹	B	C	D	A	E	B	C	D	A E
T-JOINTS LOADED BY AN AXIAL FORCE ON THE BRACE											
T1	200.7x200.7x12.8	² 140.0x140.0x5.0	0.82	2.35	2.78	6.47		2.18	3.07	3.08	6.92
T2	200.7x200.7x12.8	² 140.0x140.0x5.0		2.36		6.35			3.42		6.94
T3	200.7x200.7x12.8	² 140.0x140.0x5.0		2.33		7.30			2.91		8.12
T4	200.7x200.7x12.8	² 140.0x140.0x5.0	0.42	2.08	2.64	6.99		1.51	2.61	2.56	8.13
T5	200.6x200.6x12.6	² 140.0x140.0x5.0		2.02		7.69			3.27		9.26
T6	199.7x199.7x12.7	² 140.0x140.0x5.0	0.52	2.25		7.06		1.67	2.68		7.71
T7	200.6x200.6x12.6	² 140.0x140.0x5.0		1.86		6.48			2.70		7.09
T8	200.7x200.7x12.6	² 139.9x139.9x5.0		2.41		7.46			3.24		8.46
T9	200.6x200.6x12.7	140.0x140.0x7.6	2.27 ³	4.31	4.49	5.72		3.86 ³	5.51	4.49	6.08
T10	200.6x200.6x12.7	140.0x140.0x7.6	2.47	4.19	4.43	6.41		4.18	5.67	4.47	6.95
T11	200.6x200.6x12.7	140.0x140.0x7.6		³ 4.31					³ 5.51		
T12	200.6x200.6x12.7	140.0x140.0x7.6	2.96	4.42	4.37	7.00		4.00	5.34	5.10	7.77
T13	200.7x200.7x12.8	140.0x140.0x7.6		4.26					5.49		
T14	200.6x200.6x12.7	140.0x140.0x7.6		4.15					5.87		
T15	200.7x200.7x12.8	140.0x140.0x7.6		5.17					6.49		
T16	200.6x200.6x12.7	140.0x140.0x7.6		4.73					5.88		
T17	199.7x199.7x12.7	² 139.9x139.9x5.0		2.05		8.38			2.84		9.55
T18	199.7x199.7x12.7	² 139.9x139.9x5.0		1.83		7.99			2.34		9.18
T19	200.6x200.6x12.7	² 140 x140 x5.0		1.68		7.95			2.13		9.09
T20	200.6x200.6x12.7	² 140 x140 x5.0		2.09		7.82			2.70		8.77
T21	199.7x199.7x12.7	140 x140 x7.6	2.66	5.43	5.82	6.15		3.50	6.22	6.45	6.82
T22	199.7x199.7x12.7	140 x140 x7.6		5.73					7.08		
T23	199.7x199.7x12.7	140 x140 x7.6		4.57					6.12		
T24	199.7x199.7x12.7	140 x140 x7.6		4.92					5.71		
T-JOINTS LOADED BY AN IN-PLANE BENDING MOMENT ON THE BRACE											
T31	200.7x200.7x12.8	² 140 x140 x5.0		0.97		5.11			1.33		5.60
T32	200.7x200.7x12.8	² 140 x140 x5.0	0.23	1.30	1.22	3.95	3.59	0.33	1.67	1.33	4.24 4.21
T37	199.7x199.7x12.7	140 x140 x7.6	1.12	2.45	2.02	4.15	3.70	1.66	3.24	2.28	4.20 4.01
T38	199.7x199.7x12.7	139.8x139.8x7.8		2.80		4.15			3.28		4.49

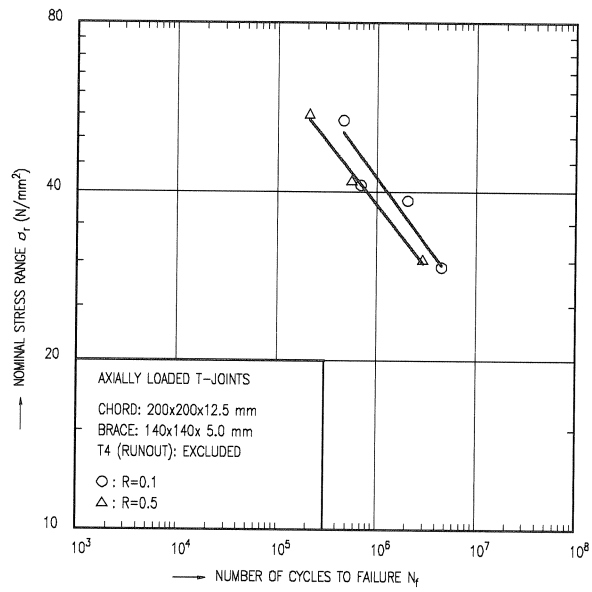


Figure 14. R infl., σ_r , t=5 mm.

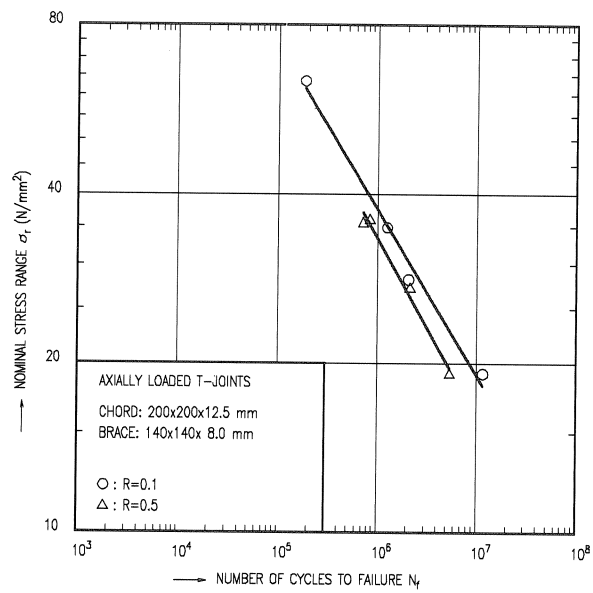


Figure 15. R infl., σ_r , t=12.5 mm.

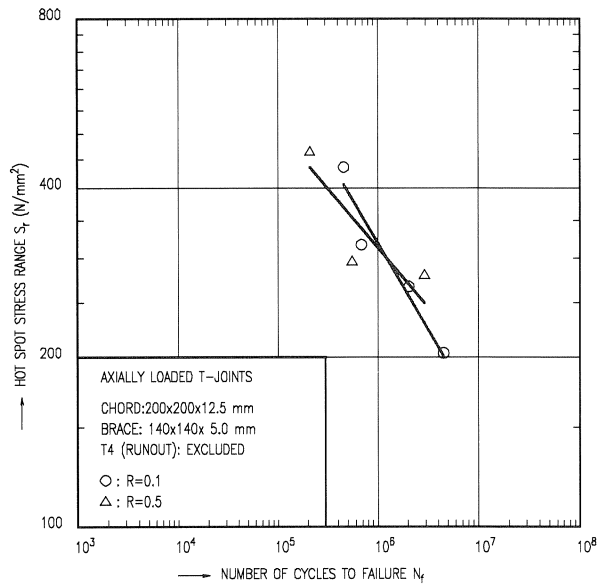


Figure 16. R infl., $S_{h.s.}$, $t=5\text{mm}$.

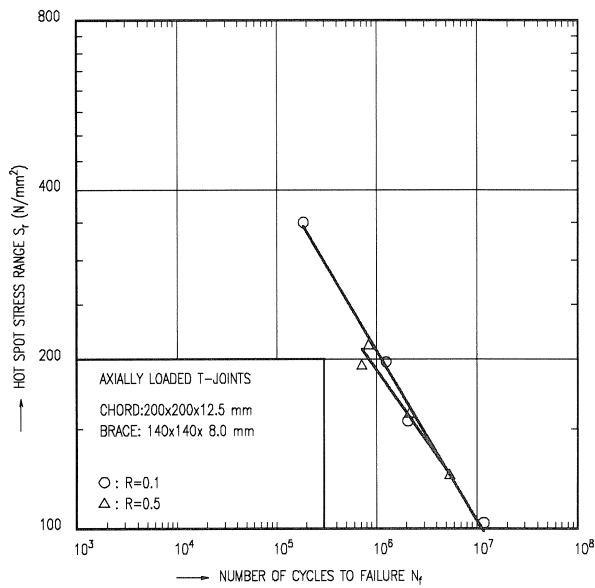


Figure 17. R infl., $S_{h.s.}$, $t=12.5\text{mm}$.

Discussion on the influence of the stress level

Consider the governing quadratically measured SNCF in Table 4 for axially loaded T-joints, which occurs in the brace for $t_1=5$ mm and in the chord for $t_1=8$ mm.

T-joints with $t_1=5$ mm

- R=0.1: the SNCFs range from 6.92 to 8.12 (T1 to T3 and T6).
- R=0.5: the SNCFs range from 7.09 to 9.26 (+11% on average) (T5, T7, T8).
- Low cycle: the SNCFs range from 8.77 to 9.55 (+23% on average) (T17 to T20).

T-joints with $t_1=8$ mm

- R=0.1: the SNCFs range from 5.34 to 5.67 (T9 to T12).
- R=0.5: the SNCFs range from 5.49 to 6.49 (+7% on average) (T13 to T16).
- Low cycle: the SNCFs range from 5.71 to 7.08 (+15% on average) (T21 to T24).

Although the overall scatter tends to cloud the comparison, causing an overlap in SNCF ranges, there is clear evidence for the relation between stress level and SNCF. Note that a dependency on R of the SNCF weakens the hot spot stress philosophy: although the relationship between $S_{h.s.}$ and N_f is maintained, the SNCFs are slightly dependent on the stress level.

A first possible explanation for the effect of the stress range might be local cyclic yielding, which causes a lower stiffness and hence a larger ratio between strain- and load range. The yield strain $\epsilon_y \approx 300/210000 = 1430 \cdot 10^{-6}$ (see Tables 2 and 3). Cyclic yielding would require $\epsilon_{h.s.} = 2860 \cdot 10^{-6}$. Note that in all cases (except for the low cycle tests) in Table 4, $\epsilon_{h.s.} = \epsilon_{nom} \cdot SNCF$ is below this value. Very local stress raisers (see Chapter 2.3) could raise this value to cause cyclic yielding. However, this does not explain the influence of R as R does not influence this strain range. Probably more important is the geometric non-linear behaviour.

Influence of the wall thickness ratio τ

The τ -ratio strongly influences the mechanism of failure. This is because for the same nominal stress in the brace, the nominal stress in the chord increases with increasing t_1 , causing a tendency towards chord failure. The value of τ at which the failure mode changes from brace to chord failure is dependent upon the other geometrical parameters β and 2γ and upon joint type and load case as these factors influence the SNCFs in the members.

Also the thickness effect plays an important role in relation to τ .

All tested specimens, except for X20 and X5 had the maximum measured SNCF in the brace, but for the axially loaded joints where the SNCFs in the chord were close to the values in the brace, chord failure occurred, due to the higher chord wall thickness and consequently lower $\epsilon_{h.s.}$ - N_f curves than for the brace.

For the T-joints with $\tau=0.4$ failure generally occurred in the brace, whereas for $\tau=0.64$ failure occurred in the chord. The only exception was specimen T4 ($\tau=0.4$), which showed crack initiation in the chord. This test was stopped at $N=10^7$, because crack growth was very slow. For X-joints with an axial load in the brace, all tests had a τ value of 0.5 or larger. In general, chord failure occurred, which agrees with the results for T-joints. However, the small specimens X-1 to X-4 with $\tau=0.64$ failed in the brace due to the very high SNCFs in the brace, sometimes as much as 5 times larger as in the chord. Except for X5, all X-joints with a bending moment in the brace had brace failures, even in cases where τ was 1.0. For the series X5 the SNCFs in the brace were larger, even for $\tau=1.0$.

Crack initiation

Table 4 shows that crack initiation begins at an early stage, typically N_{ini} was 0.1 to 0.25 N_f . N_{ini} was not determined for X-joints with a bending moment in the brace. A possible explanation for the large ratio between N_{ini} and N_f is the very steep stress gradient near the corners of the brace: the crack soon reaches areas where the strains are considerably lower, in contrast to for instance axially loaded butt welded plates.

In Figure 18, a cracked specimen is shown. The crack started in the chord at the weld toe and developed through the weld into the brace.

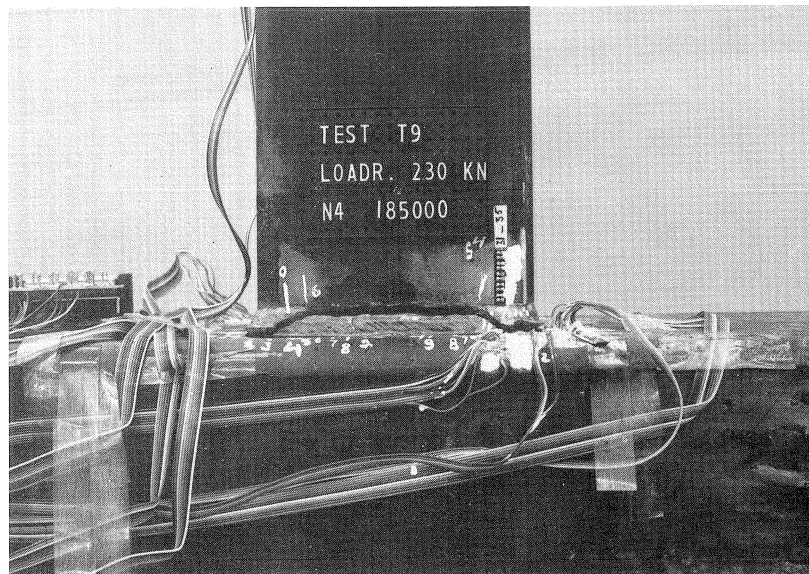


Figure 18. Detail of test specimen T9, after testing.

4 NUMERICAL RESEARCH

4.1 Introduction

The numerical work aims to investigate a parameter range in order to establish the parametric formulae for the designer. As no reliable information concerning the numerical modelling of joints between square hollow section was available at the time, a study was carried out on the influence of the FE model used upon the accuracy of the results [6]. As noted in Chapter 3.3, the SNCFs obtained are highly sensitive for small variations of the geometry of the joint. Therefore, a similar sensitivity of the SNCFs for the numerical model is to be expected. This means that simple FE models without modelling of the corner radii and weld as might be used for the analysis of the static behaviour of the joints will not be satisfactory for fatigue analysis.

Also, no sophisticated mesh generator was available at the time, leaving the task of modelling entirely to the researcher. The second purpose of the study was to gain experience and confidence in modelling the joint geometry.

Joints used for the comparison

As the numerical work for the initial ECSC-CIDECT contract was to be carried out in Delft, the experiments used for the comparison were all from Delft. All experiments on T-joints cover only two different geometries, from each of which one joint was selected (joints T4 and T12). The X-joints consisted only of one set of non-dimensional parameters in three different sizes, each of which was modelled (X1, X5 and X9). The two joints with $\beta=0.4$ and $\beta=1.0$ were also used for the comparison (X20 and X38).

Measurements of the dimensions used for the calibration of the FE model

In order to be able to follow the change in wall thickness reliably, the wall thickness was measured at various positions (see Figure 19). The measurements for T4 and T12 have been carried out at all four corners of the brace (and for the wall thickness and weld sizes also at the centres of the flat parts) to determine $t_{1_1}..t_{1_3}$, r_1 , r_{1_1} , w_1 and w_0 . The measurements for the chord were carried out at the upper half of the chord at both sides along the brace ($t_{0_1}..t_{0_6}$, r_0 , r_{0_1} and r_{0_2}). The values for b_1 ($= h_1$) were obtained from the 4 sides of the brace, whereas for the chord only the side adjacent to the brace was taken into account to determine b_0 ($= h_0$).

For X-joints, which have been calibrated with an earlier FE model (see Chapter 4.3, [6]), less measurements have been carried out. The most important measured dimensions are given in Tables 2 and 3.

General considerations for the FE model

- All FE analyses carried out are linear elastic. For the hot spot stress concept, the SNCFs are supposed to be independent on the stress level (no redistribution of strains), which is not completely true (as shown and discussed in Chapter 3.3).
- In contrast to the measurements, the length of the brace was taken as $2.5 b_1$, rather than $5.0 b_1$, to reduce the number of elements in the FE model. As the stresses can be evenly distributed at the top of the FE model, this does not influence the stress distribution near the joint, as shown in [14]. Because of co-symmetry for axially loaded T- and X-joints, only 1/4 of the T-joint, or 1/8 of the X-joint has to be modelled, applying the suitable boundary conditions. In contrast to other researchers [102], this was also found [14] to be possible for contra-symmetry as arises for joints loaded by an in-plane bending moment on the brace (for linear FE analysis only).
- To allow for a straightforward comparison, the FE analyses for the calibration are based upon strains. The parameter study is stress based, to establish formulae for the designer on the basis of stresses.
- The weld was modelled with solid elements, to allow for a clear definition of the weld toe. As an alternative, Van Dooren used a simple FE model which did not include the weld or corner radii, applying a "shift rule" for the extrapolation [20]. However, the use of solid elements to model the weld eliminates the discussion on the position of the weld toe completely and removes a possible source of errors.

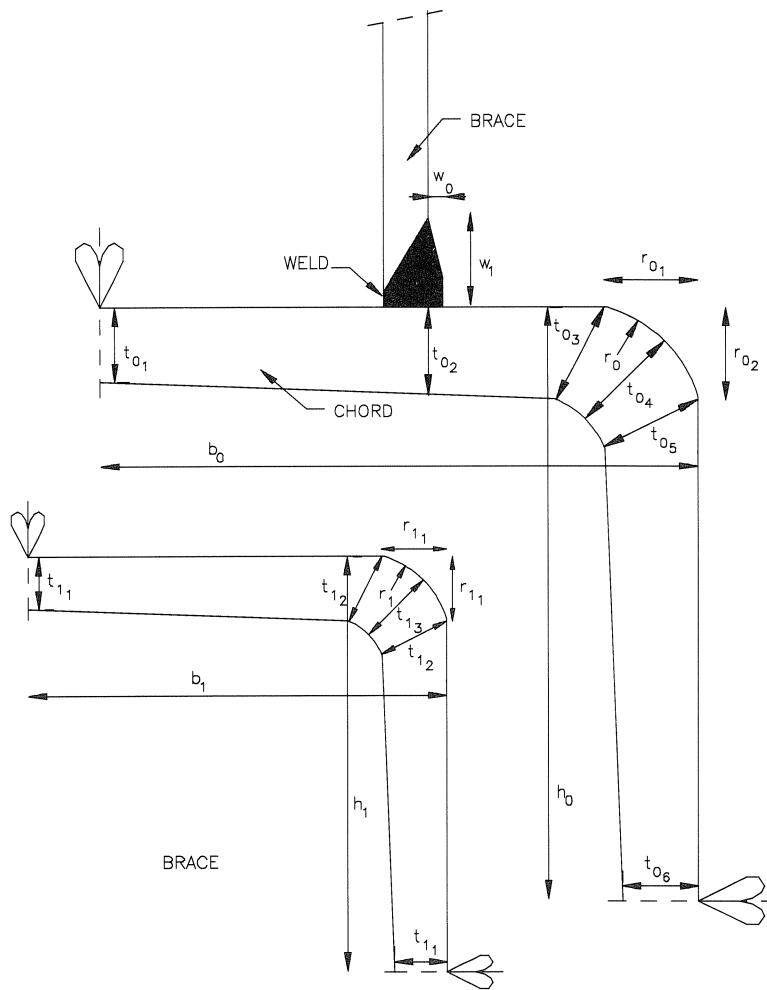


Figure 19. Summary of symbols used for the calibration of the FE model with the tests.

4.2 FE elements used

The in-house general purpose finite element program DIANA (Displacement ANALyser) is used for all the analytical work [42]. Only the linear elastic part is required for this research work. The steel properties used are always with the modulus of elasticity (E) of 210000 N/mm² and Poisson's ratio (ν) of 0.3.

Several types of elements have been used:

- 8 noded, 40 degrees of freedom thick shell elements
- 20 noded, 60 degrees of freedom solid elements
- 13 noded, 49 degrees of freedom transition elements
- 2 noded, 12 degrees of freedom beam elements

Shell elements

The main part of the model is made up of thick shell elements, shown in Figure 20. The shell element is an eight noded curved quadrilateral thick shell element, degenerated from the 20 noded solid element [30, 88]. Each node has five degrees of freedom, of which three are translational and two out-of-plane rotational degrees, giving a total of 40 degrees of freedom per element (see Figure 20).

Figure 20 also shows positions and numbering of integration points related to the element coordinates and node numbering order, where the results of analyses are output. The program allows a higher number of integration points, particularly in the thickness direction, but for the present work, a total of 12 integration points will suffice in most cases. This gives a 2x2 Gauss integration along the planes of the shell, with ξ and $\eta = \pm 1/\sqrt{3}$ (≈ 0.577) and 3 point Simpson integration in the thickness direction, with the three points corresponding to the bottom surface, mid-surface and top surface of the shell ($\zeta = -1.0, 0.0$ and $+1.0$) respectively.

Solid elements

The weld and a part of the members near the weld are modelled with solid elements, as shown in Figure 21, to allow for a clear definition of the weld toe. The extrapolations used to determine the SNCFs are carried out on data from solid elements as these elements were thought to provide the most reliable representation of reality.

The solid element used is the 20 noded isoparametric element shown in Figure 21. An isoparametric element is described as an element having the same interpolation function for displacements and geometry (shape). A second order polynomial in ξ , η and ζ (see Figure 21) is used for this element.

In general, a choice of Gauss integration order that may be used is $3 \times 3 \times 3$, $2 \times 2 \times 3$, $3 \times 3 \times 2$ and $2 \times 2 \times 2$. The minimum order of integration is $2 \times 2 \times 2$. The integration order chosen for the present work is $2 \times 2 \times 3$ in most cases. However, where solid elements are stacked together, $2 \times 2 \times 2$ order is also chosen. The order of numbering the integration points follows the sequence followed in the shell element (Figure 20). Unlike shell elements, solid elements represent three dimensional measurements and do not explicitly imply any thickness. Therefore, Simpson integration is not provided in DIANA as an option for such elements and the positions of the integration points from the middle of the solid in each of the directions ξ, η and ζ are given for $3 \times 3 \times 3$ integration as $-\sqrt{0.6}$, 0.0 and $+\sqrt{0.6}$ (≈ 0.774). For $2 \times 2 \times 2$ integration, the positions for ξ, η and ζ $-1/\sqrt{3}$ and $+1/\sqrt{3}$ only. The $3 \times 3 \times 3$ Gauss integration, with 27 integration points, requires a lot more computer storage and is only sparingly used.

Transition element

In order to combine the use of shell and solid element in the same analysis, it is useful to have "transition" elements for compatibility at the junction between the shell and solid configurations. The 13 noded transition element (see Figure 22) has only one side attached to a solid element, the opposite side to shell elements and the remaining two (adjacent) sides to other transition elements. Details of the integration points, etc., are similar to those for the shell elements described earlier.

Beam elements

The beam element is only used in the present work to distribute the applied loads at the ends of members over the total cross-section and introduce the correct boundary conditions. They are therefore only fictitious elements with properties given such as to induce uniform displacements at the ends of the members.

The beam element used for the present work is a linear beam element with two nodes.

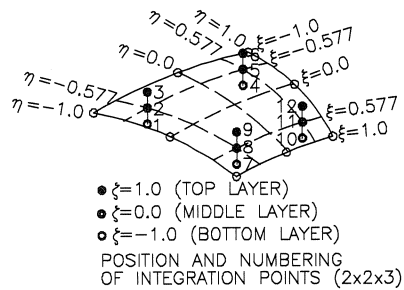
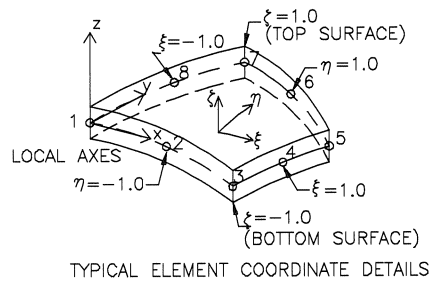


Figure 20. Thick shell element.

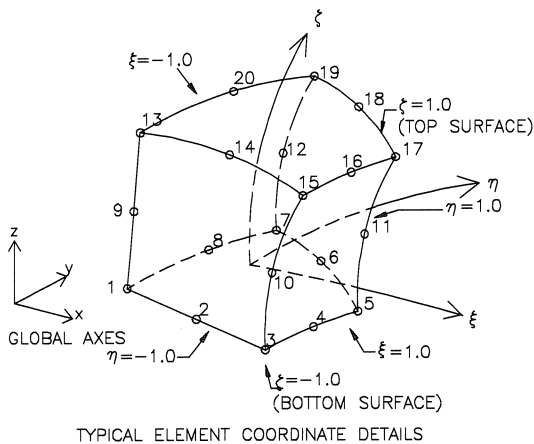


Figure 21. Solid element.

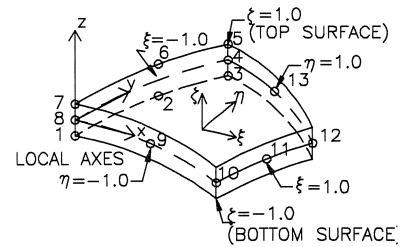


Figure 22. Transition element.

4.3 Development of the FE model

The development of the model is described extensively in [6] and [14], so that it will only be summarized here. All models contain a weld made of solid elements and a rounded element at the corner of the weld.

As a first step, the radii of chord and brace were modelled as quarter cylinders, r_0 based upon r_{0_1} and r_{0_2} and r_1 based upon r_{1_1} . In fact, the measurements at the test specimens revealed that the centres of the inner and outer radius do not coincide, as the thickness varies strongly in the corner. Also, the radii do not merge smoothly with the flat side, as a quarter of a cylinder would, but instead intersect the sides at a fairly large angle.

In order to improve the accuracy of the results, the wall thickness in the brace corners was increased to t_{1_4} . Later, the wall thickness in the chord was increased to t_{0_6} . In cases where the wall thickness in the corners was larger than the corner radii, values marginally smaller than the corner radii were used. Later on, the intermediate wall thickness t_{0_2} was also included in the model, which then contained a stepwise thickness influence in the chord of t_{0_1} , via t_{0_2} to t_{0_4} . Also, in case the wall thickness at 45° exceeds the corner radius, the radius is adapted to the wall thickness (plus 0.5 mm), rather than the other way round. This model, shown in Figures 23 and 24 performed satisfactorily for X-joints [6].

However, for T-joints, line C at 45° was often found to give the highest strains and here the stepwise increase in wall thickness resulted in poor accuracy. A smooth transition, using all wall thicknesses and radii measured (as shown in Figure 19) was used for both brace and chord. Also, more solid elements were introduced to allow all extrapolations to take place in solid elements only. Also, the corner radii were modelled more realistically instead of the quarter cylinder (as shown in Figure 19). The resulting model as shown in Figures 25 and 26 was used for the comparison. The model used for the parametric study is derived from this model, but is based on nominal wall thicknesses and corner radii, so that no tapering of the wall thickness occurs and the corners are quarter cylinders. When the nominal wall thickness and nominal corner radius are equal, the corner radius is increased by 5%, to avoid sharp inner corner radii and allow the use of shell elements in the corners.

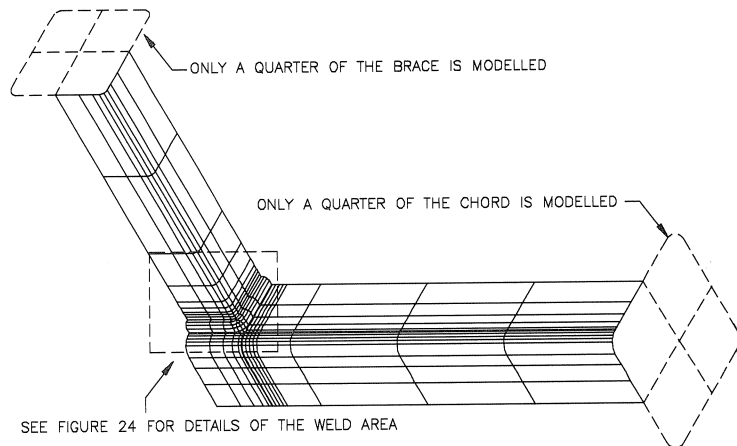


Figure 23. FE model initially used for the analysis of X-joints.

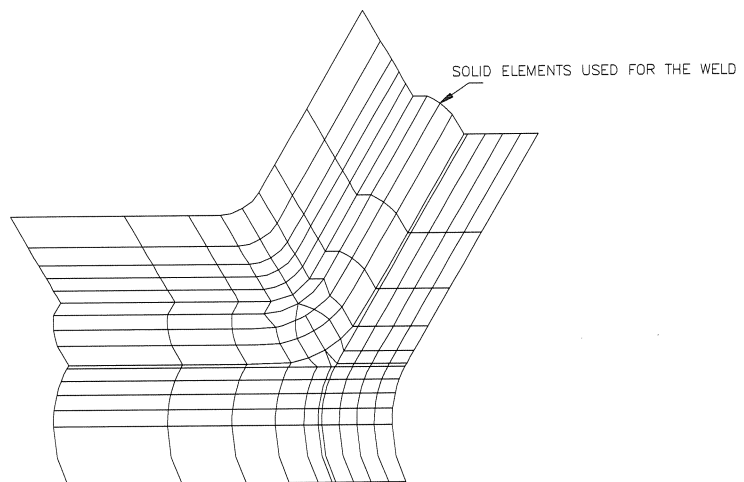


Figure 24. Detail of the FE model initially used for the analysis of X-joints.

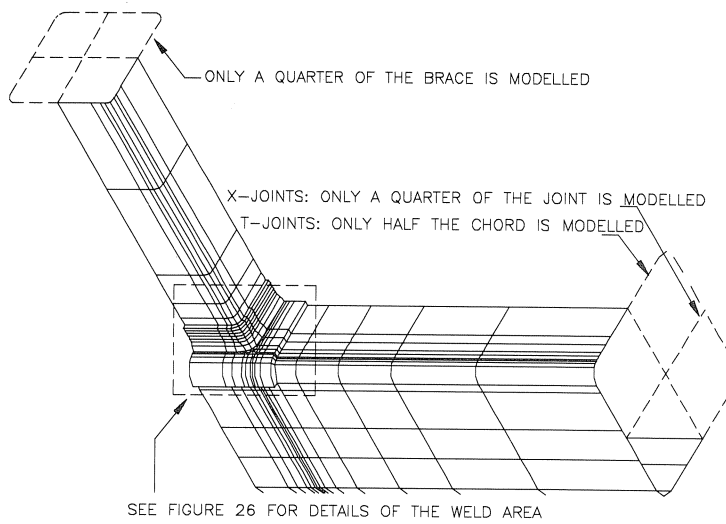


Figure 25. FE model used for the analysis of T- and X-joints.

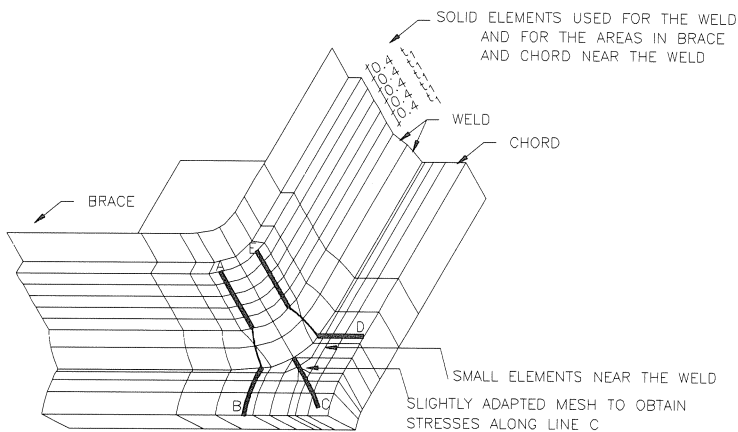


Figure 26. Detail of the FE model used for the analysis of T- and X-joints.

4.4 *Comparison of the FE model with the experiments*

A comparison is carried out between experiments and two numerical analyses for each of the 7 joints considered. The first analysis is based upon the average measured dimensions of the test specimen used for the comparison. The second analysis uses nominal (specified) dimensions. In this way, the accuracy of the numerical modelling with measured dimensions is checked against experimental measurements. Secondly, the influence of the difference between nominal and measured dimensions is studied by comparing the two numerical analyses. This provides useful background data on margins of safety with respect to actual joints.

The comparisons have been carried out along the measurement lines where the strain gauges were placed (see Figure 4). Examples of the SNCF distribution along these lines are presented in Figure 27. The SNCF distribution may be described as strains throughout the structure (brace as well as chord), all normalized with respect to uniform longitudinal strain at a cross-section of the brace which is outside the region of influence of the joint. The FE analyses were performed with a nominal strain of 1.0 in the brace, so that the values in the computer plots are all normalized and strain concentrations can be easily determined at each integration point. For the experiments, the average values at the four corners were normalized with respect to the average strain, which was measured with strain gauges, placed on the brace at a distance of $2.5 b_1$ away from the weld toe.

The SNCF values at the weld toe are summarized in Table 7 for each of the three cases: experimental measurements, analyses based on measured dimensions and analyses based on nominal dimensions. The values are obtained from extrapolations along lines A to D. This was done for the experiments and for the numerical analyses with nominal and measured dimensions. Line E was not taken into consideration, since no measurements were available along this line for the axially loaded T- and X-joints, which were used for the calibration of the FE model.

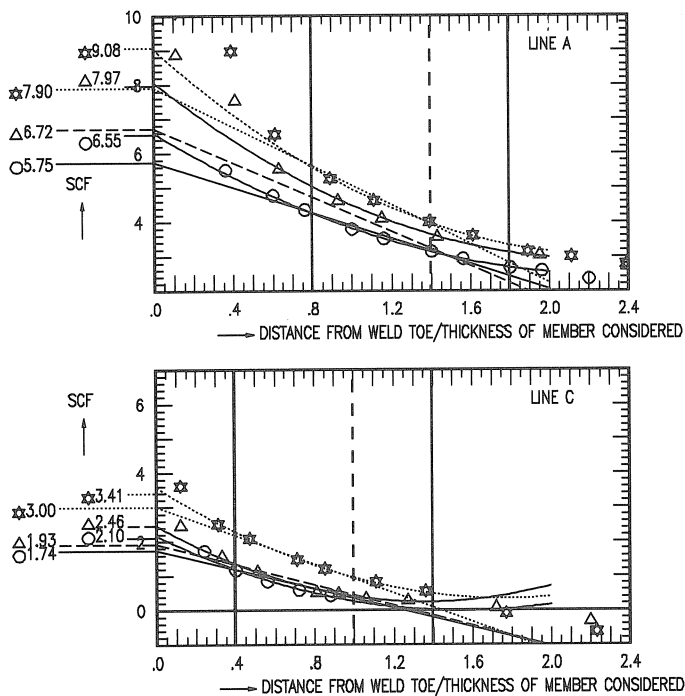
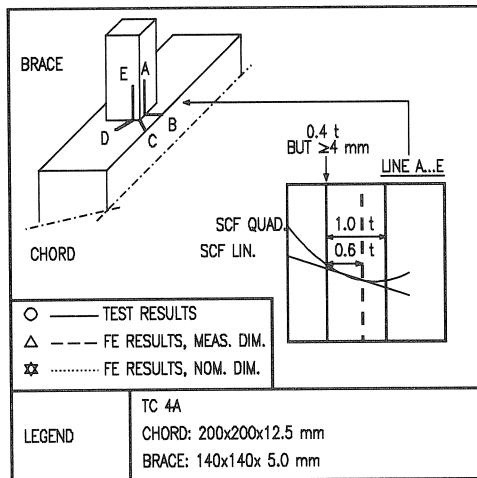


Figure 27. Comparison between SNCFs from tests and FE analyses.

Table 7. Extrapolated SNCFs from measurements and FE analyses										
JOINT	DIMENSIONS (mm)		Linear extrapolation				Quadratic extrapolation			
	CHORD	BRACE	CHORD		BRACE		CHORD		BRACE	
	$b_0 \times h_0 \times t_0$	$b_1 \times h_1 \times t_1$	B	C	D	A	B	C	D	A
SNCF MEASURED										
X1	101.0x101.0x 6.1	70.0x 70.0x 4.2	-	-	1.15	5.09	-	-	1.48	5.95
X5	200.6x200.6x12.6	139.8x139.8x 8.0	3.35	-	1.00	6.90	4.41	-	1.14	8.09
X9	259.2x259.2x17.0	180.5x180.5x10.6	2.76	-	1.10	6.20	3.60	-	1.43	6.87
X20	201.1x201.1x 8.0	80.0x 80.0x 4.1	12.50	-	-	7.80	14.50	-	-	10.80
X38	199.7x199.7x16.2	201.1x201.1x 8.0	0.86	-	0.34	2.30	0.96	-	0.48	2.38
T4	200.7x200.7x12.8	140.0x140.0x 5.0	0.21	1.74	2.64 ¹	5.75	0.89	2.10	2.56 ¹	6.55
T12	200.6x200.6x12.7	140.0x140.0x 7.6	2.90	4.31	4.37 ¹	6.44	3.57	4.98	5.10 ¹	6.86
SNCF FE WITH MEASURED DIMENSIONS										
X1	101.0x101.0x 6.1	70.0x 70.0x 4.2	0.60	-	1.20	6.18	0.59	-	1.87	7.11
X5	200.6x200.6x12.6	139.8x139.8x 8.0	3.56	-	1.00	6.10	5.77	-	1.44	8.15
X9	259.2x259.2x17.0	180.5x180.5x10.6	4.55	-	1.55	6.10	6.38	-	1.85	6.52
X20	201.1x201.1x 8.0	80.0x 80.0x 4.1	12.30	-	-	12.60	13.25	-	-	14.80
X38	199.7x199.7x16.2	201.1x201.1x 8.0	0.68	-	0.40	1.70	0.49	-	0.26	1.85
T4	200.7x200.7x12.8	140.0x140.0x 5.0	0.17	1.93	3.04	6.72	-0.20	2.46	3.30	7.97
T12	200.6x200.6x12.7	140.0x140.0x 7.6	1.88	5.08	4.57	7.10	3.09	6.08	4.89	7.95
SNCF FE WITH NOMINAL DIMENSIONS										
X1	101.0x101.0x 6.1	70.0x 70.0x 4.2	1.48	-	2.50	13.75	1.19	-	3.76	16.98
X5	200.6x200.6x12.6	139.8x139.8x 8.0	6.00	-	2.10	8.80	6.55	-	2.66	9.55
X9	259.2x259.2x17.0	180.5x180.5x10.6	4.65	-	1.90	6.80	4.99	-	2.17	7.28
X20	201.1x201.1x 8.0	80.0x 80.0x 4.1	13.65	-	5.60	13.70	15.11	-	6.30	16.40
X38	199.7x199.7x16.2	201.1x201.1x 8.0	0.55	-	0.60	1.45	0.37	-	0.82	1.37
T4	200.7x200.7x12.8	140.0x140.0x 5.0	2.56	3.00	3.45	7.90	3.12	3.41	3.82	9.08
T12	200.6x200.6x12.7	140.0x140.0x 7.6	3.70	5.35	5.33	6.48	4.33	6.40	5.73	7.18

¹ Not enough corners were measured, therefore the SNCF at the crack location was used instead of the average SNCFs.

No measurements were carried out along line E for the joints considered in this table

4.5 *Results of the comparison between FE analyses and experiments*

The following general conclusions are made from this preliminary work:

- The modelling of the finite element mesh, together with input of the measured variations of thickness in the cross-section of the brace and chord, results in a good simulation of the strains and their gradients. As an example, Figure 27 shows the comparisons between measurements and analysed strains for joint T4 at the locations in the brace and chord where the highest strains occur: lines A (brace) and C (chord).
- For close correlation with experimental measurements, it is necessary to model the variation of thickness in the cross-section of the chord and brace and the corner radii as realistically as possible. This confirms the sensitivity of the SNCF for small changes in the geometry as noted before in Chapter 3.3. Also the modelling of the weld and attached members in solid elements provides a straightforward interpretation of the output.
- Observations show a wide difference in SNCFs with measurements when the nominal dimensions are used. Analyses with nominal values mostly give higher strains, because the nominal thicknesses are smaller than measured thicknesses.
- A large number of analyses using the present type of idealization (Figures 25 and 26), is possible on a mini-computer. On the Convex C240, each analysis takes about 1 minute (less than 2 seconds CPU time), thereby allowing a large number of analyses.

Discussion on the differences between the numerical and experimental test results

- In view of the fact that a very fine mesh is required near the weld ($0.2 t_i$), it is possible that a better accuracy may be achieved by also having more than one element in the thickness direction.
- The measurements for the experimental specimens are averaged over the 4 corners. However, an average geometry need not necessarily result in an average strain, because of non-linear relationships between strain distribution and geometric aspects such as the wall thickness.
- The FE method used here is based upon a displacement approach, so that an upper bound is obtained on the stiffness even for the most optimal mesh refinement.
- A linear elastic FE analysis is carried out. However, there exists a relationship between load level and SNCF (see Chapter 3.3), suggesting a geometrical non-linearity.

5 PARAMETRIC STUDY

5.1 *Geometries and load cases considered*

After the development of the numerical model and comparison with the experimentally determined SNCFs (see Chapter 4), the next step is the stress based analysis of a large number of geometries and load cases, in order to establish a basis for the parametric formulae.

Geometries considered

In order to cover the complete range of practical geometries, variations in β , 2γ and τ have to be studied. One possible approach is to use a standard geometry and then vary each independent parameter (in this study β , 2γ and τ) in turn. The advantage of this method is that the number of geometrical combinations to be analysed increases only linear with the number of parameters: each new parameter is studied for a few values of that parameter.

This method has for instance been applied by Soh and Soh for their parametric studies in SCFs [102, 104].

A basic disadvantage of this method is that the important interaction between the geometrical parameters is completely disregarded. In case several parameters are distinctly different from the basic geometry this might cause large errors (see Chapter 7.7). Therefore, another approach has been adopted for this work, covering more or less the complete parameter range. Table 8 presents an overview of the geometries analysed. For $\beta=0.4/0.7/1.0$, three values of 2γ are analysed, each with at least 2 values of τ . For $2\gamma=16.0$, additional analyses were carried out for $\beta=0.25/0.55/0.85$ with $\tau=0.5/1.0$ to obtain more information on the complex relationship between β and the SCF. This way, 30 geometries were analysed.

The number of the geometry (see Table 8) is used consistently throughout the work for referencing all numerical analyses. In addition, the following letters are used for specifying further details.

- So for instance TC12AB indicates a numerical analysis of T-joint geometry 12 (chord 200x200x12.5 mm, brace 140x140x8 mm, see Table 8) loaded by an axial force on the brace with a butt weld.

85

Table 8. Geometries used for the parametric study											
JOINT	NON-DIM. PARAMETERS			CHORD			BRACE			WELD ¹	
no.	β	2γ	τ	b_0	t_0	r_0	b_1	t_1	r_1	w_0	w_1
41	0.25	16.0	0.50	200	12.5	25.0	50	6.3	6.3	3.2	8.3
42		16.0	1.00	200	12.5	25.0	50	12.5	12.5	6.3	14.5
20	0.40	25.0	0.50	200	8.0	16.0	80	4.0	4.0	2.0	6.0
21		16.0	0.32	200	12.5	25.0	80	4.0	4.0	2.0	6.0
22		12.5	0.25	200	16.0	32.0	80	4.0	4.0	2.0	6.0
23		25.0	1.00	200	8.0	16.0	80	8.0	8.0	4.0	10.0
24		16.0	0.64	200	12.5	25.0	80	8.0	8.0	4.0	10.0
25		12.5	0.50	200	16.0	32.0	80	8.0	8.0	4.0	10.0
43	0.55	16.0	0.50	200	12.5	25.0	110	6.3	8.8	3.2	8.3
44		16.0	1.00	200	12.5	25.0	110	12.5	17.5	6.3	14.5
26	0.70	25.0	0.63	200	8.0	16.0	140	5.0	7.0	2.5	7.0
4		16.0	0.40	200	12.5	25.0	140	5.0	7.0	2.5	7.0
27		12.5	0.31	200	16.0	32.0	140	5.0	7.0	2.5	7.0
47		16.0	0.50	200	12.5	25.0	140	6.3	8.8	3.2	8.3
28		25.0	1.00	200	8.0	16.0	140	8.0	11.2	4.0	10.0
12		16.0	0.64	200	12.5	25.0	140	8.0	11.2	4.0	10.0
29		12.5	0.50	200	16.0	32.0	140	8.0	11.2	4.0	10.0
30		16.0	1.00	200	12.5	25.0	140	12.5	17.5	6.3	14.5
31		12.5	0.78	200	16.0	32.0	140	12.5	17.5	6.3	14.5
45		16.0	0.50	200	12.5	25.0	170	6.3	12.5	3.2	8.3
46	0.85	16.0	1.00	200	12.5	25.0	170	12.5	25.0	6.3	14.5
32	1.00	25.0	0.79	200	8.0	16.0	200	6.3	12.5	3.2	8.3
33		16.0	0.50	200	12.5	25.0	200	6.3	12.5	3.2	8.3
34		12.5	0.39	200	16.0	32.0	200	6.3	12.5	3.2	8.3
35		25.0	1.00	200	8.0	16.0	200	8.0	16.0	4.0	10.0
36		16.0	0.64	200	12.5	25.0	200	8.0	16.0	4.0	10.0
37		12.5	0.50	200	16.0	32.0	200	8.0	16.0	4.0	10.0
38		16.0	1.00	200	12.5	25.0	200	12.5	25.0	6.3	14.5
39		12.5	0.78	200	16.0	32.0	200	12.5	25.0	6.3	14.5
40		12.5	1.00	200	16.0	32.0	200	16.0	32.0	8.0	18.0

All dimensions in mm.

¹ Dimensions given for butt welds. For fillet welds, $w_0=w_1=\sqrt{2}\tau_1$.

Load cases and joint types considered

To allow use of formula (2-2), SCF_{a1} , SCF_{m1} , SCF_{a0} and SCF_{m0} should be known.

As SCF_{a1} and SCF_{m1} are the most important stress concentration factors, each geometry is investigated as a T- as well as an X-joint with an in-plane bending moment and axial force on the brace.

To allow comparison between T- and X-joints and provide information on SCF_{m0} , the T-joints are also investigated for an in-plane bending moment on the chord.

Five T-joints were analysed with an axial force on the chord, to investigate SCF_{a0} .

In case of T-joints with an in-plane bending on the brace, analyses were carried out on the basis of strains and stresses, to allow comparison between SNCFs and SCFs as discussed in Chapter 5.4.

All geometries are provided with butt welds. The influence of the weld type is studied in Chapter 6, together with the influence of the corner radius. Using the extrapolation methods described in Chapter 2.5, the SCF values are determined and tabulated in Tables 10 to 16.

5.2 Comparison of T- and X-joints

In the case of T-joints, the load from the brace is transferred to the end supports of the chord, whereas for X-joints the loads in the opposite braces are in equilibrium. Especially in the case of T-joints with an axially loaded brace, large bending moments occur in the chord.

For long chords and joints with larger values of τ and β , the nominal stresses in the chord due to this bending moment can be considerably higher than the nominal stress in the brace. Therefore, it is important to consider the influence of this bending moment. The total hot spot stress at a given location according to the definition presented in Chapter 2.5 can be thought of as being the result of a nominal axial stress in the brace multiplied by the appropriate stress concentration factor plus a nominal bending stress in the chord multiplied with the corresponding stress concentration factor.

In case of axially loaded T-joints, Formula 2-2 reduces to:

$$S_{h.s.} = \sigma_{a1} \cdot SCF_{a1} + \sigma_{m0} \cdot SCF_{m0}.$$

$$\text{As } M_0 = \frac{1}{4} F_1 \cdot (l_0 - b_1), \text{ in which } F_1 = A_1 \cdot E \cdot \sigma_{a1}; \sigma_{m0} = \sigma_{a1} \cdot \frac{A_1 \cdot (l_0 - b_1)}{4W_0}$$

The total SCFs can be calculated from:

$$SCF_{tot} = SCF_{a1} + SCF_{m0} \cdot \frac{A_1 \cdot (l_0 - b_1)}{4W_0} \quad (5-1)$$

For T-joints loaded by an in-plane bending moment on the brace ($M_0 = M_1/2$) (5-1) changes to:

$$SCF_{tot} = SCF_{a1} + SCF_{m0} \cdot \frac{W_1}{2W_0} \quad (5-2)$$

An important consequence of the additional strain caused by the induced bending in the chord is the fact that the SCFs based on the total stress range (SCF_{tot}) as often given in design recommendations are dependent on α . When SCF_{tot} and SCF_{m0} have been determined by FE analyses with an axial load on the brace and a bending moment on the chord respectively, it is possible to calculate SCF_{a1} using Equation (5-1).

To check the validity of this approach, a T-joint T38 was analysed 3 times (based on strains):

- An axial load on the brace (also causing an additional bending moment in the chord) for a certain chord length $l_0 = 1290$ mm ($SNCF_{tot}$).
- A bending moment on the chord of the T-joint, without any loading on the brace ($SNCF_{m0}$).
- An axial load on the brace for a double chord length $l = 2580$ mm ($SNCF_{2tot}$).

Based on the first 2 FE analyses, it is possible to determine $SNCF_{a1}$ using Equation (5-1). Then, applying Equation (5-1) again on $SNCF_{m0}$ and $SNCF_{a1}$ for a double chord length, $SNCF_{2tot}$ can be determined. The result is compared with the (total) $SNCF$ s found for an FE analysis with the double chord length. The results are tabulated in Table 9. As can be observed, the agreement is very good (within a few percent). It should however be noted, that for very short chords, depending on the support conditions, this relationship is no longer perfect, as is known from literature (for instance Efthymiou, [54]). The SCFs of T-joints loaded by an in-plane bending moment on the chord are tabulated in Table 10.

Table 9. Influence of l_0 on the SNCFs of axially loaded T-joints											
l_0 (mm)	SNCF	Linear extrapolation					Quadratic extrapolation				
		B	C	D	A	E	B	C	D	A	E
1290	$SNCF_{tot}$	0.45	10.82	11.88	2.49	3.65	0.46	12.43	12.82	2.60	3.98
1290	$SNCF_{m0}$	-0.13	1.25	2.05	0.04	0.20	-0.13	1.37	2.15	0.05	0.24
1290	$SNCF_{a1}$	1.10	4.53	1.57	2.29	2.64	1.11	5.54	2.01	2.35	2.77
2580	SCF_{a1} +10.98 \cdot $SNCF_{m0}$	-0.33	18.26	24.08	2.73	4.84	-0.32	20.58	25.62	2.90	5.41
2580	$SNCF_{tot}$	-0.37	18.57	25.08	2.79	4.86	-0.33	19.95	26.16	2.94	5.41

TC38 -Chord:200x200x12.5, $r_0=25$ mm
 -Brace:200x200x12.5, $r_0=25$ mm
 $-A_1=8973$ mm² (determined from nominal dimensions)
 $-W_0=486102$ mm³ (determined from nominal dimensions)
 $-l_0=1290$ mm (length of test specimens)

Analyses, shown respectively in the table above:

- 1 FE analysis of TC38 with $l_0=1290$ mm and an axial load on the brace.
- 2 FE analysis of TC38 with $l_0=1290$ mm and a bending moment on the chord.
- 3 Determining $SNCF_{a1}$ for a double chord length from the two previous FE

$$\text{analyses } SNCF_{tot} = SNCF_{a1} + SNCF_{m0} * \frac{A_1 * (l_0 - b_1)}{4W_0}, \text{ or: } SNCF_{a1} = SNCF_{tot} - SNCF_{m0} * \frac{A_1 * (l_0 - b_1)}{4W_0}$$

$$\text{For TC38: } SNCF_{a1} = SNCF_{tot} - SNCF_{m0} * \frac{8973 * (1290 - 200)}{4 * 486102} = SNCF_{tot} - 5.03 * SNCF_{m0}.$$

- 4 With $SNCF_{a1}$ and $SNCF_{m0}$, the SNCF for a double chord length is determined

$$SNCF_{tot} = SNCF_{a1} + SNCF_{m0} * \frac{A_1 * (l_0 - b_1)}{4W_0}$$

$$SNCF_{tot} = SNCF_{a1} + SNCF_{m0} * \frac{8973 * (2580 - 200)}{4 * 486102} = SNCF_{a1} + 10.98 * SNCF_{m0}$$

- 5 For comparison, a FE analysis of TC38 with $l_0=2580$ mm and an axial load on the brace. The results of case 4 and 5 are very similar, showing the validity of the concept.

Table 10. SCFs T-joints, loaded by an in-plane bending moment on the chord butt welds													
JOINT	NON-DIM. PARAMETERS			SCF linear extrapolation					SCF quadratic extrapolation				
				CHORD			BRACE		CHORD			BRACE	
no.	β	2γ	τ	B	C	D	A	E	B	C	D	A	E
TC41CB	0.25	16.0	0.50	-0.14	0.69	1.34	0.01	-0.26	-0.16	0.72	1.41	0.00	-0.24
TC42CB	0.25	16.0	1.00	-0.23	0.71	1.48	0.09	-0.34	-0.26	0.75	1.56	0.09	-0.36
TC20CB	0.40	25.0	0.50	-0.12	0.79	1.44	-0.02	-0.32	-0.14	0.83	1.54	-0.02	-0.26
TC21CB	0.40	16.0	0.32	-0.09	0.74	1.38	0.07	-0.15	-0.10	0.77	1.45	0.07	-0.06
TC22CB	0.40	12.5	0.25	-0.07	0.68	1.29	0.11	-0.07	-0.09	0.71	1.36	0.11	0.03
TC23CB	0.40	25.0	1.00	-0.20	0.83	1.56	-0.04	-0.41	-0.23	0.89	1.67	-0.04	-0.40
TC24CB	0.40	16.0	0.64	-0.17	0.81	1.53	-0.02	-0.26	-0.19	0.86	1.62	-0.03	-0.23
TC25CB	0.40	12.5	0.50	-0.15	0.77	1.45	-0.01	-0.16	-0.17	0.80	1.55	-0.01	-0.12
TC43CB	0.55	16.0	0.50	-0.10	0.91	1.55	-0.02	-0.08	-0.10	0.96	1.66	-0.01	-0.03
TC44CB	0.55	16.0	1.00	-0.18	0.99	1.71	-0.08	-0.25	-0.20	1.04	1.81	-0.09	-0.24
TC26CB	0.70	25.0	0.63	-0.01	1.13	1.71	-0.00	-0.13	-0.00	1.23	1.83	0.02	-0.09
TC4CB	0.70	16.0	0.40	-0.00	0.95	1.59	0.18	0.13	-0.02	1.01	1.66	0.23	0.22
TC27CB	0.70	12.5	0.31	-0.00	0.92	1.47	0.26	0.25	0.03	1.00	1.56	0.31	0.35
TC47CB	0.70	16.0	0.50	-0.01	1.02	1.68	0.12	0.09	-0.03	1.08	1.76	0.14	0.16
TC28CB	0.70	25.0	1.00	-0.05	1.24	1.82	-0.07	-0.24	-0.05	1.33	1.93	-0.07	-0.21
TC12CB	0.70	16.0	0.64	-0.04	1.09	1.75	0.04	0.02	-0.07	1.17	1.81	0.05	0.07
TC29CB	0.70	12.5	0.50	-0.03	1.04	1.62	0.13	0.16	-0.02	1.11	1.71	0.14	0.23
TC30CB	0.70	16.0	1.00	-0.05	1.23	1.87	-0.03	-0.14	-0.05	1.28	1.93	-0.03	-0.11
TC31CB	0.70	12.5	0.78	-0.07	1.13	1.75	0.01	-0.01	-0.07	1.20	1.82	0.01	0.03
TC45CB	0.85	16.0	0.50	0.09	1.11	1.85	0.22	0.26	0.13	1.24	1.98	0.29	0.33
TC46CB	0.85	16.0	1.00	0.09	1.40	2.13	0.07	0.06	0.12	1.51	2.26	0.10	0.10
TC32CB	1.00	25.0	0.79	0.19	1.48	2.35	0.09	0.26	0.20	1.65	2.55	0.11	0.32
TC33CB	1.00	16.0	0.50	0.14	1.06	1.72	-0.00	0.16	0.15	1.15	1.82	0.00	0.18
TC34CB	1.00	12.5	0.39	0.10	0.88	1.52	-0.05	0.08	0.12	0.94	1.59	-0.05	0.09
TC35CB	1.00	25.0	1.00	0.17	1.51	2.84	0.11	0.32	0.18	1.67	3.13	0.14	0.38
TC36CB	1.00	16.0	0.64	0.12	1.26	1.99	0.02	0.20	0.13	1.37	2.11	0.03	0.22
TC37CB	1.00	12.5	0.50	0.09	0.98	1.64	-0.04	0.13	0.10	1.04	1.74	-0.03	0.14
TC38CB	1.00	16.0	1.00	0.07	1.25	2.45	0.04	0.25	0.08	1.30	2.57	0.06	0.29
TC39CB	1.00	12.5	0.78	0.05	1.09	1.83	-0.01	0.17	0.06	1.18	1.93	0.00	0.19
TC40CB	1.00	12.5	1.00	0.02	1.05	2.16	-0.00	0.20	0.03	1.12	2.29	0.01	0.24

Table 11. SCFs T-joints, loaded by an in-plane bending moment on the brace, not compensated for the influence of the bending moment in the chord, butt welds													
JOINT	NON-DIM. PARAMETERS			SCF linear extrapolation					SCF quadratic extrapolation				
				CHORD			BRACE		CHORD			BRACE	
no.	β	2γ	τ	B	C	D	A	E	B	C	D	A	E
TC41MB	0.25	16.0	0.50	0.81	1.61	1.61	1.18	1.56	0.92	1.76	1.70	1.30	1.68
TC42MB	0.25	16.0	1.00	0.73	1.95	1.98	0.70	1.38	0.84	2.11	2.11	0.76	1.46
TC20MB	0.40	25.0	0.50	4.45	6.33	5.47	3.92	4.12	5.18	7.07	6.10	4.61	4.72
TC21MB	0.40	16.0	0.32	1.46	2.06	1.89	2.36	2.48	1.61	2.27	2.03	2.72	2.76
TC22MB	0.40	12.5	0.25	0.76	1.11	1.03	1.82	1.93	0.72	1.18	1.08	2.07	2.11
TC23MB	0.40	25.0	1.00	7.16	11.12	8.59	3.28	3.62	8.05	12.55	9.41	3.65	3.95
TC24MB	0.40	16.0	0.64	2.46	3.78	3.18	2.32	2.54	2.73	4.25	3.46	2.55	2.74
TC25MB	0.40	12.5	0.50	1.28	1.98	1.77	1.87	2.07	1.38	2.17	1.91	2.04	2.21
TC43MB	0.55	16.0	0.50	3.28	4.14	3.11	3.79	3.60	3.66	4.66	3.41	4.25	3.99
TC44MB	0.55	16.0	1.00	4.94	6.60	4.56	3.11	2.89	5.60	7.19	4.93	3.47	3.16
TC26MB	0.70	25.0	0.63	9.10	10.40	6.38	7.30	6.26	10.48	11.81	7.15	8.38	7.17
TC4MB	0.70	16.0	0.40	1.79	2.61	2.10	4.38	3.94	2.49	3.07	2.27	4.96	4.41
TC27MB	0.70	12.5	0.31	0.84	1.19	1.07	3.19	2.96	1.19	1.38	1.16	3.57	3.27
TC47MB	0.70	16.0	0.50	1.99	3.27	2.58	4.70	4.08	2.97	3.93	2.88	5.25	4.49
TC28MB	0.70	25.0	1.00	13.13	15.14	8.45	7.40	5.64	15.72	17.11	9.34	8.22	6.16
TC12MB	0.70	16.0	0.64	2.74	4.15	3.11	4.86	4.03	3.72	5.09	3.42	5.34	4.37
TC29MB	0.70	12.5	0.50	1.38	1.94	1.68	3.66	3.22	1.90	2.35	1.85	3.98	3.47
TC30MB	0.70	16.0	1.00	3.72	5.75	3.99	4.39	3.36	4.94	6.81	4.36	4.87	3.66
TC31MB	0.70	12.5	0.78	1.91	2.85	2.31	3.44	2.89	2.50	3.38	2.55	3.80	3.14
TC45MB	0.85	16.0	0.50	1.81	2.50	1.79	3.69	3.41	2.23	3.07	2.08	4.05	3.76
TC46MB	0.85	16.0	1.00	2.98	4.81	3.45	4.13	3.50	3.63	5.51	3.84	4.51	3.84
TC32MB	1.00	25.0	0.79	0.91	2.69	2.49	2.76	3.01	0.92	3.30	2.90	2.83	3.14
TC33MB	1.00	16.0	0.50	0.36	1.17	0.91	1.78	1.97	0.36	1.34	1.03	1.79	1.97
TC34MB	1.00	12.5	0.39	0.20	0.71	0.55	1.37	1.48	0.21	0.83	0.62	1.36	1.45
TC35MB	1.00	25.0	1.00	1.16	3.35	4.12	3.12	3.71	1.17	4.04	4.77	3.21	3.94
TC36MB	1.00	16.0	0.64	0.46	1.89	1.47	1.93	2.18	0.46	2.14	1.63	1.95	2.23
TC37MB	1.00	12.5	0.50	0.26	1.02	0.84	1.47	1.65	0.27	1.13	0.93	1.47	1.65
TC38MB	1.00	16.0	1.00	0.64	2.58	2.98	2.28	2.88	0.64	2.88	3.26	2.34	3.04
TC39MB	1.00	12.5	0.78	0.36	1.70	1.54	1.68	1.99	0.36	1.89	1.67	1.71	2.03
TC40MB	1.00	12.5	1.00	0.41	1.95	2.39	1.80	2.37	0.41	2.16	2.59	1.86	2.51

Table 12. SCFs T-joints, loaded by an in-plane bending moment on the brace, compensated for the influence of the bending moment in the chord, butt welds													
JOINT	NON-DIM. PARAMETERS			SCF linear extrapolation					SCF quadratic extrapolation				
				CHORD			BRACE		CHORD			BRACE	
no.	β	2γ	τ	B	C	D	A	E	B	C	D	A	E
TC41MB	0.25	16.0	0.50	0.81	1.60	1.59	1.18	1.56	0.92	1.75	1.68	1.30	1.68
TC42MB	0.25	16.0	1.00	0.73	1.94	1.96	0.70	1.39	0.84	2.10	2.08	0.76	1.47
TC20MB	0.40	25.0	0.50	4.45	6.30	5.41	3.92	4.13	5.19	7.04	6.04	4.61	4.73
TC21MB	0.40	16.0	0.32	1.46	2.04	1.85	2.36	2.48	1.61	2.25	1.99	2.72	2.76
TC22MB	0.40	12.5	0.25	0.76	1.09	1.00	1.82	1.93	0.72	1.16	1.05	2.07	2.11
TC23MB	0.40	25.0	1.00	7.17	11.06	8.49	3.28	3.65	8.07	12.49	9.30	3.65	3.98
TC24MB	0.40	16.0	0.64	2.47	3.74	3.11	2.32	2.55	2.74	4.21	3.38	2.55	2.75
TC25MB	0.40	12.5	0.50	1.29	1.95	1.71	1.87	2.08	1.39	2.14	1.85	2.04	2.21
TC43MB	0.55	16.0	0.50	3.29	4.07	2.99	3.79	3.61	3.67	4.58	3.28	4.25	3.99
TC44MB	0.55	16.0	1.00	4.96	6.47	4.34	3.12	2.92	5.63	7.06	4.70	3.48	3.19
TC26MB	0.70	25.0	0.63	9.10	10.22	6.11	7.30	6.28	10.48	11.62	6.86	8.38	7.18
TC4MB	0.70	16.0	0.40	1.79	2.50	1.92	4.36	3.93	2.49	2.96	2.08	4.93	4.39
TC27MB	0.70	12.5	0.31	0.84	1.10	0.93	3.17	2.94	1.19	1.29	1.01	3.54	3.24
TC47MB	0.70	16.0	0.50	1.99	3.13	2.35	4.68	4.07	2.97	3.78	2.64	5.23	4.47
TC28MB	0.70	25.0	1.00	13.14	14.85	8.02	7.42	5.70	15.73	16.80	8.89	8.24	6.21
TC12MB	0.70	16.0	0.64	2.75	3.97	2.82	4.85	4.03	3.73	4.90	3.12	5.33	4.36
TC29MB	0.70	12.5	0.50	1.38	1.80	1.45	3.64	3.20	1.90	2.20	1.61	3.96	3.44
TC30MB	0.70	16.0	1.00	3.73	5.47	3.56	4.40	3.39	4.95	6.52	3.92	4.88	3.69
TC31MB	0.70	12.5	0.78	1.92	2.63	1.97	3.44	2.89	2.51	3.15	2.20	3.80	3.13
TC45MB	0.85	16.0	0.50	1.79	2.27	1.41	3.65	3.36	2.20	2.82	1.68	3.99	3.69
TC46MB	0.85	16.0	1.00	2.95	4.33	2.72	4.11	3.48	3.59	4.99	3.06	4.48	3.81
TC32MB	1.00	25.0	0.79	0.83	2.09	1.53	2.72	2.90	0.84	2.63	1.86	2.79	3.01
TC33MB	1.00	16.0	0.50	0.32	0.86	0.41	1.78	1.92	0.32	1.01	0.51	1.79	1.92
TC34MB	1.00	12.5	0.39	0.18	0.50	0.18	1.38	1.46	0.18	0.60	0.23	1.37	1.43
TC35MB	1.00	25.0	1.00	1.08	2.60	2.70	3.07	3.55	1.08	3.21	3.21	3.14	3.75
TC36MB	1.00	16.0	0.64	0.42	1.45	0.77	1.92	2.11	0.41	1.66	0.89	1.94	2.15
TC37MB	1.00	12.5	0.50	0.23	0.73	0.35	1.48	1.61	0.24	0.82	0.41	1.48	1.61
TC38MB	1.00	16.0	1.00	0.61	1.96	1.76	2.26	2.76	0.60	2.23	1.98	2.31	2.90
TC39MB	1.00	12.5	0.78	0.34	1.24	0.77	1.68	1.92	0.33	1.39	0.85	1.71	1.95
TC40MB	1.00	12.5	1.00	0.40	1.43	1.31	1.80	2.27	0.40	1.60	1.45	1.86	2.39

Table 13. SCFs T-joints, loaded by an axial force on the brace, compensated for the influence of the bending moment in the chord, butt welds													
JOINT	NON-DIM. PARAMETERS			SCF linear extrapolation					SCF quadratic extrapolation				
				CHORD			BRACE		CHORD			BRACE	
no.	β	2γ	τ	B	C	D	A	E	B	C	D	A	E
TC41AB	0.25	16.0	0.50	6.21	5.57	3.59	3.82	2.82	6.66	6.08	3.83	4.46	3.24
TC42AB	0.25	16.0	1.00	10.75	9.15	5.32	2.77	1.37	11.56	9.88	5.67	3.27	1.59
TC20AB	0.40	25.0	0.50	14.93	13.86	8.15	10.25	8.52	16.38	15.33	8.77	12.37	9.83
TC21AB	0.40	16.0	0.32	4.90	4.08	2.71	5.68	4.93	5.20	4.51	2.90	6.74	5.56
TC22AB	0.40	12.5	0.25	2.53	1.81	1.37	3.89	3.46	2.58	2.08	1.42	4.58	3.86
TC23AB	0.40	25.0	1.00	27.20	24.93	12.16	10.18	5.88	30.31	27.37	13.28	11.43	6.42
TC24AB	0.40	16.0	0.64	9.53	8.11	4.58	6.64	4.38	10.20	9.04	4.95	7.40	4.76
TC25AB	0.40	12.5	0.50	5.11	3.97	2.47	4.89	3.43	5.50	4.49	2.73	5.42	3.72
TC43AB	0.55	16.0	0.50	7.29	5.94	3.33	7.02	5.45	7.92	6.81	3.75	7.91	6.08
TC44AB	0.55	16.0	1.00	12.50	10.11	4.67	6.58	3.70	13.78	11.07	5.09	7.33	4.12
TC26AB	0.70	25.0	0.63	14.31	12.15	5.90	9.97	7.63	15.19	14.39	6.71	11.42	8.82
TC4AB	0.70	16.0	0.40	2.74	2.81	1.80	5.94	4.88	3.79	3.50	2.11	6.73	5.51
TC27AB	0.70	12.5	0.31	1.51	1.44	0.95	4.30	3.68	2.00	1.88	1.29	4.84	4.10
TC47AB	0.70	16.0	0.50	3.45	3.65	2.24	6.53	5.03	4.63	4.50	2.59	7.30	5.54
TC28AB	0.70	25.0	1.00	20.24	17.28	7.09	10.24	6.27	21.77	19.59	7.91	11.36	6.85
TC12AB	0.70	16.0	0.64	4.64	4.86	2.70	6.90	4.86	5.62	6.19	3.05	7.60	5.29
TC29AB	0.70	12.5	0.50	2.48	2.40	1.48	5.22	4.00	3.05	2.95	1.84	5.72	4.33
TC30AB	0.70	16.0	1.00	6.59	7.27	3.45	6.57	3.76	7.62	8.29	3.86	7.28	4.13
TC31AB	0.70	12.5	0.78	3.75	3.62	2.04	5.26	3.45	4.20	4.23	2.34	5.81	3.79
TC45AB	0.85	16.0	0.50	2.42	2.63	1.36	3.99	3.49	2.86	3.25	1.64	4.39	3.89
TC46AB	0.85	16.0	1.00	4.09	5.26	2.83	4.66	3.56	4.84	6.00	3.20	5.11	3.95
TC32AB	1.00	25.0	0.79	1.10	2.87	2.00	2.60	2.76	1.12	3.49	2.39	2.68	2.88
TC33AB	1.00	16.0	0.50	0.53	1.46	0.71	1.74	1.87	0.52	1.61	0.84	1.75	1.87
TC34AB	1.00	12.5	0.39	0.35	0.97	0.43	1.38	1.44	0.35	1.10	0.51	1.37	1.40
TC35AB	1.00	25.0	1.00	1.45	3.63	3.47	2.98	3.43	1.49	4.35	4.09	3.08	3.65
TC36AB	1.00	16.0	0.64	0.68	2.26	1.20	1.91	2.08	0.67	2.52	1.37	1.93	2.12
TC37AB	1.00	12.5	0.50	0.46	1.35	0.68	1.50	1.62	0.46	1.47	0.79	1.50	1.61
TC38AB	1.00	16.0	1.00	1.05	3.22	2.58	2.33	2.78	1.02	3.57	2.95	2.40	2.95
TC39AB	1.00	12.5	0.78	0.70	2.32	1.28	1.76	1.95	0.69	2.51	1.44	1.80	2.01
TC40AB	1.00	12.5	1.00	0.87	2.79	2.15	1.96	2.37	0.85	3.02	2.41	2.03	2.53

Table 14. SCFs X-joints, loaded by an in-plane bending moment on the brace butt welds													
JOINT	NON-DIM. PARAMETERS			SCF linear extrapolation					SCF quadratic extrapolation				
				CHORD			BRACE		CHORD			BRACE	
no.	β	2γ	τ	B	C	D	A	E	B	C	D	A	E
XC41MB	0.25	16.0	0.50	0.81	1.62	1.62	1.18	1.56	0.92	1.77	1.71	1.30	1.68
XC42MB	0.25	16.0	1.00	0.74	1.97	1.98	0.70	1.38	0.85	2.13	2.11	0.76	1.46
XC20MB	0.40	25.0	0.50	4.55	6.78	5.52	3.95	4.14	5.07	7.44	5.86	4.64	4.75
XC21MB	0.40	16.0	0.32	1.51	2.21	1.96	2.38	2.49	1.63	2.40	2.05	2.73	2.77
XC22MB	0.40	12.5	0.25	0.81	1.10	1.05	1.83	1.93	0.83	1.23	1.08	2.08	2.12
XC23MB	0.40	25.0	1.00	7.22	11.47	8.58	3.34	3.65	8.21	12.59	9.30	3.72	4.00
XC24MB	0.40	16.0	0.64	2.52	3.92	3.25	2.36	2.57	2.75	4.32	3.46	2.60	2.77
XC25MB	0.40	12.5	0.50	1.37	2.04	1.80	1.89	2.09	1.51	2.26	1.95	2.07	2.24
XC43MB	0.55	16.0	0.50	3.42	4.28	3.14	3.87	3.65	3.79	4.81	3.44	4.35	4.05
XC44MB	0.55	16.0	1.00	5.18	6.84	4.58	3.18	2.92	5.84	7.45	4.94	3.55	3.20
XC26MB	0.70	25.0	0.63	9.91	10.94	6.48	7.52	6.42	10.72	12.80	7.22	8.63	7.36
XC4MB	0.70	16.0	0.40	1.80	2.78	2.08	4.53	4.05	2.69	3.34	2.33	5.12	4.53
XC27MB	0.70	12.5	0.31	1.02	1.45	1.12	3.30	3.05	1.42	1.79	1.39	3.70	3.37
XC47MB	0.70	16.0	0.50	2.20	3.50	2.56	4.86	4.18	3.20	4.19	2.85	5.43	4.60
XC28MB	0.70	25.0	1.00	14.08	15.87	8.38	7.62	5.76	15.49	17.89	9.23	8.46	6.30
XC12MB	0.70	16.0	0.64	3.02	4.44	3.06	5.03	4.12	3.76	5.42	3.37	5.53	4.47
XC29MB	0.70	12.5	0.50	1.59	2.25	1.69	3.80	3.30	2.03	2.67	1.98	4.14	3.56
XC30MB	0.70	16.0	1.00	4.16	6.36	3.97	4.54	3.42	4.98	7.16	4.35	5.03	3.72
XC31MB	0.70	12.5	0.78	2.24	3.16	2.26	3.58	2.95	2.61	3.62	2.52	3.95	3.21
XC45MB	0.85	16.0	0.50	2.09	2.64	1.58	3.85	3.51	2.51	3.23	1.86	4.22	3.87
XC46MB	0.85	16.0	1.00	3.47	4.99	3.04	4.30	3.59	4.15	5.71	3.41	4.70	3.92
XC32MB	1.00	25.0	0.79	0.91	2.38	1.74	2.77	2.95	0.91	2.96	2.09	2.84	3.07
XC33MB	1.00	16.0	0.50	0.38	1.05	0.52	1.83	1.97	0.39	1.21	0.62	1.83	1.97
XC34MB	1.00	12.5	0.39	0.22	0.63	0.26	1.43	1.50	0.23	0.76	0.32	1.42	1.47
XC35MB	1.00	25.0	1.00	1.17	2.98	3.03	3.13	3.61	1.18	3.64	3.60	3.22	3.82
XC36MB	1.00	16.0	0.64	0.50	1.71	0.93	1.98	2.17	0.50	1.95	1.07	2.00	2.20
XC37MB	1.00	12.5	0.50	0.30	0.92	0.46	1.53	1.66	0.31	1.03	0.55	1.53	1.66
XC38MB	1.00	16.0	1.00	0.74	2.38	2.09	2.34	2.83	0.74	2.68	2.35	2.40	2.98
XC39MB	1.00	12.5	0.78	0.45	1.58	0.96	1.75	1.98	0.45	1.76	1.08	1.78	2.01
XC40MB	1.00	12.5	1.00	0.55	1.84	1.62	1.88	2.35	0.55	2.06	1.81	1.93	2.47

Table 15. SCFs X-joints, loaded by an axial force on the brace butt welds													
JOINT	NON-DIM. PARAMETERS			SCF linear extrapolation					SCF quadratic extrapolation				
				CHORD			BRACE		CHORD			BRACE	
no.	β	2γ	τ	B	C	D	A	E	B	C	D	A	E
XC41AB	0.25	16.0	0.50	6.60	5.94	3.82	4.00	2.84	7.06	6.49	4.07	4.69	3.28
XC42AB	0.25	16.0	1.00	11.46	9.73	5.65	2.93	1.26	12.29	10.50	6.00	3.46	1.47
XC20AB	0.40	25.0	0.50	16.06	14.85	8.63	10.88	8.89	17.57	16.43	9.29	13.11	10.22
XC21AB	0.40	16.0	0.32	5.36	4.46	2.95	6.05	5.17	5.67	4.91	3.15	7.20	5.83
XC22AB	0.40	12.5	0.25	2.81	2.02	1.52	4.15	3.62	2.86	2.31	1.57	4.89	4.05
XC23AB	0.40	25.0	1.00	29.21	26.60	12.78	10.83	5.94	32.49	29.17	13.95	12.15	6.49
XC24AB	0.40	16.0	0.64	10.39	8.79	4.93	7.09	4.48	11.09	9.78	5.32	7.91	4.87
XC25AB	0.40	12.5	0.50	5.68	4.36	2.70	5.23	3.51	6.03	4.92	2.98	5.80	3.81
XC43AB	0.55	16.0	0.50	8.21	6.48	3.58	7.55	5.72	8.74	7.41	4.02	8.51	6.39
XC44AB	0.55	16.0	1.00	14.01	10.83	4.92	7.04	3.73	15.22	11.82	5.35	7.84	4.15
XC26AB	0.70	25.0	0.63	15.88	12.99	6.12	10.64	8.00	16.42	15.32	6.95	12.17	9.25
XC4AB	0.70	16.0	0.40	3.25	3.04	1.87	6.38	5.13	4.33	3.78	2.18	7.23	5.80
XC27AB	0.70	12.5	0.31	1.82	1.51	0.97	4.63	3.86	2.32	1.99	1.32	5.21	4.31
XC47AB	0.70	16.0	0.50	4.06	3.90	2.30	7.00	5.24	5.25	4.81	2.65	7.82	5.77
XC28AB	0.70	25.0	1.00	22.24	18.04	7.13	10.85	6.42	23.38	20.38	7.95	12.04	7.01
XC12AB	0.70	16.0	0.64	5.34	5.13	2.71	7.36	4.99	6.38	6.58	3.06	8.12	5.43
XC29AB	0.70	12.5	0.50	2.95	2.47	1.48	5.61	4.11	3.51	3.06	1.83	6.15	4.45
XC30AB	0.70	16.0	1.00	7.48	7.37	3.32	6.98	3.74	8.48	8.43	3.71	7.73	4.10
XC31AB	0.70	12.5	0.78	4.40	3.60	1.95	5.63	3.44	4.82	4.24	2.24	6.22	3.77
XC45AB	0.85	16.0	0.50	2.77	2.43	1.10	4.02	3.41	3.19	3.04	1.35	4.42	3.79
XC46AB	0.85	16.0	1.00	4.47	4.49	2.12	4.64	3.35	5.19	5.18	2.41	5.08	3.70
XC32AB	1.00	25.0	0.79	0.86	1.80	1.06	2.27	2.29	0.86	2.26	1.33	2.33	2.37
XC33AB	1.00	16.0	0.50	0.43	0.90	0.34	1.62	1.65	0.43	1.04	0.44	1.62	1.65
XC34AB	1.00	12.5	0.39	0.28	0.59	0.20	1.32	1.32	0.29	0.71	0.25	1.31	1.29
XC35AB	1.00	25.0	1.00	1.16	2.24	1.88	2.57	2.77	1.16	2.77	2.30	2.65	2.93
XC36AB	1.00	16.0	0.64	0.56	1.44	0.62	1.75	1.79	0.57	1.65	0.74	1.77	1.82
XC37AB	1.00	12.5	0.50	0.38	0.83	0.34	1.43	1.45	0.39	0.94	0.41	1.43	1.44
XC38AB	1.00	16.0	1.00	0.91	1.99	1.35	2.13	2.29	0.91	2.26	1.57	2.18	2.42
XC39AB	1.00	12.5	0.78	0.61	1.40	0.63	1.66	1.68	0.61	1.58	0.74	1.69	1.71
XC40AB	1.00	12.5	1.00	0.79	1.66	1.09	1.86	1.99	0.79	1.89	1.26	1.92	2.11

A similar method is applied to all SCFs for T-joints loaded by in-plane bending moment on the brace, this time based on equation (5-2). In this way, Table 12 was derived from Table 11 by "subtracting" the influence of the bending moment on the chord. For axial load on the brace the results are only presented after exclusion of the influence of the bending moment according to Equation (5-1). See Table 13.

If the influence of the bending moment on the chord of T-joints is excluded, a comparison between T- and X-joints can be made (Table 14 vs. Table 12 and Table 15 vs. Table 13). Plotting the SCFs of T-joints against the SCF of X-joints with the same non-dimensional parameters for lines A to E in case of an in-plane bending moment on the brace (Figure 28) and an axial force on the brace (Figure 29) shows a very close agreement between the two joint types.

Note that:

- The minimum value for SCF_{a1} and SCF_{m1} is taken as 2.0 (see Chapter 2.5).
- For joints with $\beta=1.0$ the stress concentration factors for X-joints are lower than for T-joints. This is due to the fact that the loads in X-joints are directly transferred from brace to brace via the side wall of the chord, whereas for T-joints the loads are transferred to the ends of the chord. This results in lower SCFs for axially loaded X-joints along lines C and D, which is taken into account by applying a correction factor of 0.65 for line C and 0.5 for line D on the $SCF_{formula}$ for axially loaded X-joints with $\beta=1.0$. These correction factors are given in Tables 18 and 19.

As a result, one set of parametric formulae can be used for SCF_{a1} and SCF_{m1} for T- and X-joints, unlike many other investigations which have come up with different sets of equations for T- and X-joints. For instance Smedley [98] who derived completely different terms for the two types of joints, based on an analysis of a large database of experiments. Soh and Soh derived formulae containing an α influence for X-joints [104], which does not seem logical (except as a correction factor for short chords).

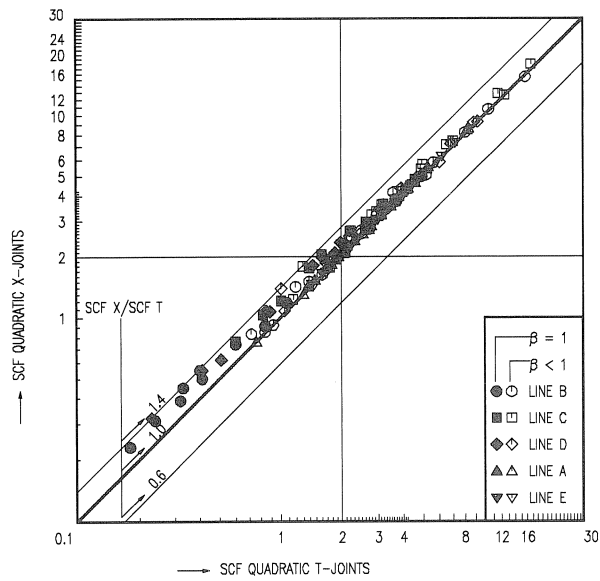


Figure 28. Comparison between T- and X-joints, loaded by I.P.B. on the brace, T-joints compensated for M_{chord} .

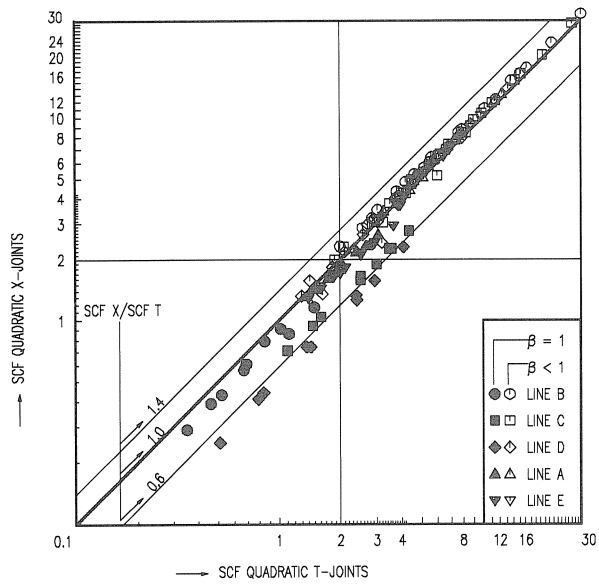


Figure 29. Comparison between T- and X-joints, loaded by an axial force on the brace, T-joints compensated for M_{chord} .

The approach of separating the influence of the bending moment in the chord has 3 distinct advantages:

- Elimination of α in the parametric formulae.

This parameter can be included in a non-dimensional way in Equation (5-1).

In order to arrive at completely non-dimensional parametric formulae, as for the types of joints and loadings, a certain idealization is necessary:

The moment of inertia of a solid square section $I_0 = \frac{b_0^4}{12}$.

The elastic section modulus of a square chord with wall thickness t_0 and no rounded corners

$$: I_0 = \frac{b_0^4 - (b_0 - 2t_0)^4}{12} = \frac{b_0^4 - b_0^4 + 8b_0^3t_0 - 24b_0^2t_0^2 + 32b_0t_0^3 - 16t_0^4}{12}$$

$$\text{As } W_0 = 2 \frac{I_0}{b_0}, \text{ this results in } W_0 = \frac{8b_0^3t_0 - 24b_0^2t_0^2 + 32b_0t_0^3 - 16t_0^4}{6b_0} \approx \frac{4}{3}b_0t_0(b_0 - 3t_0).$$

As $A_1 \approx 4t_1 \cdot (b_1 - t_1)$ (again neglecting the corner radii) and $l_0 = \alpha b_0 / 2$:

$$\frac{A_1 \cdot (l_0 - b_1)}{4W_0} = \frac{3 \cdot 4(b_1 - t_1)t_1 \cdot (\alpha b_0 / 2 - b_1)}{4b_0t_0(b_0 - 3t_0) \cdot 4} = \frac{3(\beta - \tau/2\gamma)\tau \cdot (\alpha/2 - \beta)}{(1 - 3/2\gamma) \cdot 4} = \frac{3\tau(2\gamma\beta - \tau) \cdot (\alpha - 2\beta)}{8(2\gamma - 3)}$$

$$\text{Therefore: } S_{r_{h.s.}} = \sigma_{a1} \cdot (SCF_{a1} + SCF_{m0} \cdot \frac{3\tau(2\gamma\beta - \tau) \cdot (\alpha - 2\beta)}{8(2\gamma - 3)}) \quad (5-3)$$

- Additional bending moments in the chord, asymmetrical support conditions of the chord and other effects can be elegantly included in the determination of $S_{r_{h.s.}}$: namely by determining all forces on the members and applying Equation (2-2)

$$(S_{r_{h.s.}} = \sigma_{r_{m1}} \cdot SCF_{m1} + \sigma_{r_{a1}} \cdot SCF_{a1} + \sigma_{r_{m0}} \cdot SCF_{m0} + \sigma_{r_{a0}} \cdot SCF_{a0}) \text{ for the determination of } S_{r_{h.s.}}$$

- One set of parametric formula can be used for both T- and X-joints.

5.3 Influence of axial load on the chord

In order to check whether the parametric formulae for bending moment in the chord of T-joints can also be used for an axial force on the chord, 5 T-joints are analysed by the FE method, applying an axial force on the chord. The SCFs are compared with the SCFs obtained from the parametric formulae for a bending moment on the chord. As the SCFs for lines A, B and E are negligible for all cases considered, only lines C and D need to be considered. As no differences larger than 20% are found (see Table 16, results for in-plane bending moment on the chord taken from Table 10), it is acceptable to apply the parametric formulae for T-joints loaded by an in-plane bending moment on the chord to T-joints with an axial load on the chord.

As even for more critical load cases the difference between X- and T-joints is small (see Chapter 5.2), the formulae are also applicable to X-joints.

By applying these formulae also to X-joints loaded by axial force or bending moment on the chord, the range of application of the parametric formulae is then covered for all load cases.

JOINT	NON-DIM. PARAMETERS			SCF linear extrapolation					SCF quadratic extrapolation				
				CHORD			BRACE		CHORD			BRACE	
no.	β	2γ	τ	B	C	D	A	E	B	C	D	A	E
TC41CB	0.25	16.0	0.50	-0.14	0.69	1.34	0.01	-0.26	-0.16	0.72	1.41	0.00	-0.24
TC41FB	0.25	16.0	0.50	-0.16	0.80	1.56	0.02	-0.36	-0.18	0.83	1.64	0.01	-0.35
TC43CB	0.55	16.0	0.50	-0.10	0.91	1.55	-0.02	-0.08	-0.10	0.96	1.66	-0.01	-0.03
TC43FB	0.55	16.0	0.50	-0.13	1.01	1.76	-0.08	-0.22	-0.13	1.05	1.88	-0.07	-0.17
TC28CB	0.70	25.0	1.00	-0.05	1.24	1.82	-0.07	-0.24	-0.05	1.33	1.93	-0.07	-0.21
TC28FB	0.70	25.0	1.00	-0.13	1.30	2.06	-0.14	-0.39	-0.14	1.38	2.18	-0.14	-0.37
TC33CB	1.00	16.0	0.50	0.14	1.06	1.72	-0.00	0.16	0.15	1.15	1.82	0.00	0.18
TC33FB	1.00	16.0	0.50	0.12	1.04	1.73	-0.19	-0.09	0.14	1.12	1.82	-0.18	-0.07
TC35CB	1.00	25.0	1.00	0.17	1.51	2.84	0.11	0.32	0.18	1.67	3.13	0.14	0.38
TC35FB	1.00	25.0	1.00	0.11	1.33	2.47	-0.12	-0.02	0.11	1.43	2.70	-0.10	0.02

Table 17. SNCFs T-joints, loaded by an in-plane bending moment on the brace, not compensated for the influence of the bending moment in the chord, butt welds													
JOINT	NON-DIM. PARAMETERS			SNCF linear extrapolation					SNCF quadratic extrapolation				
				CHORD			BRACE		CHORD			BRACE	
no.	β	2γ	τ	B	C	D	A	E	B	C	D	A	E
TC41MB	0.25	16.0	0.50	0.54	1.28	1.31	1.10	1.46	0.63	1.39	1.38	1.22	1.57
TC42MB	0.25	16.0	1.00	0.54	1.57	1.63	0.65	1.27	0.63	1.66	1.73	0.70	1.33
TC20MB	0.40	25.0	0.50	3.46	5.24	4.40	3.65	3.83	4.11	5.79	4.88	4.16	4.29
TC21MB	0.40	16.0	0.32	1.03	1.67	1.49	2.23	2.33	1.17	1.83	1.57	2.49	2.54
TC22MB	0.40	12.5	0.25	0.53	0.85	0.80	1.73	1.82	0.50	0.96	0.84	1.91	1.94
TC23MB	0.40	25.0	1.00	5.91	9.18	7.09	3.00	3.31	6.77	10.36	7.72	3.31	3.59
TC24MB	0.40	16.0	0.64	1.89	3.08	2.54	2.13	2.33	2.11	3.47	2.74	2.34	2.51
TC25MB	0.40	12.5	0.50	0.96	1.64	1.39	1.72	1.90	1.02	1.80	1.49	1.88	2.03
TC43MB	0.55	16.0	0.50	2.45	3.25	2.31	3.43	3.22	2.84	3.67	2.55	3.83	3.55
TC44MB	0.55	16.0	1.00	3.94	5.27	3.53	2.76	2.51	4.58	5.62	3.85	3.06	2.73
TC26MB	0.70	25.0	0.63	7.76	8.31	4.65	6.62	5.50	8.91	9.43	5.28	7.51	6.20
TC4MB	0.70	16.0	0.40	1.46	1.94	1.51	4.04	3.56	1.81	2.17	1.65	4.52	3.94
TC27MB	0.70	12.5	0.31	1.08	1.21	0.82	2.96	2.72	1.40	1.29	0.89	3.29	2.97
TC47MB	0.70	16.0	0.50	1.71	2.54	1.89	4.28	3.62	2.34	2.87	2.11	4.75	3.97
TC28MB	0.70	25.0	1.00	11.41	12.20	6.46	6.62	4.80	13.79	13.81	7.22	7.29	5.23
TC12MB	0.70	16.0	0.64	2.53	3.15	2.28	4.38	3.55	3.05	3.77	2.54	4.80	3.84
TC29MB	0.70	12.5	0.50	1.85	1.95	1.28	3.30	2.85	2.38	2.24	1.41	3.59	3.08
TC30MB	0.70	16.0	1.00	4.07	4.44	3.02	3.91	2.88	4.82	5.09	3.34	4.31	3.12
TC31MB	0.70	12.5	0.78	2.76	2.81	1.76	3.06	2.51	3.50	3.11	1.95	3.35	2.71
TC45MB	0.85	16.0	0.50	2.78	3.43	1.41	3.56	3.25	3.87	4.08	1.69	3.86	3.55
TC46MB	0.85	16.0	1.00	4.38	6.17	2.55	3.76	3.12	5.87	6.93	2.93	4.07	3.38
TC32MB	1.00	25.0	0.79	1.03	4.06	1.80	2.76	2.94	1.03	4.93	2.01	2.82	3.06
TC33MB	1.00	16.0	0.50	0.44	1.79	0.66	1.83	1.99	0.44	2.01	0.73	1.83	1.99
TC34MB	1.00	12.5	0.39	0.26	1.07	0.39	1.42	1.52	0.26	1.23	0.42	1.41	1.49
TC35MB	1.00	25.0	1.00	1.28	4.95	2.89	3.06	3.54	1.29	5.94	3.16	3.12	3.74
TC36MB	1.00	16.0	0.64	0.55	2.75	1.05	1.95	2.16	0.55	3.13	1.13	1.97	2.19
TC37MB	1.00	12.5	0.50	0.34	1.49	0.60	1.51	1.66	0.34	1.66	0.65	1.51	1.66
TC38MB	1.00	16.0	1.00	0.77	3.57	2.09	2.22	2.75	0.76	3.88	2.18	2.28	2.89
TC39MB	1.00	12.5	0.78	0.47	2.37	1.15	1.67	1.93	0.46	2.62	1.21	1.70	1.96
TC40MB	1.00	12.5	1.00	0.53	2.65	1.71	1.76	2.25	0.52	2.90	1.77	1.80	2.38

5.4 Comparison of SNCFs and SCFs

In earlier investigations, the ratio between SCF and SNCF was assumed to be approximately 1.1 as found in another research project [65]. The relationship between stresses and strains is given below:

$$\sigma_x = \frac{E}{1-\nu^2} (\epsilon_x + \nu \cdot (\epsilon_y + \epsilon_z)) \quad (5-4)$$

If x is the direction perpendicular to the weld and assuming that strains in the other directions are small, (5-4) reduces to: $\sigma_x = \frac{E}{1-\nu^2} \epsilon_x = \frac{E}{0.91} \epsilon_x \approx 1.1 E \epsilon$.

Whereas this ratio is still applied when no other data is available, for instance to compare measured strains to $S_{th.s.}$ - N_f lines based on stresses, this ratio might be dependent on the geometry of the joint.

To check this assumption, the SNCFs are also determined for the case of T-joints loaded by in-plane bending moments on the brace, presented in Table 17. The results are compared to the corresponding SCFs in Table 11. The comparison is presented in Figure 30. As can be observed in this figure, the average ratio between SCF and SNCF is about 1.1, but values lower than 0.6 and higher than 1.4 also occurred. For higher SNCFs, the ratio between SCF and SNCF approaches 1.1, suggesting that in this case the other strain components are less significant with respect to the strain perpendicular to the weld toe. As a result, comparison between SCFs and SNCFs should be carried out with great care.

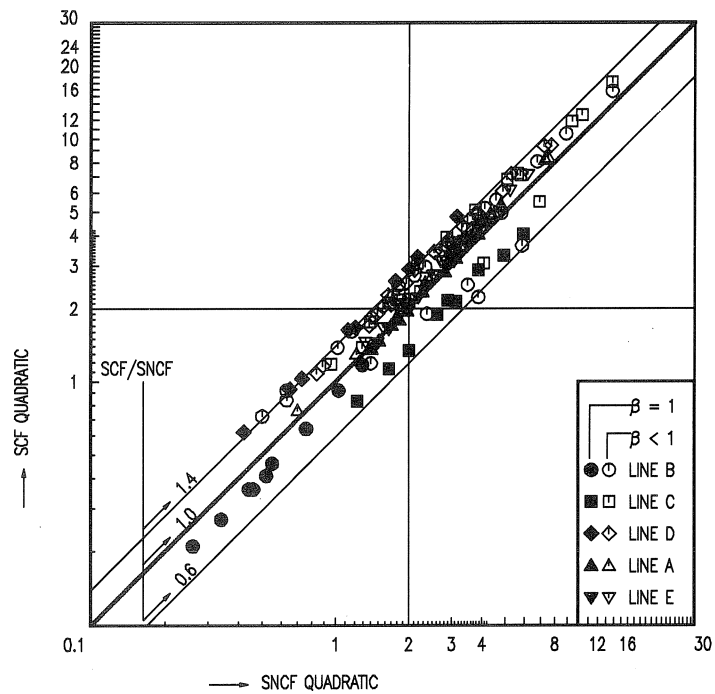


Figure 30. Comparison between SNCFs and SCFs for T-joints loaded by an in-plane bending moment on the brace, quadratic extrapolation.

Aim of the regression analysis

A computer program has been developed in order to carry out the present analyses. Many combinations of trial functions have been tested before arriving at the final formulae. The concept is to obtain the simplest possible formulae which gives a good sum of the squares of the residuals and acceptable individual residuals, both absolutely and relatively to the SCF. Also, the shape of the formulae is kept the same for all lines and load cases considered, so that only the constants in the formulae are changed.

Checks on the accuracy of the formulae

The absolute residuals are expressed as follows:

$$\text{Absolute error} = \text{SCF}_{\text{formula}} - \text{SCF}_{\text{FE analysis}}$$

The relative residuals are expressed as percentage error due to the formulae as follows:

$$\text{Percentage error} = 100 \frac{(\text{SCF}_{\text{formula}} - \text{SCF}_{\text{FE analysis}})}{\text{SCF}_{\text{FE analysis}}}$$

While the sum of the squares of the residuals gives a measure of the overall goodness of fit of a particular formula, the residuals also show whether any variables have been left out, or a higher order influence of a parameter exists. Also, the significance of errors of individual values can be observed and decisions made on their weight and as to whether a function is acceptable within the limits of engineering accuracy, without having to resort to statistical tests.

It is particularly important that either the relative error or the absolute error of all data points available is small (for instance, a relative error of 40% is no problem for SCFs close to 1 as a minimum value of 2.0 is used for SCF_{a1} and SCF_{m1} , but it is important for an SCF of 10). Furthermore, the individual importance of each data point is to be considered, taking into account which points are relatively less accurate. For $\beta=0.7$, and especially $\beta=0.85$, the SCF is very sensitive to small changes in geometry and/or FE model).

Data used for the regression analysis

The SCFs (numerical analysis with butt welds) used for the regression analysis are given in Table 10 and Tables 12 to 16. As noticed in Chapter 5.2, axially loaded X-joints with $\beta=1.0$ have a more favourable stress distribution than T-joints. To be able to treat data sets from T- and X-joints as one population, the SCFs of the parametric formulae for axially loaded X-joints with $\beta=1.0$ were multiplied by 0.65 for line C and 0.5 for line D to allow the comparison of the FE results for T- and X-joints and the determination of relative and absolute errors.

Function types investigated

It was found that the type of general function most suitable for the formulae was:

$$SCF = f_1(\tau) \cdot f_2(\beta) \cdot 2\gamma^{f_3(\beta)} \quad (5-5)$$

The types of functions to be used are limitless. However, of the two obvious choices, polynomials or Fourier series, the former has been preferred here, since it applies better to the kind of relationship needed, is easier in use for the designer and more consistent with existing formulae. As shown below, some influences can be covered by a parameter raised to a power.

It is also found that with the above formulation, by taking the regression analysis for any chosen function f_2 , iteration has to be carried out for all parameters in f_1 and f_3 (non-linear regression). First, starting values are filled in, then the parameters of the polynomial in f_2 are solved directly, then the parameters in f_1 and f_3 are improved etc., until the sum of the squares of the absolute errors reaches a minimum.

Any desired combination of polynomial (or other) functions can be used with the computer program, which then gives the constants to the functions. These constants can be rounded off to the required number of significant figures and the residuals determined. The influence of rounding off the constants to a required number of significant figures has also been observed by comparing the residuals using these rounded off constants with those obtained directly from the regression analysis (without rounding off the constants). It has been observed that the number of decimals given in the formulae cannot be rounded off to two decimal places without affecting the accuracy. This is mainly due to the difference in magnitude of the parameters: rounding off to two decimals would influence some parameters by as much as 10%, resulting in an even higher percentage difference for the SCFs.

5.6 Establishment of parametric functions for loading on the brace

The general type of formula given in equation (5-5) is split into 3 functions:

- f_1 (the influence of τ)
As can be seen in Figures 31 and 32 (see Chapter 5.8), the influence of τ can be described fairly accurately as: $f_1(\tau) = \tau^{0.75}$ for the chord and $f_1(\tau) = 1$ (no influence) for the brace. After this correction, the data points for the same β and 2γ but different τ coincide fairly well. A more accurate description would include β and 2γ in f_1 , which would complicate the graphical presentation considerably.
- f_2
The basic influence of β appears to be roughly parabolic for lines A to E. A function of the type: $f_2(\beta) = a + b\beta + c\beta^2$ is therefore used. It may be noted that the limits of β are set at 0.35 to 1.0 and not 0.25 to 1.0. This is because only 2 data points are available for $\beta = 0.25$, and although they are useful in the total regression analysis to determine the joint behaviour, they could give misleading information for 2γ values other than 16. Also, β values for rectangular hollow section joints under 0.4 are uncommon for structures loaded in fatigue. From the regression analysis an additional factor for 2γ in f_2 was found necessary for line C only: $f_2(\beta, 2\gamma) = a + b\beta + c\beta^2 + d2\gamma$.
- f_3
For the joints with $\beta = 0.4/0.7/1.0$, the SCF values increase in both members with increasing 2γ . The relationship between the SCF and 2γ is described by a parabolic function in β . Thus: $f_3(\beta) = e + f\beta + g\beta^2$.

The following formula is then established:

$$SCF = (a + b\beta + c\beta^2 + d2\gamma) \cdot 2\gamma^{(e+f\beta+g\beta^2)} \cdot \tau^h \quad (5-6)$$

- Here:
- a to h constants in the formula.
 - $h=0$ for the brace and $h=0.75$ for the chord.
 - For all lines except line C: $d=0$.
 - The other parameters are determined by the least squares method, treating the FE results for T- and X-joints as one population.

Line A always had larger SCFs than line E, or the SCFs of the two lines were within a few percent of each other, except for $\beta=1.0$. In cases where line E was more than 10% higher than line A, line E also had the highest SCFs for the other load case.

Therefore, and because the loads in the chord do not influence lines A and E, it is possible to use the maximum SCF of the brace instead of determining 2 formulae for lines A and E respectively. Note that a similar approach for the chord is less easily established, due to the influence of the bending moment in the chord and the fact that the highest SCF is also dependant on the type of loading, which causes problems for superposition of load cases.

5.7 *Establishment of parametric functions for loading on the chord*

All values of SCF_{m0} for lines A, E and B are below 0.4 and therefore negligible. So only functions for lines C and D are established. A simplified form of Equation (5-6) is used with parameters b,c,d,f and g equal to 0, leaving $SCF = a \cdot 2\gamma^e \cdot \tau^h$. Note that the influence of τ is now much smaller, about 0.2 as opposed to 0.75 for SCF_{a1} and SCF_{m1} (the data points with the same β and 2γ , but different τ generally coincide after this correction). This is due to the fact that the force on the members is not linearly related to the wall thickness of the brace as for SCF_{a1} and SCF_{m1} . Another difference is that SCF_{m0} is not limited to a minimum of 2.0, since it is to be multiplied by other nominal stresses and the stress pattern is much clearer so that less underestimation occurs by limiting the number of locations and directions where the stresses are determined. Due to the analyses carried out for an axial loading on the chord, the formulae can also be used for SCF_{a0} .

5.8 Results of the parametric study

The formulae are summarized in Table 18 (SCF based upon quadratic extrapolation) and in Table 19 (based upon linear extrapolation). A uniform type of function is obtained, usable for both X- and T-joints, chord as well as brace. The formulae are still reasonably simple to use and also agree better with the points determined by FE analyses than the preliminary formulae as established in [1, 10, and 16].

In Figures 31 to 33, the formulae are presented by plotting β against the SCF for various values of 2γ . The third parameter, τ , is included in the SCF. Note that the data points which are taken from FE analyses on T- and X-joints, show β in their position along the X-axis, 2γ in the type of symbol and τ in the size of the symbol.

The SCFs for various types of load (axial load or in-plane bending) are now known as a function of the geometry of the joint. Because fixed positions are selected, superposition is allowed, so that the determination of the hot spot stress according to Equation (2-2) becomes possible. The hot spot stress range for any arbitrary combination of loads is determined as follows:

$$S_{r.h.s.} = \sigma_{r_{m1}} \cdot SCF_{m1} + \sigma_{r_{a1}} \cdot SCF_{a1} + \sigma_{r_{m0}} \cdot SCF_{m0} + \sigma_{r_{a0}} \cdot SCF_{a0} \quad (2-2)$$

The nominal stress range σ_r , is the stress range in the member determined from beam theory, without taking the stress discontinuity due to the presence of the joint into account.

Together with appropriate $S_{r.h.s.}$ - N_f lines (established in Chapter 7), based entirely on experiments or with N_f taken from experiments and $S_{r.h.s.}$ based on the SCFs taken from the parametric formulae, the formulae form a basis for the fatigue design of T- and X-joints in square hollow sections.

Table 18. SCF formulae for T- and X-joints made with square hollow sections, quadratic extrapolation	
SCFs for T- and X-joints, loaded by a bending moment on the brace (SCF_{m1})	
LINE	
B	$SCF=(-0.011+0.085\cdot\beta-0.073\cdot\beta^2)\cdot 2\gamma^{(1.722+1.151\cdot\beta-0.697\cdot\beta^2)}\cdot\tau^{0.75}$
C	$SCF=(0.952-3.062\cdot\beta+2.382\cdot\beta^2+0.0228\cdot 2\gamma)\cdot 2\gamma^{(-0.690+5.817\cdot\beta-4.685\cdot\beta^2)}\cdot\tau^{0.75}$
D	$SCF=(-0.054+0.332\cdot\beta-0.258\cdot\beta^2)\cdot 2\gamma^{(2.084+1.062\cdot\beta+0.527\cdot\beta^2)}\cdot\tau^{0.75}$
A,E	$SCF=(0.390-1.054\cdot\beta+1.115\cdot\beta^2)\cdot 2\gamma^{(-0.154+4.555\cdot\beta-3.809\cdot\beta^2)}$
SCFs for T- and X-joints, loaded by an axial force on the brace (SCF_{a1})	
LINE	
B	$SCF=(0.143-0.204\cdot\beta+0.064\cdot\beta^2)\cdot 2\gamma^{(1.377+1.715\cdot\beta-1.103\cdot\beta^2)}\cdot\tau^{0.75}$
C	$SCF=(0.077-0.129\cdot\beta+0.061\cdot\beta^2-0.0003\cdot 2\gamma)\cdot 2\gamma^{(1.565+1.874\cdot\beta-1.028\cdot\beta^2)}\cdot\tau^{0.75}$
D	$SCF=(0.208-0.387\cdot\beta+0.209\cdot\beta^2)\cdot 2\gamma^{(0.925+2.398\cdot\beta-1.881\cdot\beta^2)}\cdot\tau^{0.75}$
A,E	$SCF=(0.013+0.693\cdot\beta-0.278\cdot\beta^2)\cdot 2\gamma^{(0.790+1.898\cdot\beta-2.109\cdot\beta^2)}$
SCFs for T- and X-joints, with loads on the chord (SCF_{m0} , SCF_{a0})	
LINE	
C	$SCF=0.725\cdot 2\gamma^{0.248\cdot\beta}\cdot\tau^{0.19}$
D	$SCF=1.373\cdot 2\gamma^{0.205\cdot\beta}\cdot\tau^{0.24}$
B,A,E	negligible i.e.: $SCF=0$
Range of validity:	
$0.35 \leq \beta \leq 1.0$ $12.5 \leq 2\gamma \leq 25.0$ $0.25 \leq \tau \leq 1.0$ $1.0 \leq r/t \leq 4.0$	
Minimum SCFs for the brace:	
$SCF_{a1}, SCF_{m1} \geq 2.0$	
X-joints, $\beta=1.0$:	
line C $SCF_{a1}=0.65\cdot SCF_{formula}$ line D $SCF_{a1}=0.50\cdot SCF_{formula}$	
Fillet welds: (if β is close to 1.0, line A cannot have a fillet weld)	
lines A,E $SCF_{a1,m1}=1.40\cdot SCF_{formula}$	

Table 19. SCF formulae for T- and X-joints made with square hollow sections, linear extrapolation	
SCFs for T- and X-joints, loaded by a bending moment on the brace (SCF_{m1})	
LINE	
B	$SCF=(-0.005+0.054\cdot\beta-0.047\cdot\beta^2)\cdot 2\gamma^{(1.596+1.798\cdot\beta-1.310\cdot\beta^2)}\cdot\tau^{0.75}$
C	$SCF=(0.826-4.694\cdot\beta+4.109\cdot\beta^2+0.0899\cdot 2\gamma)\cdot 2\gamma^{(-0.721+4.797\cdot\beta-4.038\cdot\beta^2)}\cdot\tau^{0.75}$
D	$SCF=(-0.035+0.273\cdot\beta-0.221\cdot\beta^2)\cdot 2\gamma^{(1.930-0.728\cdot\beta+0.373\cdot\beta^2)}\cdot\tau^{0.75}$
A,E	$SCF=(0.396-1.066\cdot\beta+1.119\cdot\beta^2)\cdot 2\gamma^{(-0.148+4.380\cdot\beta-3.648\cdot\beta^2)}$
SCFs for T- and X-joints, loaded by an axial force on the brace (SCF_{a1})	
LINE	
B	$SCF=(0.125-0.178\cdot\beta+0.057\cdot\beta^2)\cdot 2\gamma^{(1.394+1.794\cdot\beta-1.280\cdot\beta^2)}\cdot\tau^{0.75}$
C	$SCF=(0.068-0.125\cdot\beta+0.063\cdot\beta^2-0.0002\cdot 2\gamma)\cdot 2\gamma^{(1.596+1.802\cdot\beta-0.853\cdot\beta^2)}\cdot\tau^{0.75}$
D	$SCF=(0.168-0.310\cdot\beta+0.174\cdot\beta^2)\cdot 2\gamma^{(1.015+2.283\cdot\beta-1.931\cdot\beta^2)}\cdot\tau^{0.75}$
A,E	$SCF=(-0.067+1.075\cdot\beta-0.708\cdot\beta^2)\cdot 2\gamma^{(0.838+1.431\cdot\beta-1.573\cdot\beta^2)}$
SCFs for T- and X-joints, with loads on the chord (SCF_{m0} , SCF_{a0})	
LINE	
C	$SCF=0.708\cdot 2\gamma^{0.229\cdot\beta}\cdot\tau^{0.20}$
D	$SCF=1.322\cdot 2\gamma^{0.195\cdot\beta}\cdot\tau^{0.24}$
B,A,E	negligible i.e.: $SCF=0$
Range of validity:	
$0.35 \leq \beta \leq 1.0$ $12.5 \leq 2\gamma \leq 25.0$ $0.25 \leq \tau \leq 1.0$ $1.0 \leq r/t \leq 4.0$	
Minimum SCFs for the brace:	
$SCF_{a1}, SCF_{m1} \geq 2.0$	
X-joints, $\beta=1.0$:	
line C $SCF_{a1}=0.65\cdot SCF_{formula}$	
line D $SCF_{a1}=0.50\cdot SCF_{formula}$	
Fillet welds: (if β is close to 1.0, line A cannot have a fillet weld)	
lines A,E $SCF_{a1,m1}=1.40\cdot SCF_{formula}$	

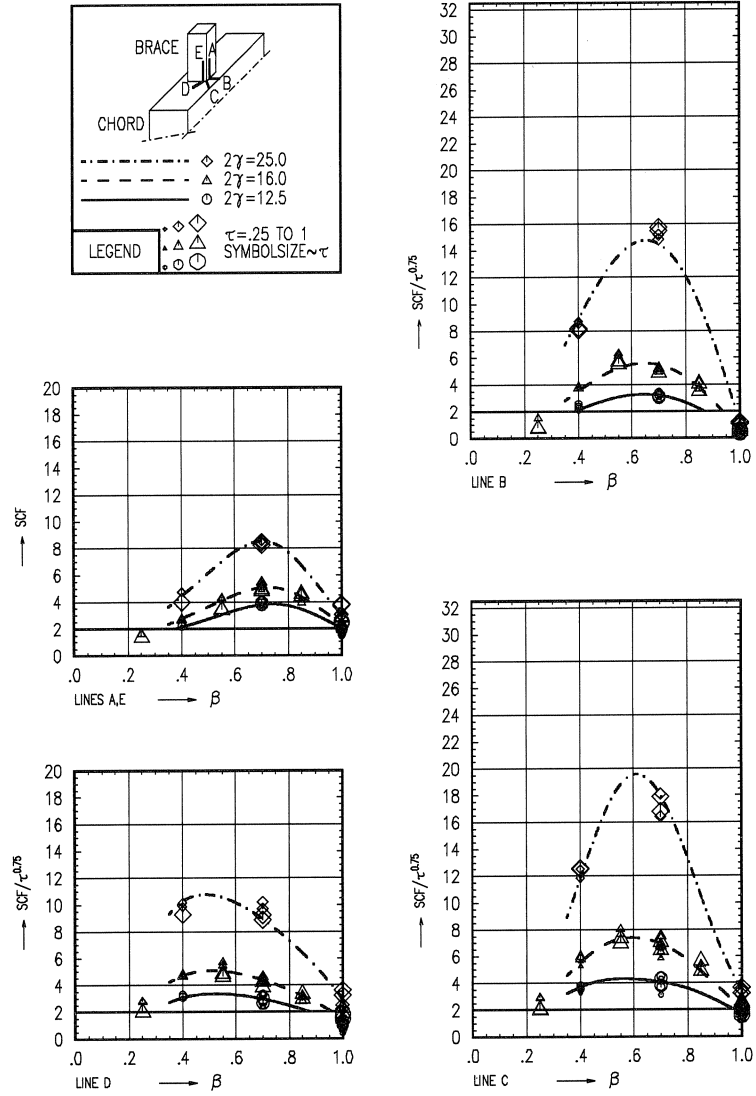


Figure 31. SCF T- and X-joints, loaded by an in-plane bending moment on the brace (SCF_{m1}), based on quadratic extrapolation.

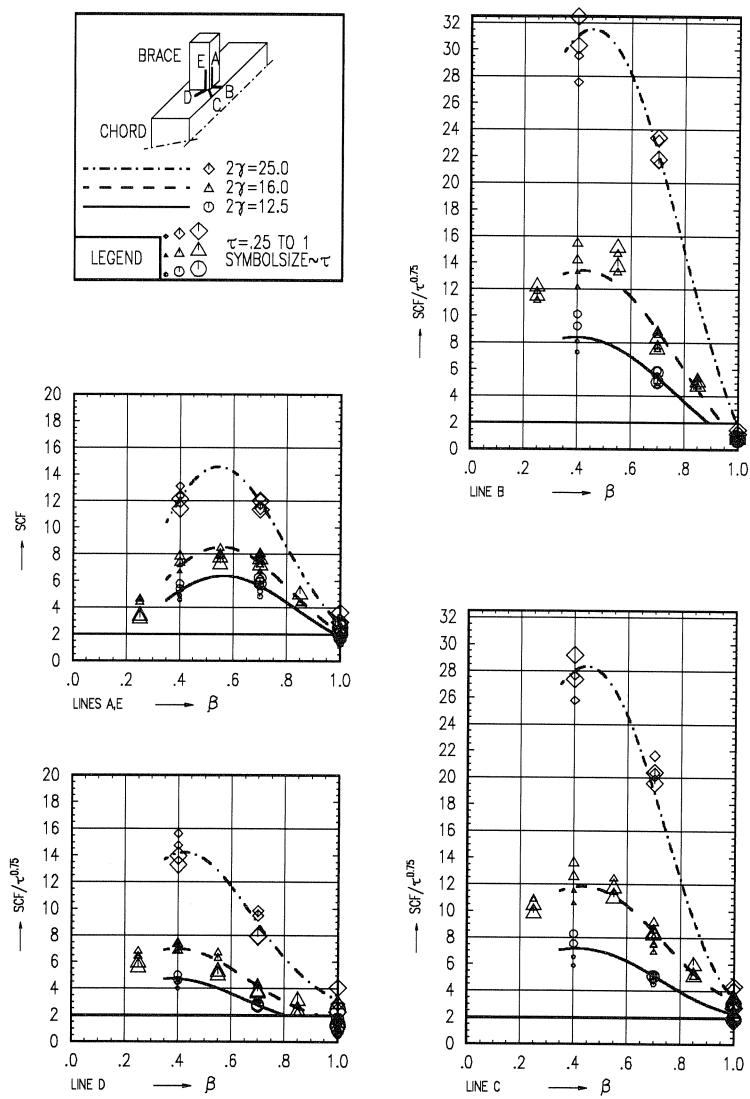


Figure 32. SCF T- and X-joints, loaded by an axial force on the chord (SCF_{a1}), based on quadratic extrapolation.

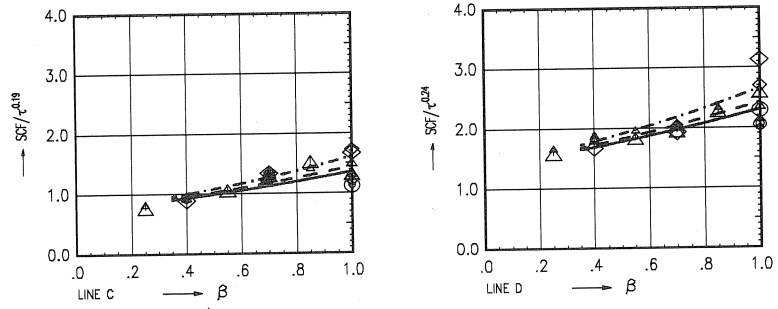


Figure 33. SCF T- and X-joints, loaded by an in-plane bending moment on the chord (SCF_{m0}), based on quadratic extrapolation.

6 INFLUENCE OF CORNER RADII AND WELD ON THE SCF

6.1 Introduction

In Chapter 5, parametric formulae for the designer have been established. However, the parametric study which forms the basis of the proposed design method concentrates entirely on butt welded joints with specific weld dimensions ($w_1=t_1+2$, $w_0=t_1/2$) and corner radii ($r/t=1$ to 2, depending on b) only. As different manufacturers supply rectangular hollow sections with different corner radii and as different welding standards and weld types demand different weld dimensions, it is important that the influence of variations of corner radii and weld dimensions on the SCFs as determined by the parametric formulae is known. The need therefore arises to study the effect of different corner radii and welds with different dimensions on the stress concentration factor and compare the results to the parametric formulae, in order to extend the range of application.

In principle, according to the method described in Chapter 5.1, many combinations of β , 2γ , τ , r_0 , r_1 , w_0 and w_1 for welds with and without full wall penetration should be analysed. Studying 3 cases per parameter results in $3^8=6561$ combinations per type of joint and per load case. The resulting parametric formulae would have to cover the complete range and incorporate terms for all parameters and cross terms. It is obvious that the number of FE analysis required, the subsequent statistical analysis and the resulting complexity of the parametric formulae effectively prohibit application of this method.

Therefore a simpler form is used for the parameters r_0 , r_1 , w_0 , w_1 and wall penetration. This is based on variation of the parameter considered on a basic geometry. To allow for a study of the interaction between β , 2γ , τ and the parameter considered, this is done for 7 basic geometries, listed in Table 20. Four geometries study the effect of the β ratio for $2\gamma=16$ and $\tau=0.5$. For $\beta=0.7$ and $\tau=0.5$, two additional values of 2γ are considered, namely $2\gamma=12.5$ and $2\gamma=25$, in order to get an impression of the influence of 2γ . The influence of τ is studied by including a joint with $\tau=1.0$ for $2\gamma=16$ and $\beta=0.7$. All studies were carried out on T-joints with an axial load on the brace. Therefore, this method does not cover interactions between, for instance, variations in r_0 and r_1 .

Table 20. Basic geometries, used for the investigation of the influence of corner radii and weld										
CHORD (mm)			BRACE (mm)			Non-dimensional parameters			Weld Size (external)	
b ₀	t ₀	r ₀	b ₁	t ₁	r ₁	β	2γ	τ	w ₀	w ₁
200	12.5	25.0	50	6.3	6.3	0.25	16.0	0.50	3.2	8.3
200	12.5	25.0	80	6.3	6.3	0.40	16.0	0.50	3.2	8.3
200	12.5	25.0	110	6.3	8.8	0.55	16.0	0.50	3.2	8.3
200	12.5	25.0	140	6.3	8.8	0.70	16.0	0.50	3.2	8.3
200	8.0	16.0	140	4.0	5.6	0.70	25.0	0.50	2.0	6.0
200	16.0	32.0	140	8.0	11.2	0.70	12.5	0.50	4.0	10.0
200	12.5	25.0	140	12.5	17.5	0.70	16.0	1.00	6.3	14.5

6.2 Setup of the numerical work

Analyses carried out

- In order to study the influence of the brace corner radius, 4 FE analyses per basic geometry have been carried out with $r_1/t_1 = 1, 2, 3$ and 4 respectively.
- The influence of the chord corner radius is studied by carrying out 4 FE analyses per basic geometry with $r_0/t_0 = 1, 2, 3$ and 4 respectively.
- In order to investigate the influence of the weld, all basic geometries are investigated for 3 welds (see Figure 34):
 - fillet welds ($w_0=w_1=t_1 \cdot \sqrt{2}$)
 - fillet welds with full wall penetration ($w_0=w_1=t_1 \cdot \sqrt{2}$)
 - butt welds ($w_0=t_1/2, w_1=t_1+2$), as used in Chapter 5.

As a consequence of the choice of parameters, some sections are outside the normal manufacturing ranges. These cases, which all have $r_0/b_0 > 0.25$ or $r_1/b_1 > 0.25$ are shown as dashed lines in Figures 36 and 37 and are commented upon wherever necessary.

Measurement lines considered

Because of the definition of lines A to E (see Figure 4), the position shifts with r_1 (see Figure 35), so that lines A and E coincide for $r_1=3.41 t_1$ and for larger brace corner radii even cross each other. For the establishment of parametric formulae for the brace, lines A and E have been combined by always choosing the higher SCF of the two, see Chapter 5. For all cases considered in this chapter, line A has higher SCFs than line E (see Table 13). Therefore, line E is not considered in this chapter.

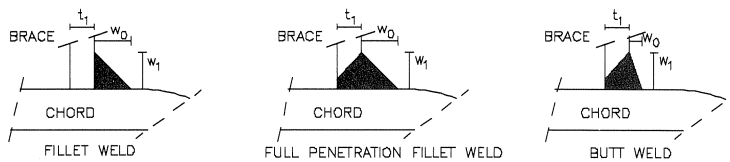


Figure 34. Types of weld investigated.

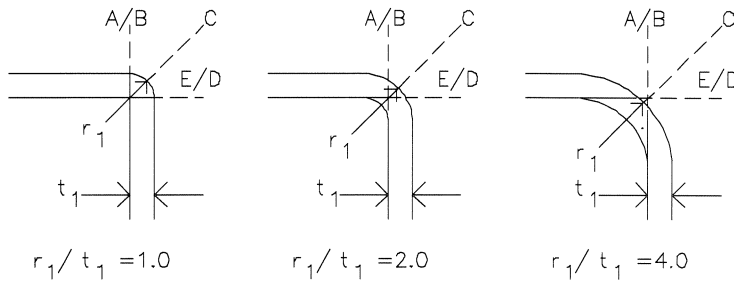


Figure 35. Relationship between r_1 and the position of lines A to E.

6.3 Influence of the corner radii on the SCF

For the corner radii, the ratio of SCF/SCF_{formula} is plotted against the radius divided by the radius used for the determination of the formulae, as presented in Table 20. This presentation in Figures 36 and 37 shows directly the influence of the corner radius compared to the accuracy of the formulae, as for $r=r_{\text{formula}}$, the SCF obtained should be SCF_{formula} . It should be noted that the formulae can sometimes give a deviation of up to 20%, compared to the FE analyses on which they are based, due to the curve fitting (see also Figures 31 to 33). After exclusion of the unrealistic geometries ($r/b > 0.25$), shown as dashed lines in Figures 36 and 37, the general tendencies can be given for the influence of r_1 and r_0 on the SCFs of lines A, B, C and D. These tendencies are summarized in Table 21, by giving the relative change in SCF per relative change in corner radius, ie. the slope of the lines in Figures 36 and 37. The slope is the change in SCF (in %) when r is changed by r_{formula} (for instance from 1 to 2 times r_{formula}).

Table 21. Influence of corner radii on the SCF									
CHORD CORNER RADIUS					BRACE CORNER RADIUS				
average SCF/SCF_{formula}					average SCF/SCF_{formula}				
r/r_{formula}	LINE A	LINE B	LINE C	LINE D	r/r_{formula}	LINE A	LINE B	LINE C	LINE D
0.75	1.07	1.04	1.03	1.12	0.52	1.07	1.03	0.96	1.10
2.86	0.90	0.91	0.90	0.92	2.00	0.78	0.84	0.88	1.15
$\frac{\Delta SCF(\%)}{\Delta r}$ (SLOPE)	-12	-9	-9	-14	$\frac{\Delta SCF(\%)}{\Delta r}$ (SLOPE)	-14	-9	-4	+2

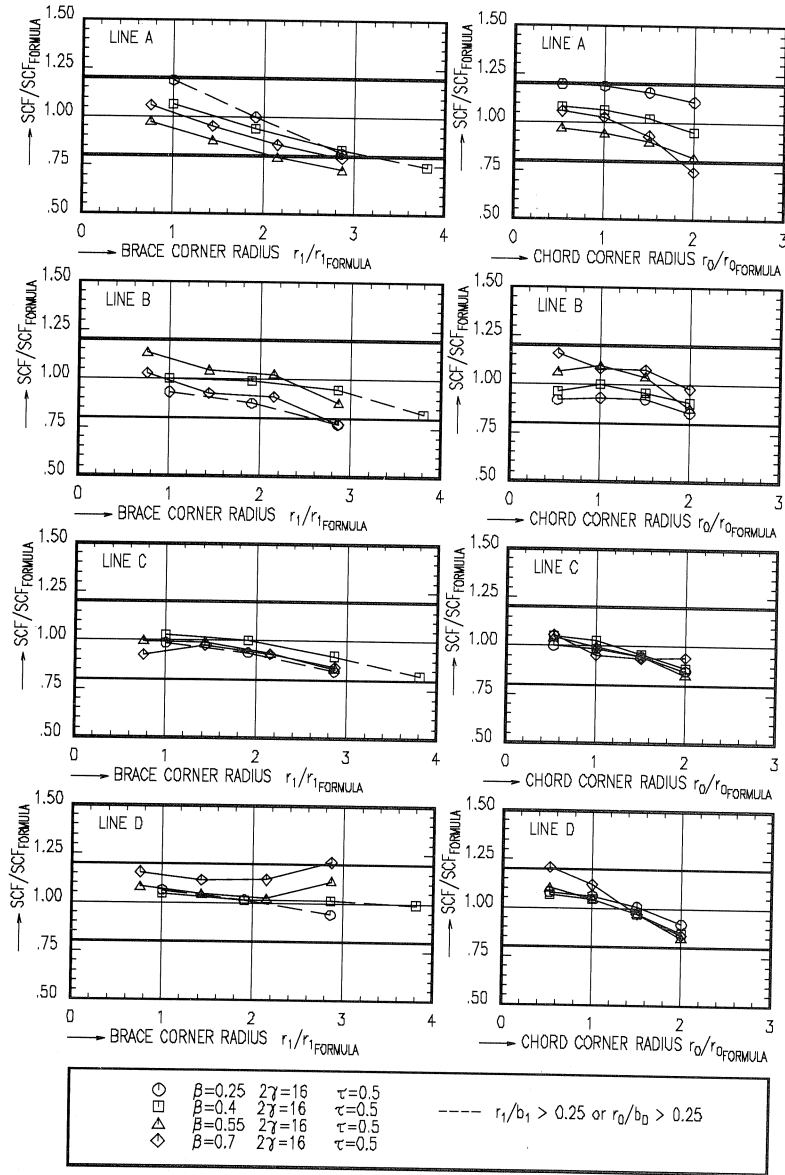


Figure 36. Influence of r_0 and r_1 on the SCF for various values of β .

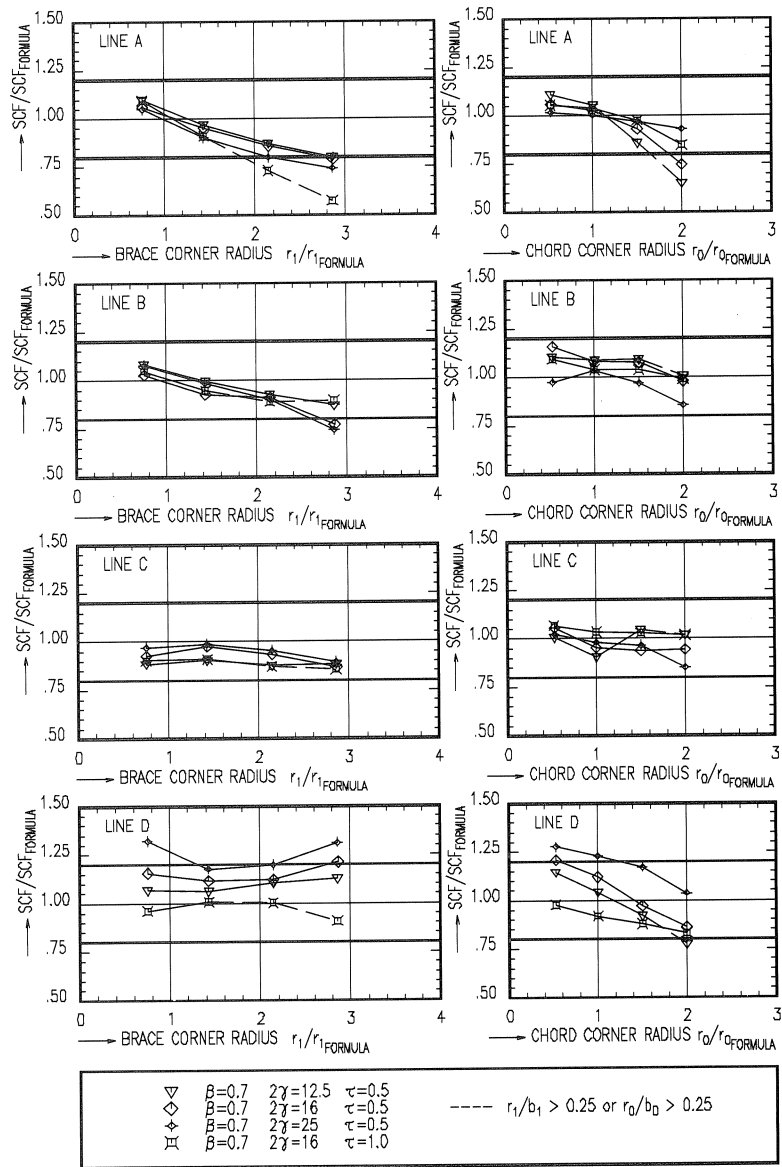


Figure 37. Influence of r_0 and r_1 on the SCF for various values of 2γ and τ .

Influence of the corner radius of the brace on the SCF

Of all brace corner radii investigated, only a few cases differ substantially more than 20% from the formulae. This is only the case for $r_1/t_1=4$ and as the SCFs are lower than the parametric formulae, the formulae are safe. The only substantial underestimation is line D, $2\gamma=25$ $\beta=0.7$. This is mainly caused by the parametric formula, which slightly underestimates the SCF in this case.

Relationship between the SCF and the brace corner radius per line.

Line A A clear influence can be found, independent of the geometry. The SCF decreases somewhat linearly with increasing r_1 for all geometries investigated, allowing a correction factor to be established.

Line B The influence is smaller than for the brace and slightly non-linear in r_1 .

Line C The influence of the corner radius of the brace on the SCF along line C is rather small for all geometries investigated.

Line D The average influence of the brace corner radius for line D is small, but varies for different geometries. Especially for larger values of β and 2γ , there appears to be an increase of SCF with increasing brace corner radii. No uniform correction factor can be given or seems necessary.

Influence of the corner radius of the chord on the SCF

The comparison of the FE analyses with the parametric formulae shows aspects which are very similar to the observations for the influence of the brace corner radii. Only a few cases differ substantially more than 20% from the formulae. This is only the case for $r_0/t_0=4$ and as the SCFs are lower than the parametric formulae, the formulae are safe. The only underestimation is found for line D, $2\gamma=25$ $\beta=0.7$ (as was the case for the influence of the brace corner radius).

Relationship between the SCF and the chord corner radius per line.

Line A The SCF is not linearly dependent on r_0 . An influence can be found, which is dependent on the geometry. A correction factor can be established, but in order to be accurate, β , 2γ and τ may have to be incorporated.

Line B The influence is strongly dependent on the geometry of the joint and non-linear in r_0 .

Line C The influence of the chord corner radius on the SCF along line C is linear in r_0 and constant for various β ratios. But for smaller values of 2γ the relationship between the SCF and r_0 is not very clear.

Line D The SCF decreases somewhat linearly with increasing r_0 so that a correction factor could be established.

6.4 Influence of the weld on the SCF

Influence of the type of weld on the SCF

The first comparison, shown by the filled symbols in Figure 38, is between a normal fillet weld ($w_0=w_1=t_1\sqrt{2}$) and a fillet weld with the same external weld dimensions, but with full wall penetration. As can be seen in Figure 38, the influence of the full wall penetration on the SCF is negligible in all cases investigated. The fillet welded joints with full wall penetration and the fillet welds with the same weld dimensions and joint geometry but no wall penetration have virtually the same SCF.

Influence of the shape of the weld on the SCF

The influence of the size of the weld is more important (the open symbols). Two cases are analysed, namely $w_0=t_1/2$, $w_1=t_1+2$ (a typical butt weld size) and $w_0=w_1=t_1\sqrt{2}$ (a typical fillet weld size, but with full wall penetration). In case t_1 is small, the weld dimension along the brace w_1 is about the same for both weld shapes: $t_1+2\approx t_1\sqrt{2}$ (less than 10% difference if $3.5 \leq t_1 \leq 7$ mm), so that the main difference between both weld shapes occurs for w_0 . For the case with $\tau=1.0$ ($t_1=12.5$ mm), $w_1=14.5$ mm for the butt weld shape and 17.68 mm for the fillet weld shape, a difference of about 20%. As can be seen in Figure 38 and Table 22, the difference in weld dimensions has an important influence on the SCF.

Relationship between the SCF and the weld dimensions per line

- | | |
|------------|---|
| Line A | The SCFs of the fillet weld dimensions were about 33% higher than those of butt welded joints with the same geometry. The recommended factor of 1.4 for the determination of the SCF of fillet welds for line A [3] is confirmed by the results. |
| Line B,C,D | For $\beta < 0.7$ the SCFs of fillet welded joints were generally slightly lower than for butt welded joints (15% on average). For $\beta = 0.7$ the SCFs were 35% lower. For the geometry with $\tau = 1.0$, the difference was even larger (50%). So the SCFs in the chord were generally lower for fillet welded joints, but the differences with butt welded joints varied from 0 to 50%, depending upon the joint geometry. |

Table 22. Influence of the weld on the SCF				
$SCF_{\text{fillet weld}}/SCF_{\text{butt weld}}$				
	LINE A	LINE B	LINE C	LINE D
minimum	1.32 (1.22)	0.66 ¹ (0.45)	0.73 ² (0.63)	0.79 (0.62)
maximum	1.37	0.99	0.93	0.88
average	1.33	0.84	0.85	0.83

Note: $\tau=1.0$ in brackets and not used to determine to average.

- ¹ $\beta=0.7$, $2\gamma=12.5$ or 16.0 ,
² $\beta=0.7$, $2\gamma=16.0$

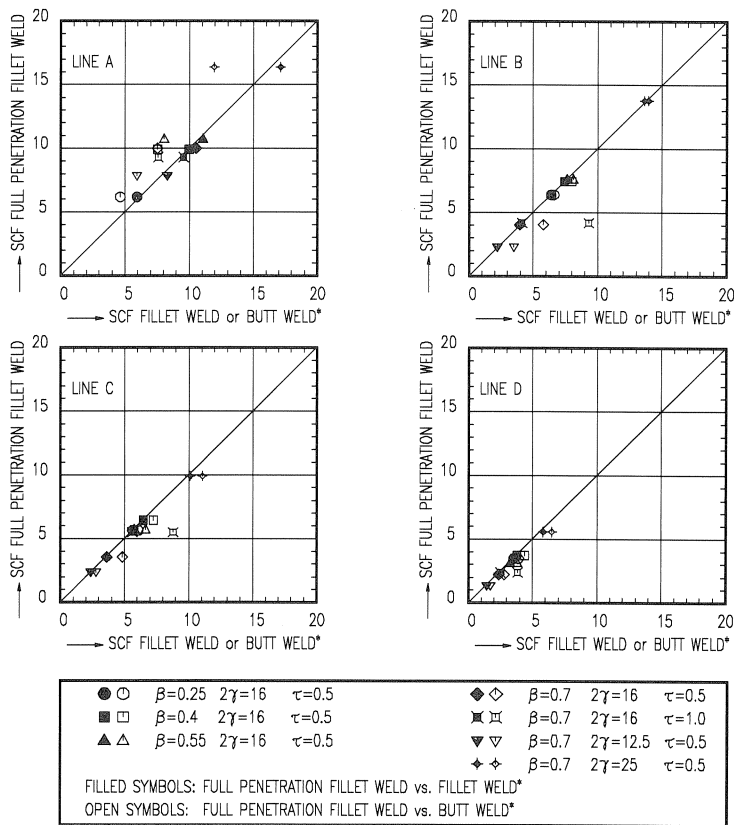


Figure 38. Influence of the weld penetration and weld dimension on the SCF.

Experimental data on the influence of the corner radii

No experiments have been carried out to verify the numerically determined influences of corner radii in this research programme. However, some experimental evidence is provided by tests carried out on K-joints. Some of the joints were made of hot finished sections, other joints were made from cold finished sections (the latter usually having a larger corner radius). In this case the cold formed sections had a slightly better fatigue behaviour. This is in agreement with the numerical investigations which generally predict lower SCFs for larger corner radii. See Figure 39 (taken from an earlier research programme [74, 83]). In other cases, the slightly larger wall thickness in the corners of hot finished sections, which is known to decrease the SCFs [13], might cause the hot finished sections to exhibit a slightly better behaviour than cold finished sections.

Influence of corner radii

The influence of the corner radii is usually within the scatter band of the parametric formulae, as shown in [119]. For some lines, the correction factor would be dependent on the joint geometry (requiring extensive additional investigations to cover the complete range of validity of the parametric formulae) and be non-linear in r . Incorporating all the influences would complicate the formulae considerably. Furthermore, differences in manufacture and fabrication of the joints tend to cause much larger differences (see Chapter 4, [120], [13]). Specifying an influence of the corner radii would also limit the designer in that a specified corner radius would have to be used in order to gain profit in terms of lower SCFs.

Influence of the weld

The parametric formulae determined in Chapter 5 can be used for fillet welded joints, provided that the SCFs found from the formulae for lines A and E in the brace are multiplied by a factor of 1.4. To profit from the favourable influence of the weld dimensions on the SCFs in the chord, additional research would be necessary. Based upon the limited number of geometries investigated, no general correction factor can be given for the chord.

Results

As a result, the parametric formulae from Chapter 5, together with correction factors on the SCF in case of fillet welds of 1.4 for the brace and 1.0 for the chord are recommended for fillet welded joints. These correction factors are given in Tables 18 and 19.

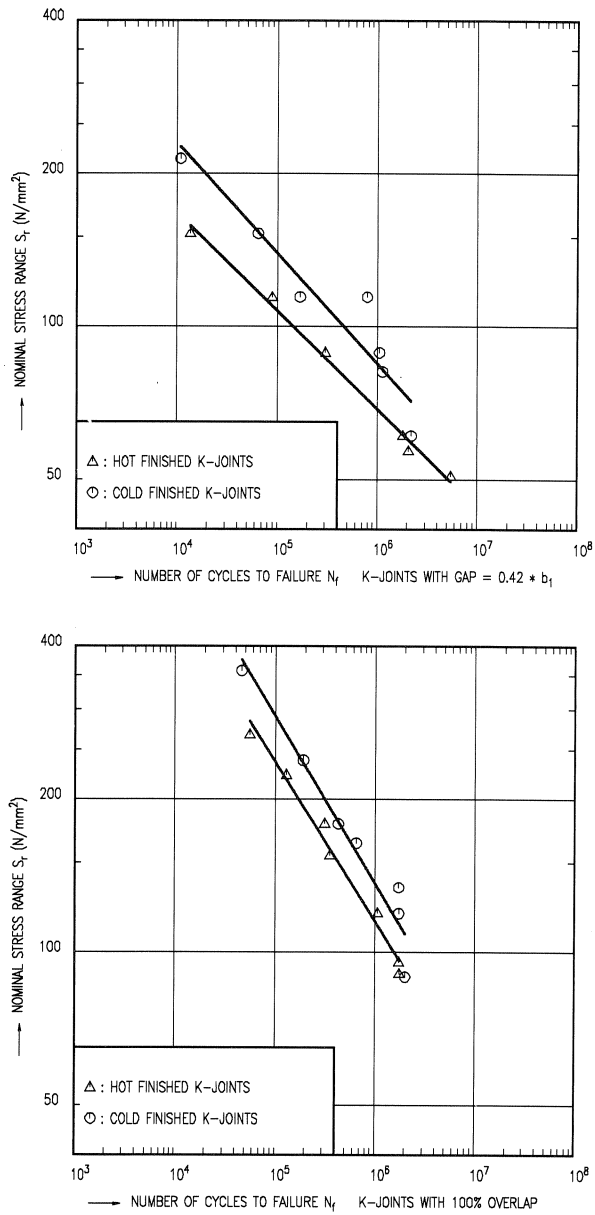


Figure 39. Test results on hot and cold finished K-joints [74, 83]

7 ESTABLISHMENT OF $S_{r_{h.s.}}$ - N_f LINES AND THICKNESS EFFECT

7.1 *Establishment of the S-N line based on experimental data*

After closer inspection of the available results and further analysis, the following data have been excluded from the main data base and marked in Tables 1 and 4:

- For the X-joints loaded by an in-plane bending moment on the brace, the welding at the joint started at the corners of the braces, except for one series of 4 joints X1Ba to X1Bd. All other series of test joints were welded according to accepted procedure, starting and stopping weld runs at the middle of the brace. All such joints where welding started at the corners are not used for the analysis.
- Furthermore, for the X-joints loaded by a bending moment, strain measurements were not carried out for all joints, so that the SNCF and SCF values have been used from one joint per test series with identical dimensions, where the measurements were carried out. All such data have been discarded from the main analyses based on measured hot spot stresses. However, they can still be used for the analysis based on the parametric formulae.
- Testing of joint X38 was abandoned since the test rig required repeated repair due to the large fatigue strength of the joint.

The remaining experiments which can be used consist of 13 axially loaded X-joints, 24 axially loaded T-joints as well as 4 X-joints loaded by an in-plane bending moment of which the hot spot strains were measured for only 1 specimen and 4 T-joints loaded by an in-plane bending moment. The test results are summarized in Table 4.

Other tests have been plotted in the $S_{r_{h.s.}}$ - N_f lines, but are excluded for the determination of the characteristic $S_{r_{h.s.}}$ - N_f lines.

- | | |
|----------------|---|
| Runouts: | the test was stopped before complete failure, because of large number of cycles to failure. |
| Weld failures: | the weld itself fails, rather than cracking of a member at the weld toe. |
| Overloads: | large loadings which can eliminate residual stresses and may influence the fatigue behaviour. |

These tests are marked in Tables 1 and 4 and by arrows in the $S_{r_{h.s.}}$ - N_f lines.

Figures 40 (based on quadratic extrapolation) and 41 (based on linear extrapolation) show a plot of $S_{h.s.}-N_f$ for all these data points, with the size of the symbols proportional to the wall thickness of the failed member in a joint. The influence of thickness can clearly be seen. A mean line is determined through all these points along with lines at ± 2 times the standard deviation, parallel to the mean line. As expected, the deviation from the mean is large. The line minus 2 times the standard deviation can be used as a characteristic line. For comparison, the characteristic lines of IIW line A [68] and the new DEn line [107] are plotted in for 16 mm thickness as well as the EC3 class 90 $S_{h.s.}-N_f$ line. Although not used in this work, the test results of K-joints also fit in nicely with the $S_{h.s.}-N_f$ lines derived in this chapter [3].

7.2 Establishment of the thickness effect

A statistical analysis has been carried out of all the data presented in Table 4, from which it was found that only the influence of wall thickness of the failed member in relation to the fatigue life (N_f) was significant.

The main data used in the analysis after exclusions as summarized in chapter 7.1, consists of 34 specimens, with wall thicknesses of 4, 5, 8, 12.5 and 16 mm. For the thicknesses considered (between 4 mm and 16 mm), there is sufficient evidence from earlier work [52, 112], the IIW rules [68] and the work by Van Delft, et al [45] on the European fatigue tests on tubular joints, that the slope of the $S_{h.s.}-N_f$ lines may vary with wall thickness. The difference in the two approaches is that in the IIW rules [68], the size effect is taken to begin at 10^4 cycles and increase with increasing N_f , while Van Delft, et al [45] assume the size effect to begin at 1 cycle. The latter approach gives simpler formulae, of the form as given by equation (7-1), which is why a similar approach is adopted here.

A large number of statistical analyses have been carried out to get an optimum constant x for the following thickness correction on the data points to an equivalent fatigue strength for $t=16$ mm:

$$S_{h.s.(16 \text{ mm})} = S_{h.s.(t \text{ mm})} \cdot (16/t)^{x \log_{10}(N_f)}$$

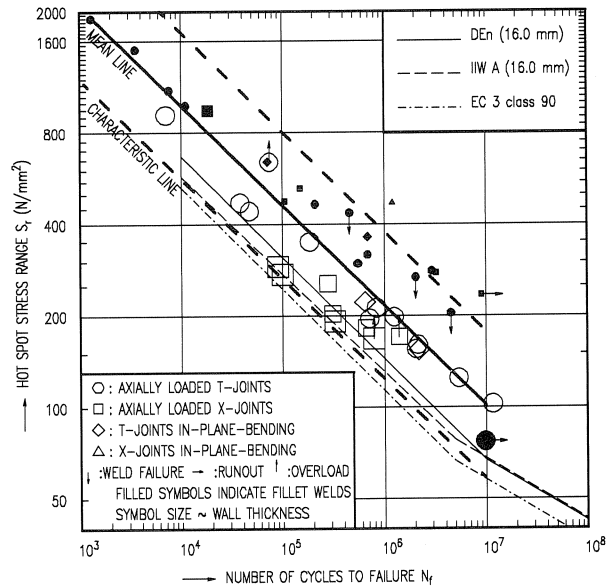


Figure 40. $S_{th.s.}$ - N_f line, based on tests, without thickness correction, quadratic extrapolation.

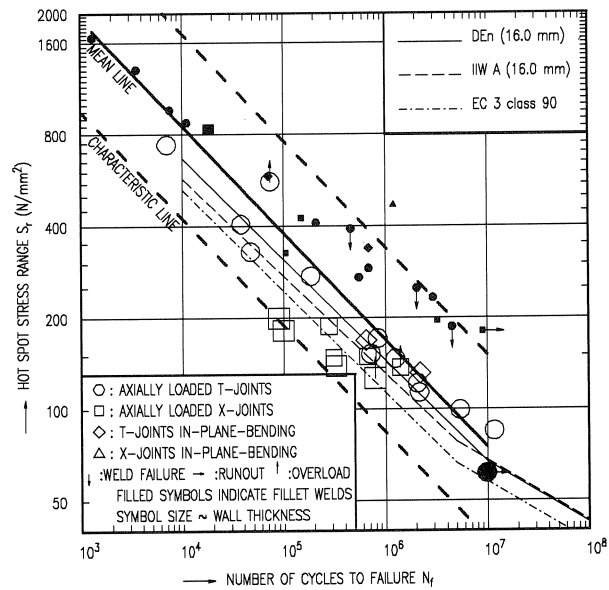


Figure 41. $S_{th.s.}$ - N_f line, based on tests, without thickness correction, linear extrapolation.

Then x is varied for all the analyses, until a minimal scatter in the $S_{r_{h.s.}}-N_f$ line is obtained. The optimum value of x is -0.11, so that the thickness correction for the data points is:

$$S_{r_{h.s.}(16 \text{ mm})} = S_{r_{h.s.}(t \text{ mm})} (16/t)^{-0.11 \log_{10}(N_f)} \quad (7-1)$$

Design $S_{r_{h.s.}}-N_f$ lines for other wall thicknesses can then be derived from the $S_{r_{h.s.}}-N_f$ line for $t=16$ mm by applying the equation above, rewritten to give a direct thickness correction relationship:

$$S_{r_{h.s.}(t \text{ mm})} = S_{r_{h.s.}(16 \text{ mm})} (16/t)^{0.11 \log_{10}(N_f)} \quad (7-2)$$

Applying equation (7-1) to the experimental data gives Figures 42 and 43 (for quadratic and linear extrapolation respectively), which shows the main data, plotted together with the mean line. The lines for 2 times the standard deviation are also plotted, parallel to the mean line.

The figures show that:

- The scatter is reduced very much by applying the thickness correction, as can be observed by comparing Figures 40 and 42 (or 41 and 43).
- The characteristic line for the test results for 16 mm thickness based on quadratic extrapolation (Figure 42) is slightly below the IIW and DEn lines.
- The 3 T-Joints with weld failures ($a = t_1$) were in this case not below the mean line.
- The joints that were accidentally overloaded for a few cycles also fit in nicely with the other results, with the exception of specimen T21, ($N_f=7.4 \cdot 10^4$) which seems to be influenced by the high peak load at the start of the test.
- In the case of runouts, the joints were sufficiently cracked, suggesting that the number of cycles to failure would be within the scatter band.
- Since the experiments contain butt welded and fillet welded specimens ($t_1 < 8$ mm), the $S_{r_{h.s.}}-N_f$ lines can be used for both types of weld.
- The experiments do not indicate the position of the fatigue limit for constant amplitude loading, since insufficient information is available in the high cycle area (for instance 10^8 cycles).
- The low cycle tests with hot spot stresses of up to $5\sigma_e$ are in the scatter band. This indicates that limitations of the hot spot stress range to $2\sigma_e$ as in the DEn design guide are not necessary.

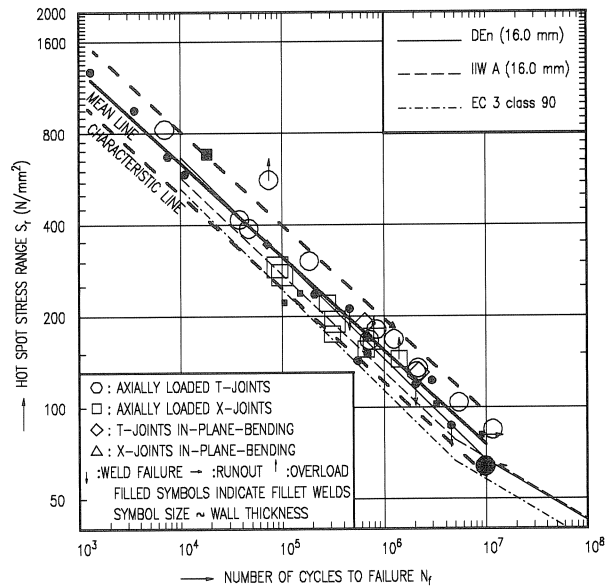


Figure 42. S_h - N_f line, based on tests, th. correction by $(t/16)^{0.11 \log N_f}$, quadratic extrapolation.

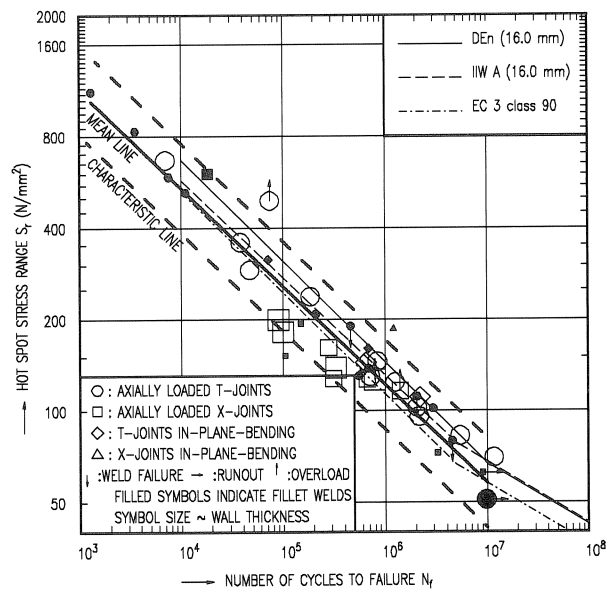


Figure 43. S_h - N_f line, based on tests, with th. correction by $(t/16)^{0.11 \log N_f}$, linear extrapolation.

Since the fatigue strength depends on the wall thickness, both chord and brace have to be checked for the critical locations in relation to the $S_{f,h.s.}$ - N_f line relevant to the thickness of the member considered. Therefore equation (2-2) has to be applied to locations A and E (combined) for the brace together with the $S_{f,h.s.}$ - N_f line for the brace wall thickness as well as for locations B, C and D for the chord, however now related to the $S_{f,h.s.}$ - N_f line for the chord wall thickness.

Because of the larger influence of welding defects, the equations are not valid for thicknesses below 4 mm, because, as shown in [3], the fatigue life is adversely affected for small thicknesses. This conclusion is also supported by earlier work [112].

7.3 Establishment of the $S_{f,h.s.}$ - N_f line based on the parametric formulae

In order to use the parametric formulae, the nominal stress range σ_r must be determined. This stress range is obtained by multiplying the nominal strain range ϵ_r from Table 4 with $1.1 \cdot E$. Multiplying this stress range with the SCF values, determined from the formulae (Table 18 for quadratic extrapolation or Table 19 for linear extrapolation) or graphs (Figures 31 to 33) gives the 'numerical' hot-spot stress range $S_{f,h.s.}$. These values have been adjusted to 16 mm thickness by using Equation (7-1) and plotted against the fatigue life determined from tests (Table 4) in Figure 44 (quadratic extrapolation) and in Figure 45 (linear extrapolation).

The SCFs in the brace for fillet welded specimens are about 1.4 times higher than for butt welded joints with the same basic geometry (see Chapter 6). Therefore the hot spot stresses in the brace are multiplied with this factor for fillet welded specimens. The same (existing) design $S_{f,h.s.}$ - N_f lines as plotted in Figures 40, 42, 41 and 43 are plotted in these figures as well. The $S_{f,h.s.}$ - N_f curve is determined using the highest SCF of the cracked member, applying the SCF formula for the nominal dimensions of the test specimen considered. Nearly all results for the axially loaded specimens (with the exception of X1) are above the characteristic lines IIW-A and DEn T'. However, in Figure 44, based on quadratic extrapolation, a few cases the results are slightly below the characteristic curves:

- The X-joint X1Bb with a bending moment on the brace had an SCF from the measurements of 4.76 (see Table 5). However, other measurements with an even smaller wall thickness in the chord (higher τ and 2γ) had SCFs of about 3, which agrees better with the parametric formulae (see Figure 31: the SCF in line A for $\beta=1.0$, $2\gamma=12.5$ is about 2.5). As the results of all experimental SCFs of the 4 data points of X-joints with a bending moment on the brace are based on a single measurement, and as this measurement seems to be out of range compared to other measurements, no evidence exists suggesting that the parametric formulae underestimate the SCF in this case.
- Specimen X12 is also low in the scatter band. This specimen had a higher measured SCF when compared to X9 to X11 (see Table 5), which had the same nominal dimensions. These 'individual' deviations due to different dimensions are of course not included in the parametric formulae, but they do influence the fatigue life. Therefore specimen X12 seems to exhibit a slightly worse fatigue behaviour when the SCF is determined by parametric formulae.
- Two other X-joints, X1 and X2 are also somewhat below the characteristic $S_{r_{h.s.}}-N_f$ lines, but this is also the case for the $S_{r_{h.s.}}-N_f$ lines, based on the experiments. Here, the agreement between measured SCFs and SCFs from the parametric formulae is good.
- Two T-joints, T17 and T18 were also rather low in the scatter band, but close enough to the DEn line and still above the IIW line.

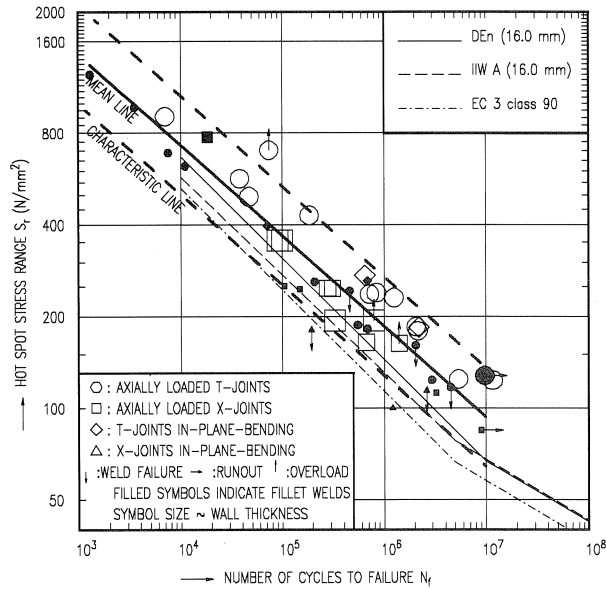


Figure 44. $S_{r,th.s.}$ - N_f line, based on σ_r and N_f from tests and SCF from formulae th. correction by $(t/16)^{0.11 \log N_f}$, quadratic extrapolation.

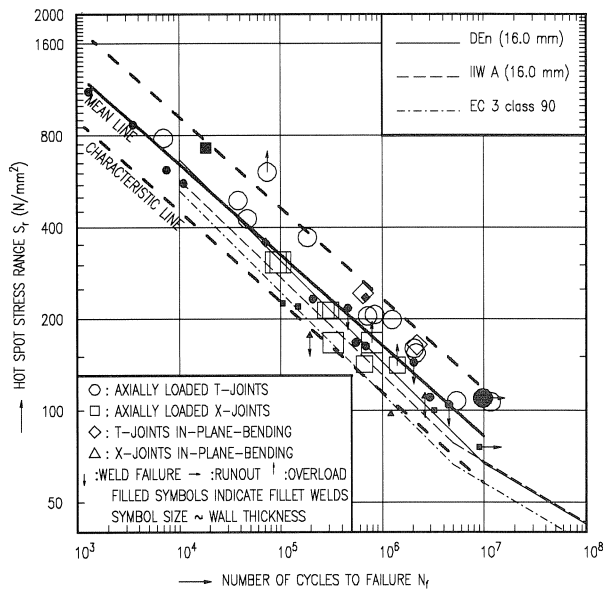


Figure 45. $S_{r,th.s.}$ - N_f line, based on σ_r and N_f from tests and SCF from formulae th. correction by $(t/16)^{0.11 \log N_f}$, linear extrapolation.

7.4 *Comparison between parametric formulae and experimental results*

The SCF values derived from the numerical analyses are, in general, higher than from the experimental work. It can be observed that the scatter band is slightly wider than for the tests. However, as the hot spot stress ranges found by applying the SCF formulae are generally higher (compare the mean lines in Figures 42 and 44), the characteristic line based on quadratic extrapolation is about the same.

There are different causes for this larger scatter in the $S_{t_{h.s.}}-N_f$ line, based on the parametric formulae:

- The FE analyses are based on nominal dimensions. In reality, the wall thickness in the corners was found to be 30% higher in some cases, causing significantly lower SCFs. See Chapter 4 and [13].
- The parametric formulae are based on curve-fitting through all data of T- and X-joints, with errors of about 20%. See Figures 31 to 33.
- The factor of 1.1 to convert from measured SNCFs to SCFs can vary, depending on the geometry (see Chapter 5.4).

7.5 Classification of the $S_{r_{h.s.}}-N_f$ line according to Eurocode 3, document 9.03

The $S_{r_{h.s.}}-N_f$ line to be used for the fatigue design of T- and X-joints between square hollow sections is determined by a statistical evaluation according to Eurocode 3, document 9.03 [43]. This document is established to determine fatigue strength curves for joints between structural hollow sections and is based on the following starting-points:

- Priority is given to full sized specimens (this is especially important for circular hollow sections).
- The governing parameters are the stress level and the number of cycles to failure. In case of the hot spot method, the stress level to be considered is the hot spot stress. Also, the thickness correction has to be taken into account, as shown in Figures 42 to 45.
- The minimum number of test specimens required is 12. In this case, the $S_{r_{h.s.}}-N_f$ line is based upon 34 data points.

The analysis is carried out as follows:

- 1) Only test results of specimens where strain gauge measurements were carried out are used for the statistical analysis to derive the classification according to EC3. Runouts, weld failures, overloads and specimens with incorrect weld sequence are excluded from the analysis.
- 2) A least squares fit is carried out, minimizing the error in N_f on the data points:

$$N_{f(i)} = a S_{r_{h.s., 16 \text{ mm}(i)}}^b, \text{ with } a \text{ and } b \text{ constants.}$$

This concept slightly deviates from the least squares fit used in the $S_{r_{h.s.}}-N_f$ lines in this work, as these $S_{r_{h.s.}}-N_f$ lines are based on a least squares fit on both $S_{r_{h.s.}}$ and N_f . This concept acknowledges that the scatter in the $S_{r_{h.s.}}-N_f$ lines has two causes:

- variation in N_f for a certain $S_{r_{h.s.}}$.
- variation in $S_{r_{h.s.}}$ itself, due to measurement and extrapolation inaccuracies, or inaccuracies of the parametric formulae.

This can be seen by comparing Figures 42 and 44: the same N_f is used for all the tests, but due to the slightly less accurate prediction of the $S_{r_{h.s.}}$ by the formulae, the scatter in Figure 44 is larger.

Also, the result of this least squares fit on both N_f and $S_{r_{h.s.}}$, is a slightly smaller scatter (the characteristic lines are closer together) and a better visual fit (the mean line fits better through the data points). A disadvantage of the least squares fit on both N_f and $S_{r_{h.s.}}$ is that this method is slightly more complicated.

- 3) Once the mean $S_{r_{h.s.}}-N_f$ line is established, the mean class is $S_{r_{h.s.}}$ at $N_f=2 \cdot 10^6$.
- 4) Now the characteristic class has to be determined with a confidence of 95%. For an infinite number of data points, this class would be the mean class-1.64 σ , with σ the standard deviation in N_f .

For less data points, a larger margin between mean class and characteristic class is required to fulfil the 95% confidence margin. Assuming a Student's " t " distribution of the residual of N_f , the characteristic strength is determined by the mean strength minus $t(95\%) \cdot \sigma$. The number of data points minus the number of degrees of freedom in the formulae $=34-7=27$. The percentile of the t distribution (95%) for 27 degrees of freedom is 1.73, so that the characteristic class is the mean class-1.73 σ .

The results of the analysis are given in Table 23 where the mean and characteristic classes based on linear and quadratic extrapolation are presented for the experiments with and without thickness correction, as well as for the formulae with thickness correction. Characteristic classes based on quadratic extrapolation and including the thickness of 95 and 97 are found for experiments and parametric formulae respectively. The nearest existing EC3 class is 90, therefore this is the most appropriate class for the hot spot stress based fatigue assessment of the joints covered in the work.

Table 23. Classes based on hot spot stress, according to EC3

Class	MEAN CLASS			CHARACTERISTIC CLASS		
Extrapolation method	Linear	Quadratic	L/Q	Linear	Quadratic	L/Q
Experiments, no thickness correction	119	160	0.74	54	87	0.62
Experiments, thickness correction	95	122	0.78	66	95	0.69
Stress from Formulae thickness correction	129	146	0.88	88	97	0.90

7.6 Comparison of $S_{r_{h.s.}}-N_f$ lines using linear and quadratic extrapolation

The difference in SCF between linear and quadratic extrapolation can be up to 40%, as can be observed in Figure 46, where the two extrapolations are compared to each other (for T-joints loaded by an in-plane bending moment on the brace).

Both linear and quadratic extrapolation were applied all through the research programme. This approach provides a solid basis for the choice of the extrapolation method. Rather than comparing the various steps in the process, such as the comparison between numerical and experimental results or the difference between the parametric formulae and the FE results, an overall comparison can be made. This is done by comparing the $S_{r_{h.s.}}-N_f$ lines based on the quadratic extrapolation method of Figures 40, 42 and 44 with Figures 41, 43 and 45, which are based on linear extrapolation.

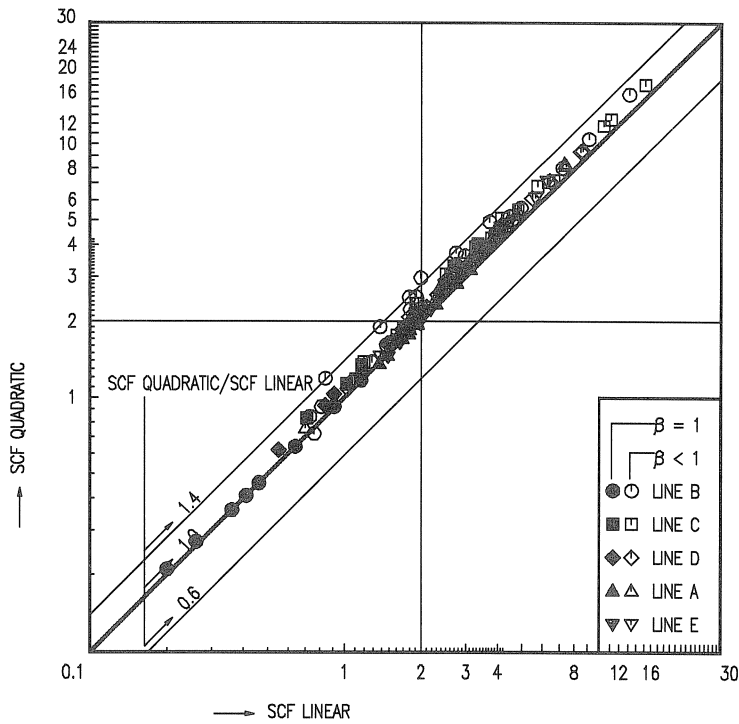


Figure 46. Comparison between linear and quadratic extrapolation for T-joints loaded by an in-plane bending moment on the brace.

Compared to the quadratic extrapolation, the mean $S_{t_{h.s.}}-N_f$ lines of the linear extrapolation are approximately 25% lower based on experimental SCFs and about 10% lower based on numerical SCFs. As the linear extrapolation for experiments gives about 25% lower SCFs and the parametric formulae give about 10% lower SCFs, the number of cycles found for a given geometry and nominal stress would be the same. However, the designer has to apply the characteristic lines (for instance 95% survival), so that the scatter of the lines becomes important. Looking at the characteristic lines the differences become clear: for experimentally determined hot spot stresses, the linear extrapolation gives about 35% lower results than the quadratic $S_{t_{h.s.}}-N_f$ line, due to a larger scatter in the $S_{t_{h.s.}}-N_f$ lines, compare Figure 42 with Figure 43. For the parametric formulae, the characteristic line is about 10% lower for linear extrapolation, as can be seen by comparing Figures 44 and 45.

So analysing an experiment on the basis of linear extrapolation with a given nominal stress would result in a 25% lower hot spot stress, to be used in conjunction with a 35% lower (on stress basis) $S_{t_{h.s.}}-N_f$ line. Hence the number of cycles to failure would correspond to that of an analysis based on quadratic extrapolation with a 10% higher nominal stress. If the analysis is carried out with the parametric formulae, the analysis based on linear extrapolation would give only 10% lower hot spot stresses, to be used with a 10% lower $S_{t_{h.s.}}-N_f$ line. So here the result would be the same as for an analysis on the basis of quadratic extrapolation.

Another way of comparing both extrapolation methods is shown in Table 23, where the ratio between the class based on linear and quadratic extrapolation is presented, to show quantitatively the difference between both methods.

The table confirms the advantage of quadratic extrapolation over linear extrapolation for evaluation of the experiments: the ratio between the characteristic class based on linear extrapolation and the characteristic class based on quadratic extrapolation is 0.69 (experiments with thickness correction). This is about 10% smaller than the ratio between the mean class based on linear extrapolation and the mean class based on quadratic extrapolation, which is 0.78. The difference in ratios indicates a larger scatter for linear extrapolation.

For the SCFs based on the parametric formulae the results for linear extrapolation are about the same.

Another advantage of the quadratic extrapolation is a better agreement between the characteristic $S_{r,h.s.}-N_f$ line based on experiments and the $S_{r,h.s.}-N_f$ line based on parametric formulae (compare the characteristic lines in Figures 42 and 44). This would allow one $S_{r,h.s.}-N_f$ line for experimentally determined hot spot stresses and the parametric formulae, without any correction factor being necessary.

This is confirmed by the classification according to EC3 as shown in Table 23: for quadratic extrapolation the characteristic class of the SCFs from experiments with thickness correction is 95 whereas the characteristic class of the SCFs from parametric formulae is 97. This would not be feasible for linear extrapolation without a correction factor on the parametric formulae being necessary, as the characteristic classes are 66 and 88 respectively.

Therefore, although the quadratic extrapolation is slightly more difficult to carry out and more sensitive to small changes in the data points, this method is preferred over linear extrapolation.

7.7 Comparison with parametric formulae derived by Soh

The only other parametric formulae available for the SCFs of T- or X-joints between square hollow sections are those recently derived by Soh and Soh [102]. Their parametric formulae (only valid for T-joints) are tabulated in Table 24.

Table 24. SCF formulae for T- and made with square hollow sections derived by Soh [102], including the influence of the bending moment on the chord (SCF_{m0}).	
SCFs for T-joints, loaded by a bending moment on the brace (SCF_{m1})	
Chord	$SCF = 0.6343 \cdot \beta^{1.173} \cdot 2\gamma^{1.347} \cdot \tau^{1.134} \cdot \alpha^{-0.248}$
Brace	$SCF = 0.7058 \cdot \beta^{0.880} \cdot 2\gamma^{0.952} \cdot \tau^{0.748} \cdot \alpha^{0.045}$
SCFs for T-joints, loaded by an axial force on the brace (SCF_{a1})	
Chord	$SCF = 0.2134 \cdot \beta^{0.701} \cdot 2\gamma^{1.304} \cdot \tau^{1.003} \cdot \alpha^{-0.283}$
Brace	$SCF = 0.3014 \cdot \beta^{0.312} \cdot 2\gamma^{0.875} \cdot \tau^{0.829} \cdot \alpha^{-0.017}$
Range of validity:	
$0.20 \leq \beta \leq 0.75$	
$15.78 \leq 2\gamma \leq 47.62$	
$0.40 \leq \tau \leq 1.00$	
$6.66 \leq \alpha \leq 36.66$	

A direct comparison between the formulae derived by Soh with the formulae derived in Chapter 5 is not straightforward since slightly different concepts were used. The formulae by Soh only give one value for the chord, which should be compared with the highest SCF of the lines B, C and D of this work. The Soh formulae are also used for the analysis of the X-joints, although the formulae are valid only for T-joints. The X-joints with an in-plane bending moment on the brace are even further outside the range of validity because for those joints $\beta=1.0$, whereas the Soh formulae are valid only for $\beta \leq 0.75$. Therefore, the comparison is carried out by plotting the resulting $S_{n.s.}-N_f$ line, based on N_f and σ_f from the experiments multiplied with the SCFs from the Soh parametric formulae [102].

Equation (7-1) from the experiments is applied to incorporate the thickness effect in the results. The correction factor for the SCF in the brace of fillet welded specimens is taken to be 1.4, analogous to the correction factor derived in Chapter 6. The resulting graph, shown in Figure 47, can then be compared to Figures 44 and 45.

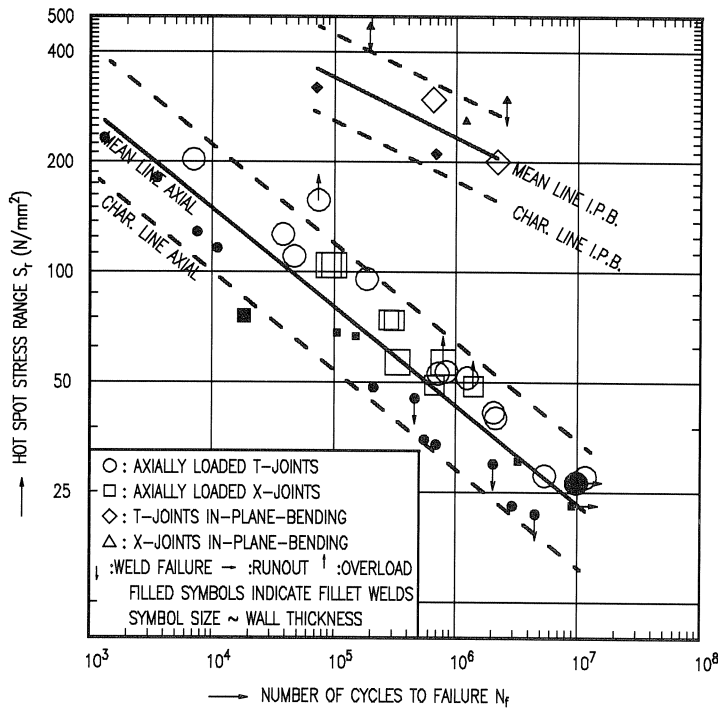


Figure 47. $S_{r,th.s.}$ - N_f line, based on σ_r and N_f from tests and SCF from the formulae of Soh, th. correction by $(t/16)^{0.11 \log N_f}$. These formulae are valid for T-joints only.

Influence of the chord length

The Soh formulae include the effect of the bending moment on the chord introduced by the axial force or in-plane bending moment on the brace, rather than establishing separate parametric formulae for that load case. Instead they contain a term for the influence of the chord length (even in case of an in-plane bending moment on the brace!).

According to the Soh parametric formulae the SCF in the chord decreases with increasing chord length. The SCF in the brace decreases also, but to a lesser degree.

Except for very short chords, where the end conditions influence the stress distribution in the joint, the result of a larger chord length is only a larger bending moment in the chord. Looking at Table 10, SCF_{m0} is negative for line B ($\beta \leq 0.70$) and in some cases in the brace. This might account for the negative exponent found by Soh and Soh. However, for lines C and D SCF_{m0} is positive, increasing the hot spot stresses at these locations for increasing chord length. In many practical cases the highest SCF occurs along lines C or D (see Table 6), so that the exponent in the α -term should be positive, rather than negative.

Comparison between T- and X-joints

The X-joints fit in quite nicely, although the formulae were not meant for this type of joint:

- For the brace, this is quite understandable, since X- and T-joints were found to differ mainly because of the bending moment in the chord, which does not influence the SCF in the brace (see chapter 5.2).
- For the chord, the bending moment in the chord, which causes the difference between T- and X-joints (see Chapter 5.2) does not seem to influence the governing SCF in the chord very much for the joints used in the experiments. For the T-joints, line D is governing the fatigue strength, due to the bending moment in the chord. However, the SCF in the T-joints along line D (see Table 6) was not much higher than the SCF along line B of the X-joints with the same non-dimensional parameters ($\beta=0.7$, $2\gamma=16$ and $\tau=0.64$). Therefore, for the joints tested in this research programme, the difference in SCF between T- and X-joints is not large.

Comparison of the Soh formulae with the formulae derived in Chapter 5

As can be seen by comparing Figures 47 and 45, the scatter in results of the analysis based on the Soh formulae is considerably larger than for the formulae derived in Chapter 5. There are several reasons for this:

- One reason for the scatter is the difference between axial loading and in-plane bending: the formulae for axial force give noticeably lower SCFs in comparison with the experiments. This causes the test specimens with an axial force on the brace to be significantly lower in the $S_{t.h.s.}-N_f$ lines than the specimens loaded by an in-plane bending moment. Figure 47 shows separate sets of mean and characteristic lines for axially loaded specimens and for specimens loaded by an in-plane bending moment.

- A second cause might be the correction factor for fillet welds. The thinner specimens are all at the lower bound of the scatter band, but the applied thickness correction comes directly from the experiments and does not work out bad for the Delft formulae of Chapter 5. However, the factor used for fillet welds does not have such a solid experimental basis. If a larger correction factor would be used, the overall scatter would be much less. However, the results in Chapter 6 do in no way hint that a larger correction factor might be justified.
- Especially serious is the result for test specimen X20, an axially loaded X-joint with $\beta=0.4$, $2\gamma=25$ and $\tau=0.5$ ($N_f=1.8 \cdot 10^4$). Although it is only one test result, the data point fitted in nicely with all other experimental or numerical $S_{r_{h,s}}-N_f$ lines, even to the higher bound of the scatter band. According to the Soh formulae, the fatigue strength of this joint is by far the worst among the axially loaded joints.

The cause for the discrepancy of especially X20 and maybe also for the thin walled joints (which have a different τ value) is probably the lack of interaction between the various non-dimensional parameters in the Soh formulae, as commented upon in Chapter 5.1. The basic geometric parameters of the Soh formulae are $\beta=0.50$, $2\gamma=30$, $\tau=0.64$, $\alpha=22$ and the angle between brace and chord 45° . First, the influence of β was studied by analysing $\beta=0.22/0.30/0.50$ (basic geometry)/ 0.60 and 0.75 , keeping all other parameters constant. Then the other parameters are analysed in turn, but never varied together. As a result, geometries that differ in more than one parameter from the basic geometry might not be properly analysed with the Soh formulae.

8 DESIGN RECOMMENDATIONS

8.1 *Proposed design rules*

In the previous chapters, parametric equations for the determination of the stress concentration factor SCF have been established, together with their range of validity and correction factors for axially loaded X-joints and fillet welds. Also, a basic $S_{t_{h.s.}}-N_f$ line ($t=16$ mm) according to the EC3 has been determined for use in combination with the parametric formulae (see Table 18) or with experimentally measured hot spot stresses. A thickness correction for $t < 16$ mm has been determined from the test results, whereas for $t > 16$ mm, the thickness correction of the new DEn design guidelines [93] is proposed to be retained in the absence of further information. In this chapter, the main aspects needed for the design recommendations are considered.

Scope

These recommendations concern the design and analysis of welded joints in braced structures and Vierendeel girders where rectangular hollow sections are used which may be either cold or hot finished. They cover structures using steel grades Fe 360, Fe 430 and Fe 510 in compliance with Euronorm 10025 or equivalent. The tolerances should conform to requirements given in ISO 657/XIV and ISO 4019.

Symbols, Notation and Definitions

The symbols and notations used in these design recommendations are the same as those used throughout this work. They are given after the introduction.

The definitions of fatigue related terms used in this chapter are given in Chapter 2.2

Stresses to be considered

For nodal joints consisting of braces and chords, the stress to be used for fatigue design is the range of hot-spot stress adjacent to the weld toe of the members. With experimental models or finite element analyses, care should be taken in obtaining geometric stress extrapolated to the weld toe as described in Chapter 2.5. In chapter 7, the linear and quadratic extrapolation are compared to each other. The quadratic extrapolation, as shown in Figure 5, is found to be more accurate because of the highly non-linear stress gradients obtained in RHS-joints.

The SCF values obtained from measurements, FE analyses or parametric formulae should be determined for all lines A to E, so that the position and value of the highest hot spot stress in the brace and in the chord can be found using the formula below for lines A to E :

$$S_{r.h.s.} = \sigma_{r_{m1}} \cdot SCF_{m1} + \sigma_{r_{a1}} \cdot SCF_{a1} + \sigma_{r_{m0}} \cdot SCF_{m0} + \sigma_{r_{a0}} \cdot SCF_{a0}$$

A minimum value of 2.0 should be taken for SCF_{a1} and SCF_{m1} . This is because the SCFs of line A to E can underestimate the "true" hot spot stress, as the stresses at other locations or in different directions can exceed the stresses along the lines of measurement. Also, the possibility of cracking from inside the member, which is especially critical for large values of β , is taken into account by this factor.

Determination of the hot-spot stress

The hot spots stress may be determined in three ways:

- 1) Through experimental model studies, where strips of strain gauges are to be positioned at the lines of measurement A to E, at a proper distance from the weld toe to allow enough strain gauges to be positioned within the area from which the quadratic extrapolation is carried out. For the determination of SNCFs, the nominal strain should be measured at least 2.5 b from the joint and end supports, to exclude the "end effects" from the measurement of the nominal strain. Extensive information on the test method used as a basis for the determination of the design guidelines described in this chapter can be found in reference [7, 12].
- 2) Applying finite element analysis. The mesh refinement should provide enough reliable information for the quadratic extrapolation along lines A to E. Near the corner of the weld, this means small elements, without sudden changes in size or a large aspect ratio, see Figure 26. The weld and corner radii should be modelled for the FE analysis and solid elements should be used to model at least the weld and the intersection area between brace and chord to ensure a proper definition of the weld toe. An analysis based solely on solid elements is preferred if the FE program used cannot provide a good interface between solid and shell elements. The FE models with mixed solid and shell elements have been found to occupy more disk space and consume more CPU time than FE models with only solid elements [95] for the same number of elements used. This is the case even though a FE model completely made up of solid elements has considerably more degrees of freedom [95].

In case of critical joints, a calibration of the FE model with experimental results is to be carried out, to ensure the validity of the results for use with this design method. The FE model and calibration with experiments is commented upon more extensively in [13 to 15].

- 3) Use of the parametric formulae, within their range of validity and applying the correction factors given in this chapter. The parametric formulae are restricted to T- and X-joints made of square hollow sections loaded by arbitrary combinations of axial forces or in-plane bending moments on the members.

The formulae and correction factors are summarized in Table 18.

Axially loaded X-joints with $\beta=1.0$ have lower SCFs than axially loaded T-joints with $\beta=1.0$, due to a direct transfer of forces from one brace to the opposite brace via the sides of the chord. This is taken into account by multiplying the SCFs from the parametric formulae along lines C and D for axially loaded X-joints with $\beta=1.0$ with 0.65 and 0.5 respectively.

Basic design $S_{h.s.}-N_f$ curve

The basic design $S_{h.s.}-N_f$ curve established for the hot spot stress based fatigue assessment of joints between square hollow sections is EC3 class 90. This line has $N_f = 2 \cdot 10^6$ cycles for a (hot spot) stress $S_{h.s.} = 90 \text{ N/mm}^2$ [53]. The $S_{h.s.}-N_f$ line can be used down to $N_f = 10^3$ cycles (see Figures 40 to 45 and Chapter 7.2). It is based on a wall thickness of 16 mm and can be used independent of stress ratio or type of weld.

For $N_f = 10^3$ to $N_f = 5 \cdot 10^6$, this line has a slope of 1:3.

- For joints with a constant amplitude loading in a non-corrosive environment, or with adequate protection against corrosion, a fatigue cut-off limit is adopted at $N_f = 5 \cdot 10^6$, so that the $S_{h.s.}-N_f$ line is horizontal.
- In case of random loading in a non-corrosive environment, or with adequate protection against corrosion when a linear cumulative damage calculation is used, the slope of the $S_{h.s.}-N_f$ line between $N_f = 5 \cdot 10^6$ and $N_f = 10^8$ is 1:5. After $N_f = 10^8$, the fatigue cut-off limit, the line is horizontal, therefore stress ranges below the value corresponding to the cut-off limit may be neglected.

The EC3 design recommendations do not apply for joints in a corrosive environment which are not adequately protected, therefore the IIW [68] and DEn [48] design recommendations are suggested. A penalty factor of 2 is to be applied on the fatigue life. Also the slope of the line remains 1:3 without any fatigue limit.

The American guidelines account for the effect of corrosion by adapting the fatigue limit: the API (for random loading in a sea environment) has a much higher fatigue limit than the AWS as shown in Figure 2.

Thickness correction factors

As noted in Chapter 7, a thickness correction factor is required in order to obtain the fatigue strength for other thicknesses.

The correction on $S_{t.h.s.}$ has to be made, between $N_f = 10^3$ and $N_f = 5 \cdot 10^6$.

$$t < 16 \text{ mm: } S_{t.h.s.}(t \text{ mm}) = S_{t.h.s.}(16 \text{ mm}) \cdot (16/t)^{0.11 \log_{10}(N_f)}$$

$$t > 16 \text{ mm: } S_{t.h.s.}(t \text{ mm}) = S_{t.h.s.}(16 \text{ mm}) \cdot (16/t)^{0.30}$$

After $N_f = 5 \cdot 10^6$, all the $S_{t.h.s.}$ - N_f lines are parallel to the line for $t=16$ mm, see Figure 48 for the appropriate $S_{t.h.s.}$ - N_f lines.

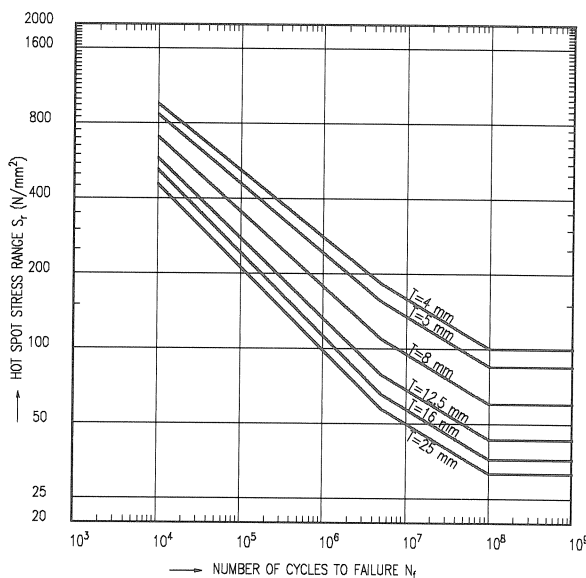


Figure 48. $S_{t.h.s.}$ - N_f lines according to EC3 class 90, th. correction by $(t/16)^{0.11 \log_{10} N_f}$.

Table 25 contains the equations for the $S_{r_{h.s.}}-N_f$ lines, for $N_f=10^3$ to 10^8 , inclusive of the thickness effect.

For thicknesses below 4 mm, welding imperfections may adversely affect fatigue strength. In earlier investigations for K-joints with a wall thickness of 2.9 mm, the thickness correction could only be used after applying a factor of 2.3 on $S_{r_{h.s.}}$ [3].

Another aspect is the extrapolation method which influences the hot spot stress of these joints, as the extrapolation is based on points that are at least 4 mm from the weld toe (see Chapter 2.4), which is relatively large for small wall thicknesses.

Table 25. Equations for the $S_{r_{h.s.}}-N_f$ lines		
t	N_f	$10^3 < N_f < 5 \cdot 10^6$
t<16mm	$10^3 < N_f < 5 \cdot 10^6$	$\log(S_{r_{h.s.}}) = \frac{1}{3} (12.151 - \log(N_f)) + \log\left(\frac{16}{t}\right) \cdot 0.11 \cdot \log(N_f)$ $\log(N_f) = \frac{12.151 - 3 \cdot \log(S_{r_{h.s.}})}{1 - 3 \cdot 0.11 \cdot \log\left(\frac{16}{t}\right)}$
	$5 \cdot 10^6 < N_f < 10^8$ (variable amplitude only)	$\log(S_{r_{h.s.}}) = \frac{1}{5} (15.786 - \log(N_f)) + \log\left(\frac{16}{t}\right) \cdot 0.737$ $\log(N_f) = 15.786 - 5 \cdot \log(S_{r_{h.s.}}) + 5 \cdot \log\left(\frac{16}{t}\right) \cdot 0.737$
t≥16mm	$10^3 < N_f < 5 \cdot 10^6$	$\log(S_{r_{h.s.}}) = \frac{1}{3} (12.151 - \log(N_f)) + \log\left(\frac{16}{t}\right) \cdot 0.30$ $\log(N_f) = 12.151 - 3 \cdot \log(S_{r_{h.s.}}) + 3 \cdot \log\left(\frac{16}{t}\right) \cdot 0.30$
	$5 \cdot 10^6 < N_f < 10^8$ (variable amplitude only)	$\log(S_{r_{h.s.}}) = \frac{1}{5} (15.786 - \log(N_f)) + \log\left(\frac{16}{t}\right) \cdot 0.30$ $\log(N_f) = 15.786 - 5 \cdot \log(S_{r_{h.s.}}) + 5 \cdot \log\left(\frac{16}{t}\right) \cdot 0.30$

Welding recommendations and correction factors

As the data base contains both fillet welds and butt welds, the $S_{r_{h.s.}}-N_f$ line is applicable to both types of welds. For use of the parametric formulae, the effect of the weld type is taken into account as a correction factor.

For fillet welded joints, the SCF from the parametric formulae for the brace (line A/E) should be corrected by the factors given below:

brace: lines A/E	:1.4
chord: lines B, C and D	:1.0 (no correction)

If welding of joints commences at the corners of the brace, instead of in the middle of the sides as in normal welding practice, the fatigue strength deteriorates. For $t=4$ mm, a factor of 2.0 should be applied to the $S_{r_{h.s.}}$ [3].

The connections at the welded joints should be carried out over the entire perimeter of the hollow sections by means of a full penetration weld, partial penetration weld, fillet weld, or a combination. Full penetration welds should be used if:

- The brace has a wall thickness larger than 8 mm.
- The angle at the toe of the brace is larger than 120°
- For $\beta=1.0$, fillet welds can only be used at the side of the brace perpendicular to the axis of chord. Therefore, the sides parallel to the chord axis should be welded by a full penetration butt weld.

Attention should be given to the proper selection of materials and the welding procedure. In order to avoid failure of the weld under static loading, the throat thickness of the fillet weld is equal to or greater than the wall thickness of the brace ($a \geq t_1$). For Fe 510 the throat thickness should exceed the brace wall thickness: $a \geq 1.1 \cdot t_1$. Recommended details of welds are given in Figure 7 (Chapter 3.2).

Partial safety factors

A safety factor has to be included depending on the type of structure (whether the joint is "fail-safe" or not), the inspection scheme and the accessibility of the joint. In Eurocode 3 [53], a partial safety factor has to be applied to the hot spot stress range. These partial safety factors are presented in Table 26.

Table 26. Partial safety factor γ_m according to EC3 on the hot spot stress range		
Inspection and access	'Fail-safe' structures	Non 'fail-safe' structures
Periodic inspection and maintenance. Accessible joint detail.	$\gamma_m = 1.00$	$\gamma_m = 1.25$
Periodic inspection and maintenance. Poor accessibility.	$\gamma_m = 1.15$	$\gamma_m = 1.35$

Design procedure

For each potential crack location the long term distribution of relevant stress ranges should be established and the probable fatigue life should satisfy the Palmgren-Miner's linear cumulative damage rule: $\sum n_i/N_i \leq 1.0$.

An arbitrary joint could be checked by following the steps given below, also shown in a concise flow chart in Figure 49.

1. Load and geometry of the joint should be determined first.
2. From simple formulae such as $\sigma_{a1} = F_1/A_1$, $\sigma_{m1} = M_1/W_1$ and $\sigma_{m0} = M_0/W_0$, the nominal stresses in the members can be determined.
3. Determine the joint parameters $\beta = b_1/b_0$, $2\gamma = b_0/t_0$ and $\tau = t_1/t_0$.
4. From the SCF formulae or graphs the SCFs for the various load cases can be determined for lines A to E.
5. Determine the hot spot stress for lines A to E from:

$$S_{h.s.} = \sigma_{t_{m1}} \cdot SCF_{m1} + \sigma_{t_{a1}} \cdot SCF_{a1} + \sigma_{t_{m0}} \cdot SCF_{m0} + \sigma_{t_{a0}} \cdot SCF_{a0}$$

Only the highest stress in the chord and the highest stress in the brace need to be considered.
6. The number of cycles to failure N_f for both brace and chord is obtained from the $S_{h.s.}$ - N_f line for the appropriate wall thickness. The lowest number of cycles in brace or chord determines the fatigue strength of the joint.

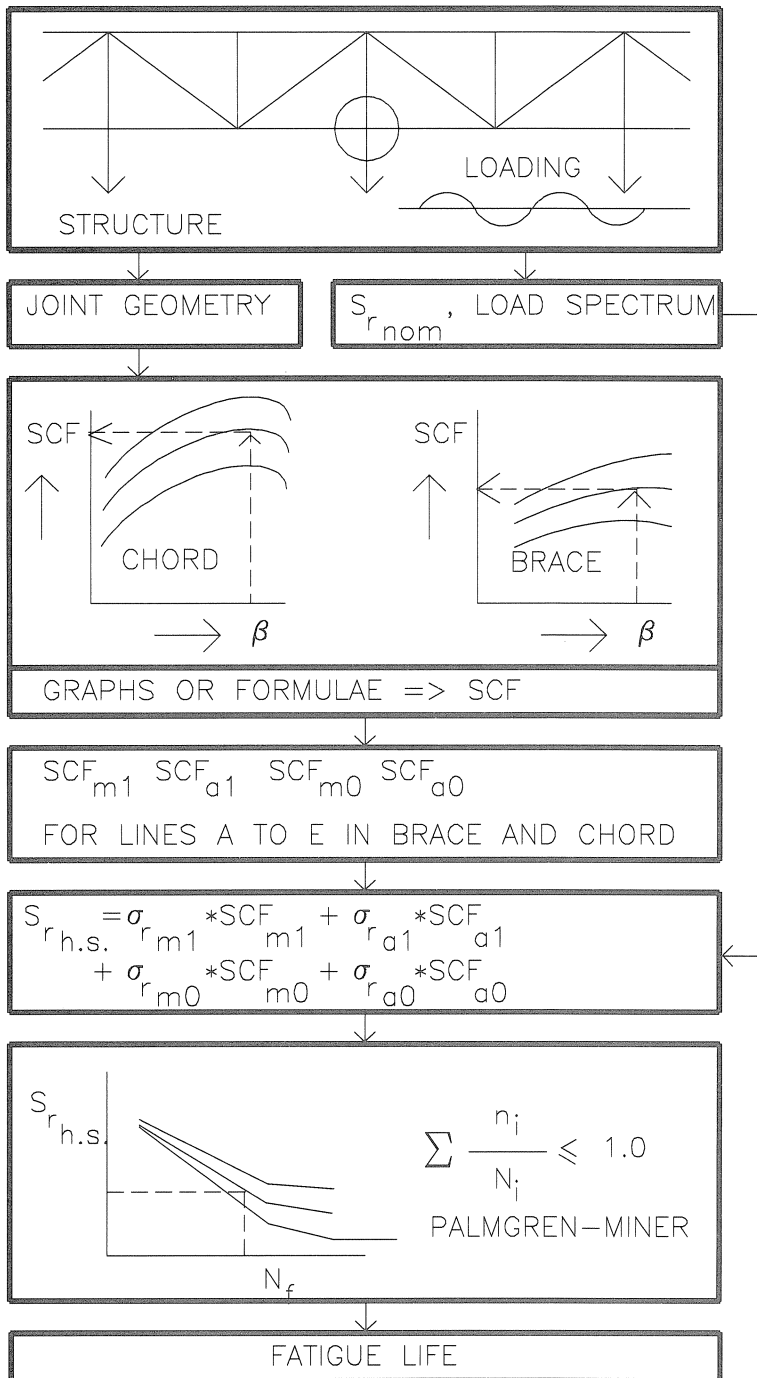


Figure 49. Design procedure for RHS T- and X-joints loaded in fatigue.

8.2 Comparison with existing design rules

Comparison of the $S_{r_{h.s.}}-N_f$ lines with the DEN and IIW design lines

The evaluation of the test results in Table 23 results in EC3 class 95, although class 90 is adopted for the design recommendations. Class 95 is about 20% lower than that for circular hollow section joints as given by the DEN $S_{r_{h.s.}}-N_f$ line [107] and 11% lower than the IIW $S_{r_{h.s.}}-N_f$ line [68], see also Chapter 2.7. This difference between CHS and RHS joints might be caused by the deviation of the direction of the principal stresses in comparison to the assumed measurement lines, in combination with a slightly lesser weld quality in the corners of the joint.

Because of the thickness correction, which extends downwards to 4 mm, the $S_{r_{h.s.}}-N_f$ lines for smaller wall thicknesses are higher than the DEN $S_{r_{h.s.}}-N_f$ line, which is valid for all thicknesses of 16 mm and below.

In comparison with the IIW, the thickness correction is larger, so that for smaller wall thicknesses, the $S_{r_{h.s.}}-N_f$ line is also higher than IIW line A.

Comparison of the $S_{r_{h.s.}}-N_f$ lines with EC3

EC3 would allow a hot spot stress design of joints between structural hollow sections based on class 36 for fillet welded joints, class 71 for butt welded joints and class 90 for but welded joints with a controlled weld profile [53], or alternatively a fatigue strength curve obtained from "adequate fatigue tests". In Chapter 7, the $S_{r_{h.s.}}-N_f$ line has been determined, according to accepted EC3 criteria.

As a direct result, the hot spot stress design method of joints between square hollow sections loaded in fatigue has become considerable more economic, due to the omission of over-conservative $S_{r_{h.s.}}-N_f$ lines for the hot spot method. For smaller wall thicknesses, the advantages are even larger.

8.3 Design examples

Two design examples below serve to illustrate the design procedure.

Example I

T-joint in square hollow sections, made of Fe 430, see Figure 50.

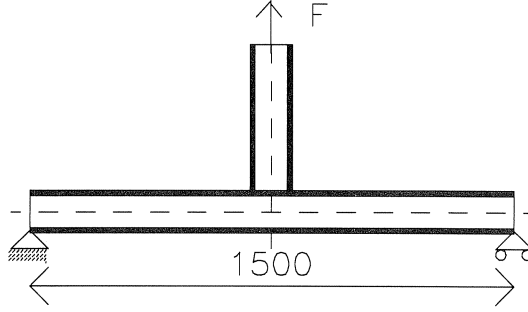


Figure 50. T-joint, used in the design example.

Chord: 200 x 200 x 12.5, $A_0 = 8973 \text{ mm}^2$, $W_0 = 513444 \text{ mm}^3$, $l_0 = 1500 \text{ mm}$

Brace: 140 x 140 x 5, $A_1 = 2661 \text{ mm}^2$, $W_1 = 114711 \text{ mm}^3$

$\beta = 140/200 = 0.7$; $2\gamma = 200/12.5 = 16$; $\tau = 5/12.5 = 0.40$.

Weld: the brace is 5 mm thick and therefore a fillet weld with $a = 5 \text{ mm}$ is assumed ($w_0 = w_1 = t_1 \cdot \sqrt{2} = 7.1 \text{ mm}$)

Problem: To determine the nominal axial force range for the design of a T-joint at $2 \cdot 10^6$ cycles for a constant amplitude loading.

Factor of safety: Depending upon the code of practice, a factor of safety should be applied to the hot spot stress range or fatigue life. In this example, the T-joint is supposed to be fail-safe (failure of the joint does not result in failure of the whole structure). The joint is supposed to be poorly accessible. According to EC3 [53], a partial safety factor of 1.15 is to be applied to the hot spot stress range, see Table 26.

An axial stress σ_{a1} causes a stress in the chord of: $\sigma_{m0} = \sigma_{a1} \cdot \frac{A_1 \cdot (l_0 - b_1)}{4W_0}$

Therefore, the total hot spot stress becomes:

$$S_{r_{h.s.}} = \sigma_{a1} \cdot (SCF_{a1} + SCF_{m0} \cdot \frac{A_1 \cdot (l_0 - b_1)}{4W_0}), \text{ in this case: } S_{r_{h.s.}} = \sigma_{a1} \cdot (SCF_{a1} + SCF_{m0} \cdot 1.76)$$

The SCFs and the ratio between the total hot spot stress and the nominal axial stress in the brace are tabulated below for lines B, C and D in the chord and lines A and E (combined) in the brace. The SCFs can be determined with the formulae in Table 18, or read from Figures 32 and 33.

Table 27. SCFs in the T-joint considered			
LINE	AXIAL FORCE IN THE BRACE SCF _{al}	BENDING MOMENT IN THE CHORD SCF _{m0}	S _{r.h.s.} / σ _{al}
A, E	10.26 ¹	-	10.26
B	4.50	-	4.50
C	4.27	0.99	6.01
D	2.11	1.64	5.00

¹ The SCF in the brace (lines A,E) is multiplied by 1.4, to correct for the weld type. See Table 18 and Figures 32 and 33.

The S_{r.h.s.} at 2·10⁶ cycles can be determined from either the S_{r.h.s.}-N_f lines in Figure 48 or the equations in Table 25:

$$\text{Brace: } t=5.0 \text{ mm: } S_{r.h.s.} = 11300 \cdot (2 \cdot 10^6)^{-1/3} \cdot (16/5.0)^{0.11 \cdot \log_{10}(2 \cdot 10^6)} = 201 \text{ N/mm}^2.$$

$$\text{Chord: } t=12.5 \text{ mm: } S_{r.h.s.} = 11300 \cdot (2 \cdot 10^6)^{-1/3} \cdot (16/12.5)^{0.11 \cdot \log_{10}(2 \cdot 10^6)} = 106 \text{ N/mm}^2.$$

Due to the smaller wall thickness of the brace, the S_{r.h.s.} at N_f=2·10⁶ is almost twice as high as for the chord.

A factor of safety of 1.15 on S_{r.h.s.} has been used, so that the above values are changed to : 201/1.15=175 and 106/1.15=92 for brace and chord respectively.

$$F_{\text{range}} = A_{\text{brace}} \cdot S_{r.h.s., N_f=2 \cdot 10^6} / (S_{r.h.s.} / \sigma_{al})$$

$$F_{\text{range}} (\text{chord}) = 2661 \cdot 92 / 6.01 = 40.7 \cdot 10^3 \text{ N} = 40.7 \text{ kN}$$

$$F_{\text{range}} (\text{brace}) = 2661 \cdot 175 / 10.26 = 45.4 \cdot 10^3 \text{ N} = 45.4 \text{ kN}$$

The lower value = 40.7 kN

Example II

Problem: For the joint of example I, the nominal axial force range F_{\max} for the design of a T-joint at $2 \cdot 10^6$ cycles and a given load spectrum is to be determined.

Load Total number of loading cycles of 2×10^6 , for the load spectrum given below:

0.95 F_{\max}	20 cycles
0.90 F_{\max}	180 cycles
0.80 F_{\max}	1800 cycles
0.65 F_{\max}	18000 cycles
0.45 F_{\max}	180000 cycles
0.20 F_{\max}	<u>1800000 cycles</u>
	2×10^6 cycles (N_{tot})

Calculations for cumulative damage:

The analysis is carried out by using the Palmgren-Miner's linear cumulative damage rule. The percentage fatigue strength used for each nominal stress range $S_{r_{h.s.i}}$ is to be determined, which is $\frac{n_i}{N_i} \cdot 100\%$. Here, n_i is the number of stress cycles at the hot spot stress range $S_{r_{h.s.i}}$, and N_i the number of stress cycles to failure in Figure 48 or Table 25 for $S_{r_{h.s.i}}$.

The following condition is to be satisfied: $\sum \frac{n_i}{N_i} = 1.0$.

The analysis is carried out in an iterative way, for various values of F_{\max} .

From example I:

$$S_{r_{h.s.}}(\text{chord}) = 6.01 \cdot F/2661$$

$$S_{r_{h.s.}}(\text{brace}) = 10.26 \cdot F/2661$$

A fatigue strength of 40.7 kN was found for constant amplitude loading. Of course, the maximum force F_{\max} will exceed this value, since most of the cycles occur at a considerable lower force range.

As an example, the check has been carried out for $F_{\max} = 150$ kN, with a partial safety factor according to EC3 [53] of 1.15. This is shown in Table 28.

Table 28. Check on damage, $\sum n_i/N_i \leq 1.0$					$F_{\max} = 1.15 \cdot 150 \text{ kN}$		
n_i	$F_i \text{ (kN)}$	Brace (line A)			Chord (line C)		
		$S_{h.s.i}$	$N_i \cdot 10^6$	n_i/N_i	$S_{h.s.i}$	$N_i \cdot 10^6$	n_i/N_i
20	163.9	632	0.03	0.001	370	0.04	0.000
180	155.3	599	0.04	0.005	351	0.05	0.004
1800	138.0	532	0.06	0.031	312	0.07	0.026
18000	112.1	432	0.12	0.145	253	0.13	0.136
180000	77.6	299	0.47	0.387	175	0.42	0.434
1800000	34.5	133	10.66	0.169	78	5.28	0.341
2000000				0.737			0.941

The damage in the chord is close to 1.0, so $F_{\max} = 150 \text{ kN}$.

9 CONCLUSIONS

9.1 *General conclusions*

Hot spot stress definition

A consistent hot spot stress or strain definition is required to allow comparison of test results and design recommendations. The determination of the hot spot stress at predetermined locations and in the direction perpendicular to the weld toe allows a well defined comparison between test results. Parametric formulae established in this way allow an elegant superposition of load cases. The hot spot stress definition used in this work is based on a number of considerations:

- The hot spot stresses are determined at fixed positions rather than using the maximum value in a member, to allow a better comparison between test results and to allow superposition of load cases.
- Two extrapolation methods (linear and quadratic) are used for the extrapolation of the stresses to the weld toe. Since the strain distribution is rather non-linear, a quadratic extrapolation yields better agreement with the failure mode. This is confirmed by the experimental $S_{h.s.}$ - N_f lines, where the scatter is smaller for quadratic extrapolation than for linear extrapolation.
- Although strains are more easily measured and probably describe the fatigue tests better, a stress based analysis is preferred because it is more consistent with current design practice.
- Stresses perpendicular to the weld toe are preferred over principal stresses for a number of reasons:
 - Primary stresses can be measured and extrapolated more easily than principal stresses.
 - Primary stresses can be superpositioned for different load cases, unlike principal stresses which differ in direction, depending on the load case.
 - As only the stress component perpendicular to the weld is increased by stress concentrations caused by the global weld shape and the wall of the adjacent member, this stress component would give the best basis for a fatigue design method.

Conclusions from the experiments

- The SCFs are found to be very sensitive to small changes in the geometry of the joint. Also, due to the tapering of the wall thickness that occurs in square hollow sections and to differences in corner radii, larger differences in SCF occur than for CHS joints.
- In general, a strong thickness influence can be observed from the tests, suggesting that the thickness effect can be applied well below 16 mm. The following thickness correction factors on the basic $S_{t_{h.s.}}-N_f$ line for 16 mm are proposed for inclusion in the design guidelines:
 $t < 16 \text{ mm: } (16/t)^{0.11 \log_{10}(N_f)}$
 $t > 16 \text{ mm: } (16/t)^{0.3}$.
- Crack initiation generally starts at about 10% to 25% of the total fatigue life.
- The fillet weld size $a=t_1$ may become critical in fatigue, resulting in weld failures as shown in the specimens T_1 to T_3 , and in many of the X-joints with a bending moment in the brace. However, the fatigue life was observed not to be substantially influenced in all cases.
- The influence of the R-ratio on the relationship between hot spot strain and number of cycles to failure is small. The influence seems to be larger for the relationship between nominal strain and number of cycles to failure. This is due to the fact that the SCFs are somewhat dependent on the R ratio, which is also shown by Yura.
- There exists an influence of the stress level on the SCF, which is probably caused by geometric non-linearity: for higher stress levels, the SCF is also higher. This might also explain the observed influence of the stress ratio R on the relationship between nominal strain and number of cycles to failure.
- The welding sequence was found to influence the fatigue strength [3]. Most of the X-joints loaded by an in-plane bending moment on the brace were welded starting and ending in the corners of the brace, rather than at the middle of the sides of the brace. These joints exhibit a notably lower fatigue strength, which is accounted for by a penalty factor of 2.0 on the hot spot stress.
- The τ ratio has a strong influence on the mode of failure: for low values of τ , brace failure occurs, whereas for higher values of τ the chord fails. However, no precise value of τ can be given for which brace failure changes to chord failure, since this also depends on other geometric parameters and on the type of loading. Also, for lower τ ratios, the wall thickness of the brace is lower than the chord wall thickness. Therefore, the thickness effect plays an important role on the mode of failure.

Conclusions from the comparison of experiments with FE analyses

- Since the SNCFs are very sensitive to small changes in geometry, it is necessary to model the variation of thickness in the cross-section of the chord and brace as realistically as possible, if close correlation with experimental measurements is required for calibration.
- The modelling of the finite element mesh, together with input of measured variations in thickness in the cross-section of the brace and chord, results in a good simulation of the strains and their gradients.
- The SNCF values for analyses with measured dimensions are, in general, either about the same as or above the experimentally measured values. The values for analyses with nominal values are, in general, higher than those for analyses with measured dimensions. This is caused by the square hollow sections used in the experimental specimens having a larger thickness (especially at the corners) than the specified nominal dimensions.

Conclusions from the numerical work

- The parametric formulae presented in this work allow the determination of the hot spot stress for a given range of T- or X-joints in square hollow sections and form a basis for future design recommendations.
- It is shown that one set of parametric equations can be used for both T- and X-joints, provided that the influence of the induced bending moment in the chord of T-joints is taken into account separately and a correction factor is given for axially loaded X-joints with $\beta=1.0$.
- The range of validity of the formulae can be extended for $r/t = 1$ to 4, without correction factors being necessary. This is confirmed by the (few) available experimental results.
- The conversion between strains and stresses is not straightforward and deserves attention when for instance strain and stress based results are compared. The ratio between SCF and SNCF for the joints considered varies from 0.6 to 1.4, with an average value of 1.1.
- The weld penetration (i.e. full penetration fillet or normal fillet weld) does not have much influence on the SCFs at the weld toe.
- The influence of the weld type can be taken into account by multiplying the SCF found from the parametric formula (which are derived for butt welds) for the brace by 1.4. For the chord, the SCFs of fillet welded joints are generally lower, but this is dependent on the geometry of the joint, so that a preliminary (correction) factor of 1.0 is recommended.

Conclusions regarding existing design recommendations

- EC3 class 90 for both fillet and butt welds is proposed as a basis for the design of rectangular hollow section joints. This class 90 agrees better with the test results than the current classes and is closer to the DEn and IIW lines, which are unconservative for the joints considered here.
- Ignoring the thickness effect below 16 mm as in the DEn or below 25 mm as in EC3 is not in accordance with the test results and is prohibitively conservative for small wall thicknesses. Based on the test results, a thickness correction down to 4 mm is allowed.
- The current practice of specifying the $S_{h.s.}$ - N_f line without giving detailed guidelines regarding the determination of the hot spot stress should be abandoned.
- The $S_{h.s.}$ - N_f lines of the various design codes are relatively in good agreement with each other for 25 mm wall thickness at $N_f=2 \cdot 10^6$ cycles. However, due to different slopes of the $S_{h.s.}$ - N_f lines, the results for other N_f vary more widely. For other thicknesses, the results vary even more, due to the present inconsistent thickness corrections.
- Tests carried out at Rice University [77] do not seem to support the AWS design recommendations regarding the influence of the weld profile when runouts are excluded. However, the remaining data is not enough to reject the influence of the weld profile altogether.
- The range of validity of the classification method in EC3 is too wide.
- The low cycle test results show that there is no need to limit the hot spot stress range to $2\sigma_e$, as in the DEn design guidelines.

9.2 Recommendations for future work

Work on K-joints

The ECSC research programme "Fatigue strength of welded unstiffened RHS-joints in latticed structures and Vierendeel girders", consisted of T- X- and K-joints. However, the parametric formulae obtained [24, 28] are not consistent with those for X- and T-joints, since:

- The formulae are based on axial forces plus implicitly included secondary bending moments. As the ratio between axial forces and secondary bending moments is dependent on the structure and the type of loading, it would be preferable to give separate parametric formulae for axial forces and bending moments as done for T- and X-joints.

- The use of maximum stress on a member as a basis for the design formulae rather than at a number of specified positions, such as lines A to E as for T- and X-joints, only allows a rather conservative superposition for different load cases, as the maximum stresses might occur at different positions in the members for different load cases.
- In view of the additional parameters for K-joints (gap, angle of the brace) many more FE analyses would be necessary to cover the parametric range.
- Another type of FE model has been adopted in comparison to T- and X-joints, with a simple weld modelling and without corner radii. This did not result in differences for the stresses in the gap area. However, in comparison with the experiments, differences with respect to the stresses in the chord face (line B) have been found [22], so that a mesh refinement here is necessary.
- The parametric formulae obtained for the determination of stress concentration factors of K-joints with gap [24] and overlap [28] are also of a completely different form in comparison to T- and X-joints [3].

The philosophy used for K-joints is different than that for X- and T-joints. To bring the K-joints in line with T- and X-joints, alternative FE analyses for K-joints with a similar FE model as used for X- and T-joints, followed by a new regression analysis to establish parametric formulae is advised.

With the new parametric formulae to be established for K-joints, test results of research programmes carried out earlier can be re-evaluated.

Extension for non-square rectangular sections

The use of rectangular rather than square hollow sections would in some cases work out very economical. Considering a beam-column framework, the beams could now be rectangular sections with the larger height used to take the in-plane bending moments. By choosing equal width of brace and chord ($\beta=1.0$) a very favourable SCF is obtained. Allowing rectangular sections gives an extra parameter to reach an optimum design. However, no analyses or tests have been carried out for non-square hollow sections so that the range of validity of the parametric formulae for the h/b ratios of the members is not established, thus preventing the proper use of rectangular hollow sections.

Extension for Y- and N-joints

By studying a few cases where the brace is not perpendicular to the chord, the range of validity of the parametric formulae for T- X- and K-joints might be extended to cover Y- and N-joints. In case no simple correction factors can be established, different sets of parametric formulae can be established.

Study on the hot spot stress

During the IIW conference in The Hague (the Netherlands), 1991, the need became obvious to reach an agreement on the definition of the hot spot stress. In this research programme, some considerations have already been made.

The influence of the non-linearities on the SCF, as noted in Chapter 3.3, might require further study, based on non-linear FE analyses. A comparison might be carried out between the use of primary stresses and the use of principal stresses as a basis for the fatigue analysis. The extrapolation method might also be investigated in more detail.

Study on alternative fatigue assessment methods

The inclusion of more information on the shape of the stress field near the weld toe, rather than just one stress value as in the hot spot stress method, might be a better basis for fatigue analysis. For instance including the slope of the stress field near the weld toe might cover the thickness effect as well as some sources of scatter.

Extensive study for fillet welded joints

As indicated in Figure 38, fillet welds in some cases have considerably lower SCFs in the chord than butt welds. In these cases, the parametric formulae for SCFs in the chord are conservative for fillet welded joints. In case of lines B and C, $\beta=0.7$, $2\gamma=16$, $\tau=1$ the SCFs for fillet welds are about 50% lower than for butt welds. Therefore, by carrying out extra FE analyses and/or tests, correction factors or separate parametric formulae can be established, allowing the designer to take advantage of this effect.

Establishment of design guidelines for multi-planar hollow section joints

Obviously, there is considerable interest at present time in multi-planar joints because of an almost complete lack of data. However, there is an ECSC-CIDECT programme of tests and numerical analyses on isolated joints and joints in multi-planar girders, carried out at the University of Karlsruhe, the Delft University of Technology and TNO Building & Construction Research.

10 REFERENCES

10.1 *Reports on the research projects carried out*

FINAL REPORTS

- [1] Wingerde, A.M. van
Puthli, R.S.
Koning, C.H.M. de
Verheul, A.
Wardenier, J.
Dutta, D. Fatigue strength of welded unstiffened R.H.S.
joints in latticed structures and Vierendeel
girders
Final Report, Part 1 "X- and T-joints"
TNO-IBBC report BI-89-064/63.5.3820
Stevin report 25.6-89-23/A1

- [2] Mang, F.
Herion, S.
Bucak, Ö.
Dutta, D. Fatigue strength of welded unstiffened R.H.S.
joints in latticed structures and Vierendeel
girders
Final Report, Part 2 "K-joints with gap and
overlap"
Versuchsanstalt Für Stahl, Holz und Steine
Universität Karlsruhe, May 1989 (in German)

- [3] Puthli, R.S.
Koning, C.H.M. de
Wingerde, A.M. van
Verheul, A.
Wardenier, J.
Dutta, D. Fatigue strength of welded unstiffened R.H.S.
joints in latticed structures and Vierendeel
girders
Final Report, Part 3 "Evaluation for design
rules"
TNO-IBBC report BI-89-097/63.5.3820
Stevin report 25.6-89-36/A1

- [4] Puthli, R.S.
Koning, C.H.M. de
Wingerde, A.M. van
Verheul, A.
Wardenier, J.
Dutta, D. Fatigue strength of welded unstiffened R.H.S.
joints in latticed structures and Vierendeel
girders
Final Report, Part 4 "Design recommendations"
TNO-IBBC report BI-89-102/63.5.3820
Stevin report 25.6-89-37/A1

- [5] Wingerde, A.M. van
Wardenier, J.
Dutta, D. Fatigue Behaviour of Uniplanar Joints Part 1
"T- and X-joints between square hollow sections"
CIDECT report 7K-91\3
TNO-IBBC report BI-91-017/63.5.3820
Stevin report 25.6-91-04/A1.12.03
(to be published)

X-joints

- [6] Puthli, R.S.
Koning, C.H.M. de
Wardenier, J.
Dutta, D. "A study on strain concentration factors of square hollow section X-joints with brace in tension"
TNO-IBBC report BI-86-63/63.5.3820
Stevin report 6-86-7
- [7] Koning, C.H.M. de
Puthli, R.S.
Wardenier, J.
Dutta, D. Fatigue behaviour of joints between rectangular hollow sections
X-joints, Part 1 "Experimental investigation on strain concentration factors and fatigue behaviour with brace in tension"
TNO-IBBC report BI-87-27/63.5.3820
Stevin report: 6-87-2.
- [8] Puthli, R.S.
Koning, C.H.M. de
Wardenier, J.
Dutta, D. Fatigue behaviour of joints between rectangular hollow sections.
X-joints, Part 2: "Comparison of strain concentration factors between results of numerical analyses and experimental work, with brace in tension"
TNO-IBBC report BI-87-52/63.5.3820
Stevin report 6-87-7
- [9] Puthli, R.S.
Koning, C.H.M. de
Wardenier, J.
Dutta, D. Fatigue behaviour of joints between rectangular hollow sections.
X-joints, Part 3 "Numerical analyses of strain concentration factors using nominal dimensions, with brace in tension"
TNO-IBBC report BI-87-66/63.5.3820
Stevin report: 6-87-8
- [10] Puthli, R.S.
Koning, C.H.M. de
Wardenier, J.
Dutta, D. Fatigue behaviour of joints between rectangular hollow sections.
X-joints, Part 4 "Analyses, conclusions and suggested recommendations from work done on X-joints in R.H.S., with brace in tension"
TNO-IBBC report BI-88-039/63.5.3820
Stevin report: 6-88-5, Stevin 25-88-11
- [11] Mang, F.
Herion, S.
Klingler, J.
Bucak, Ö.
Dutta, D. Zeit- und Dauerfestigkeit von geschweißten unverteiften Rechteck-Hohlprofilverbindungen von Fachwerken und Vierendeelträgern
X-Knoten "Experimentelle Untersuchungen und Dauerfestigkeit unter Momentenbelastung der Diagonalen"
Versuchsanstalt Für Stahl, Holz und Steine
Universität Karlsruhe,
November 1987 (in German)

T-joints

- [12] Verheul, A.
Noordhoek, C.
Wardenier, J.
Dutta, D. Fatigue behaviour of joints between rectangular hollow sections
T-joints, Part 1 "Experimental investigation on strain concentration factors and fatigue behaviour with brace in tension"
TNO-IBBC report BI-87-118/63.5.3820
Stevin report: 6-87-10.
- [13] Wingerde, A.M. van
Puthli, R.S.
Koning, C.H.M. de
Wardenier, J.
Dutta, D. Fatigue behaviour of joints between rectangular hollow sections.
T-joints, Part 2: "Comparison of strain concentration factors between results of numerical analyses and experimental work (brace in tension)"
TNO-IBBC report BI-87-82/63.5.3820
Stevin report 6-87-11
- [14] Wingerde, A.M. van
Puthli, R.S.
Koning, C.H.M. de
Wardenier, J.
Dutta, D. Fatigue behaviour of joints between rectangular hollow sections.
T-joints, Part 2, Appendix I: "A Study on Strain Concentration Factors on Square Hollow Section T-Joints with Braces in Tension or Bending"
Stevin report 6-87-13 (included in 6-87-11)
- [15] Wingerde, A.M. van
Puthli, R.S.
Koning, C.H.M. de
Wardenier, J.
Dutta, D. Fatigue behaviour of joints between rectangular hollow sections.
T-joints, Part 3 "Numerical analyses of strain concentration factors using nominal dimensions, (brace in tension or bending)"
TNO-IBBC report BI-87-83/63.5.3820
Stevin report: 6-87-12
- [16] Wingerde, A.M. van
Verheul, A.
Wardenier, J.
Dutta, D. Fatigue behaviour of joints between rectangular hollow sections.
T-joints, Part 4 "Analyses, conclusions and suggested recommendations from work done on T-joints in R.H.S"
TNO-IBBC report BI-88-126/63.5.3820
Stevin report: 6-88-15, M and C 25-88-47
- [17] Verheul A.
Wardenier, J. "The low cycle fatigue behaviour of axially loaded T-joints between rectangular hollow sections"
Cidect report 7H-89/1-E
Stevin report 25.6.89.22/A1
TNO-IBBC report BI-99-060/63.5.3820

- [18] Verheul, A.
Wardenier, J.
Back, J. de
The fatigue behaviour of axially loaded T-joints between rectangular hollow sections under random loading"
TNO-IBBC report BI-90-093/63.5.3820
Stevin report 25.6-90-11/A1/12.05
- [19] Verheul, A.
Wingerde, A.M. van
Wardenier, J.
The fatigue behaviour of T-joints between rectangular hollow sections loaded by an in-plane bending moment",.
CIDECT report 7K-91\18
TNO-IBBC report BI-91-109
Stevin report 25.6-91-19/A1

K-joints with gap

- [20] Dooren F.J. van
Puthli R.S.
Wardenier, J.
Fatigue behaviour of joints between rectangular hollow sections.
"Numerical determination of strain concentration factors of K-gap-joints made of rectangular hollow sections"
TNO-IBBC report BI-88-074/63.5.3820
Stevin report: 6-88-9, Stevin 25-88-29
- [21] Mang, F.
Herion, S.
Klingler, J.
Bucak, Ö.
Dutta, D.
Zeit- und Dauerfestigkeit von geschweißten unverteiften Rechteck-Hohlprofilverbindungen von Fachwerken und Vierendeelträgern von K-Knoten mit Spalt, Teil 1 "Experimentelle Untersuchungen und Dauerfestigkeit unter axialer Belastung der Diagonalen"
Versuchsanstalt Für Stahl, Holz und Steine Universität Karlsruhe, February 1988.
(in German)
- [22] Mang, F.
Herion, S.
Klingler, J.
Bucak, Ö.
Dutta, D.
Zeit- und Dauerfestigkeit von geschweißten unverteiften Rechteck-Hohlprofilverbindungen von Fachwerken und Vierendeelträgern von K-Knoten mit Spalt, Teil 2 "Berechnungen nach der Methode der Finiten Elemente und Vergleich mit den Versuchsergebnissen zur Bestimmung von Dehnungskonzentrationsfaktoren"
Versuchsanstalt Für Stahl, Holz und Steine Universität Karlsruhe, January 1988.
(in German)

- [23] Mang, F.
Herion, S.
Klingler, J.
Bucak, Ö.
Dutta, D.
- Zeit- und Dauerfestigkeit von geschweißten unverteiften Rechteck-Hohlprofilverbindungen von Fachwerken und Vierendeelträgern K-Knoten mit Spalt, Teil 3 "Bestimmung von Dehnungskonzentrationsfaktoren"
Versuchsanstalt Für Stahl, Holz und Steine
Universität Karlsruhe, July 1988.
(in German)
- [24] Mang, F.
Herion, S.
Bucak, Ö.
Dutta, D.
- Zeit- und Dauerfestigkeit von geschweißten unverteiften Rechteck-Hohlprofilverbindungen von Fachwerken und Vierendeelträgern K-Knoten mit Spalt, Teil 4 "Analyse, Folgerungen und Empfehlungen"
Versuchsanstalt Für Stahl, Holz und Steine
Universität Karlsruhe, April 1989.
(in German)

K-joints with overlap

- [25] Mang, F.
Herion, S.
Klingler, J.
Bucak, Ö.
Dutta, D.
- Zeit- und Dauerfestigkeit von geschweißten unverteiften Rechteck-Hohlprofilverbindungen von Fachwerken und Vierendeelträgern K-Knoten überlappt, Teil 1 "Experimentelle Untersuchungen und Dauerfestigkeit unter axialer Belastung der Diagonalen"
Versuchsanstalt Für Stahl, Holz und Steine
Universität Karlsruhe, March 1988.
(in German)
- [26] Mang, F.
Herion, S.
Klingler, J.
Bucak, Ö.
Dutta, D.
- Zeit- und Dauerfestigkeit von geschweißten unverteiften Rechteck-Hohlprofilverbindungen von Fachwerken und Vierendeelträgern K-Knoten überlappt, Teil 2 "Berechnungen nach der Methode der Finiten Elemente und Vergleich mit den Versuchsergebnissen "
Versuchsanstalt Für Stahl, Holz und Steine
Universität Karlsruhe, July 1988.
(in German)
- [27] Mang, F.
Herion, S.
Klingler, J.
Bucak, Ö.
Dutta, D.
- Zeit- und Dauerfestigkeit von geschweißten unverteiften Rechteck-Hohlprofilverbindungen von Fachwerken und Vierendeelträgern K-Knoten überlappt, Teil 3 "Bestimmung von Dehnungskonzentrationsfaktoren"
Versuchsanstalt Für Stahl, Holz und Steine
Universität Karlsruhe, January 1989.
(in German)

- [28] Mang, F.
Herion, S.
Bucak, Ö.
Dutta, D. Zeit- und Dauerfestigkeit von geschweißten
unversteiften Rechteck-Hohlprofilverbindungen
von Fachwerken und Vierendeelträgern
K-Knoten überlappt, Teil 4 "Analyse,
Folgerungen und Empfehlungen"
Versuchsanstalt Für Stahl, Holz und Steine
Universität Karlsruhe, April 1989.
(in German)
- 10.2 *Other publications*
- [29] Abel, A. "The effect of stress relieving on the fatigue of large scale
welded tubulars"
8th INTERNATIONAL OFFSHORE MECHANICS AND
ARCTIC ENGINEERING SYMPOSIUM (OMAE '89)
Volume III, p.383-388
American Society of Mechanical Engineers (ASME)
The Hague, The Netherlands, 1989.
- [30] Ahmed, S.
Irons, B.M.
Zienkiewicz, O.C. "Analysis of thick and thin shell structures by
curved finite elements"
INTERNATIONAL JOURNAL FOR NUMERICAL
METHODS IN ENGINEERING, Volume. 2, p.419-451
London, U.K., 1970.
- [31] American Petroleum
Institute "Recommended Practice for Planning, Designing
and Constructing Fixed Offshore Platforms"
API Recommended Practice 2A (RP 2A), 19th Edition
Washington, U.S.A., August 1991.
- [32] American Welding
Society "Structural Welding Code /Steel"
ANSI/AWS D1.1-92, 13th edition, Miami, Florida
U.S.A., 1992.
- [33] Back, J. de
Wardenier, J.
Kurobane, Y. "The fatigue behaviour of hollow section joints"
2nd INTERNATIONAL CONFERENCE WELDING OF
TUBULAR STRUCTURES p.419-430
IIW
Boston, U.S.A., 1984.
- [34] Back, J. de "The design aspects and fatigue behaviour of
tubular joints"
STEEL IN MARINE STRUCTURES (SIMS '87), p.205-223
Elsevier applied science publishers ltd.
Amsterdam/London/New York/Tokio
Delft, the Netherlands, June 1987.

- [35] Back, J. de
Delft, d.R.V. van
Noordhoek, C. "The effect of plate thickness on the fatigue life of welded tubular joints and flat specimens"
8th INTERNATIONAL OFFSHORE MECHANICS AND ARCTIC ENGINEERING SYMPOSIUM (OMAE '89)
Volume III, p.21-39
American Society of Mechanical Engineers (ASME)
The Hague, The Netherlands, 1989.
- [36] Back, J. de "Recent developments in the fatigue design rules in the Netherlands"
INTERNATIONAL SYMPOSIUM ON THE OCCASION OF THE RETIREMENT OF PROF. J. DE BACK
p.189-205
Delft University Press
Delft, The Netherlands, September 1989.
- [37] Berge, S.
Webster, S.E. "The size effect on the fatigue behaviour of welded joints"
STEEL IN MARINE STRUCTURES (SIMS '87), p.179-203
Elsevier applied science publishers ltd.
Amsterdam/London/New York/Tokio
Delft, the Netherlands, June 1987.
- [38] Bignonnet, A. "Improving the fatigue strength of welded steel structures"
STEEL IN MARINE STRUCTURES (SIMS '87), p.99-118
Elsevier applied science publishers ltd.
Amsterdam/London/New York/Tokio
Delft, the Netherlands, June 1987.
- [39] Bignonnet, A.
Papadopoulos, Y.
Barrere, F.
Lieurade, H.P.
Lecoq, H. "The influence of cathodic protection and post weld improvement on the fatigue resistance of steel welded joints"
STEEL IN MARINE STRUCTURES (SIMS '87), p.737-746
Elsevier applied science publishers ltd.
Amsterdam/London/New York/Tokio
Delft, the Netherlands, June 1987.
- [40] Booth, G.S. "The effect of thickness on the fatigue strength of plate welded joints"
STEEL IN MARINE STRUCTURES (SIMS '87), p.259-268
Elsevier applied science publishers ltd.
Amsterdam/London/New York/Tokio
Delft, the Netherlands, June 1987.
- [41] Booth, G.S. "Improving the fatigue strength of welded joints by grinding - techniques and benefits"
The Welding Institute report 268/85, 1985.

- [42] Borst, R. de
Kusters, G.M.A.
Nauta, P.
Witte, F.C. de "DIANA - A comprehensive but flexible
finite element system"
Finite Element Systems Handbook, Editor
Brebbia, C.A. Springer-Verlag, Berlin, 1985.
- [43] Brozetti, J.
Wardenier, J.
Mang, F.
Sedlacek, G.
Dutta, D.
Grotmann, D. Eurocode 3: Chapter 9
Document 9.03
CIDECT 7M 1/91.
- [44] Delft, D.R.V. van "A two dimensional analyses of the stresses at the
vicinity of the weld toes of tubular structures"
Stevin report 6-81-8
Stevin Laboratory, Delft University of Technology
Delft, The Netherlands, 1981.
- [45] Delft, D.R.V. van
Noordhoek, C.
Back, de J. "Evaluation of the european fatigue tests data on
large-sized welded tubular joints for offshore
structures"
OFFSHORE TECHNOLOGY CONFERENCE
(OTC '85), paper 4999
Offshore Technology Conference
P.O. Box 833868, Richardson, U.S.A.
Houston, U.S.A., May 1985.
- [46] Delft, D.R.V. van
Dijkstra, O.D.
Snijder, H.H. "The calculation of fatigue crack growth in
welded tubular joints using fracture mechanics"
OFFSHORE TECHNOLOGY CONFERENCE
(OTC '86), paper 5352
Offshore Technology Conference
P.O. Box 833868, Richardson, U.S.A.
Houston, U.S.A., May 1986.
- [47] Delft, D.R.V. van
Noordhoek, C.
Da Re, M. L. "The results of the European fatigue tests
on welded tubular joints compared with SCF
formulas and design lines"
STEEL IN MARINE STRUCTURES (SIMS '87), p.565-577
Elsevier applied science publishers ltd.
Amsterdam/London/New York/Tokio
Delft, the Netherlands, June 1987.
- [48] Department of Energy "Offshore Installation: Guidance on Design and
Construction", Department of Energy
London, U.K., 1990.

- [49] Dijkstra, O.D.
Back, J. de "Fatigue strength of tubular X- and T-joints"
12th OFFSHORE TECHNOLOGY CONFERENCE
(OTC '80), paper 3696
Offshore Technology Conference
P.O. Box 833868, Richardson, U.S.A.
Houston, U.S.A., May 1980.
- [50] Dijkstra, O.D.
Noordhoek, C. "The effect of grinding and special weld profile
on the fatigue behaviour of large-scale
tubular joints"
17th OFFSHORE TECHNOLOGY CONFERENCE
(OTC '85), paper 4866
Offshore Technology Conference
P.O. Box 833868, Richardson, U.S.A.
Houston, U.S.A., May 1985.
- [51] Dutta, D.
Mang, F.
Wardenier, J. "Fatigue behaviour of welded hollow section
joints"
CIDECT MONOGRAPH No. 7.
- [52] Dutta, D.
Würker, K.G. "Handbuch Hohlprofile in Stahlkonstruktionen"
Verlag TÜV Rheinland
Cologne, Federal Republic of Germany, 1988.
(in German)
- [53] EC Eurocode no. 3, Design of Steel Structures.
Part 1 - General Rules and Rules for Buildings,
Final Draft (november 1990), Issued to Liaison
Engineers, February 1989, Report prepared for the
Commission of the European Communities,
Directorate General, Internal Market and
Industrial Affairs, 1990.
- [54] Efthymiou, M.
Durkin, S. "Stress concentration factors in T/Y and gap/
overlap K-joints"
BEHAVIOUR OF OFFSHORE STRUCTURES 1985
(BOSS '85), p.429-440
Elsevier applied science publishers ltd.
Amsterdam/London/New York/Tokio
Delft, the Netherlands, July 1985.
- [55] Efthymiou, M. "Development of SCF formulae and generalised
influence functions for use in fatigue analysis"
OFFSHORE TUBULAR JOINTS CONFERENCE (OTJ '88)
UEG Offshore research
Englefield Green Near Egham, U.K., 1988.
(some printing errors were corrected later on,
contact Shell)

- [56] Elliot, K.S. "Stress distribution at weld toes in improved and ordinary fillet welds in X-type tubular joints"
4th INTERNATIONAL SYMPOSIUM ON TUBULAR STRUCTURES, p.190-203
Delft University Press
Delft, The Netherlands, June 1991.

- [57] Ferreira, J.M.
Branco, C.M. "Fatigue behaviour of welded nodes of square tubes"
8th INTERNATIONAL OFFSHORE MECHANICS AND ARCTIC ENGINEERING SYMPOSIUM (OMAE '89)
Volume III, p.369-375
American Society of Mechanical Engineers (ASME)
The Hague, The Netherlands, 1989.

- [58] Fessler, H.
Hyde, T.H.
Buchan, A.W. "Assessment of parametric equations for stress concentration factors in welded tubular connections"
4th INTERNATIONAL SYMPOSIUM ON TUBULAR STRUCTURES, p.219-228
Delft University Press
Delft, The Netherlands, June 1991.

- [59] Frater, G.S. "Performance of welded rectangular hollow structural section trusses"
University of Toronto, Canada, 1991.
(Ph.D. thesis)

- [60] Gibstein, M.B. "Parametrical stress analysis of T-joints"
ECSC seminar, Cambridge, U.K., 1978.

- [61] Gurney, T.R. "Fatigue of welded structures", 2nd edition,
Cambridge University press
Cambridge, U.K., 1979.

- [62] Gurney, T.R. "The influence of thickness on fatigue of welded joints -10 years on " (A review of British work)
8th INTERNATIONAL OFFSHORE MECHANICS AND ARCTIC ENGINEERING SYMPOSIUM (OMAE '89)
Volume III, p.1-8
American Society of Mechanical Engineers (ASME)
The Hague, the Netherlands, March 1989.

- [63] Haagensen, P.J.
Drågen, A.
Slind, T.
Ørjasæter, O. "Prediction of the improvement in fatigue life of welded joints due to grinding, TIG dressing, weld shape control and shot peening"
Elsevier applied science publishers ltd.
STEEL IN MARINE STRUCTURES (SIMS '87), p.689-698
Amsterdam/London/New York/Tokio
Delft, the Netherlands, June 1987.
- [64] Haagensen, P.J. "Improvement techniques"
INTERNATIONAL SYMPOSIUM ON THE OCCASION
OF THE RETIREMENT OF PROF. J. DE BACK
p.77-95
Delft University Press
Delft, The Netherlands, September 1989.
- [65] Hertogs, A.A.
Puthli, R.S.
Wardenier, J. "Stress concentration factors in plate-tube connections"
8th INTERNATIONAL OFFSHORE MECHANICS AND ARCTIC ENGINEERING SYMPOSIUM (OMAE '89)
Volume II, p.719-727
American Society of Mechanical Engineers (ASME)
The Hague, the Netherlands, March 1989.
- [66] Hoadley, P.W.
Yura, J.A. "Ultimate strength of tubular joints subjected to combined loads"
Phase II, Department of Civil engineering/
Phil M. Ferguson Structural Engineering Laboratory
University of Austin, U.S.A.
PMFSEL report 83-3, December 1983.
- [67] Iida, K. "State of the art in Japan"
STEEL IN MARINE STRUCTURES (SIMS '87), p.71-98
Elsevier applied science publishers ltd.
Amsterdam/London/New York/Tokio
Delft, the Netherlands, June 1987.
- [68] International
Institute of
Welding IIW-XVE, Recommended fatigue design procedure for hollow section joints.
Doc. SC-XV-582-85, XIII-1158-85.
Strasbourg, France, 1985.
- [69] International
Institute of
Welding "Design recommendations for hollow section joints - predominantly statically loaded - "
2nd Edition, 1989
IIW DOC: XV-701-89.

- [70] Kohoutek, R.
Hoshyari, I. "Semi-rigid tubular joints applied to offshore structures"
INTERNATIONAL OFFSHORE AND POLAR
ENGINEERING CONFERENCE (ISOPE '91), p.61-66
International Society of Offshore and Polar
Engineers, P.O. Box 1107 Golden, Colorado, U.S.A.
Edinburg, U.K., August, 1991.
- [71] Kuang, J.G.
Potvin, A.B.
Leick, R.D. "Stress concentration in tubular joints"
OFFSHORE TECHNOLOGY CONFERENCE
(OTC '75), paper 2205
Offshore Technology Conference
P.O. Box 833868, Richardson, U.S.A.
1975.
- [72] Kurobane, Y. "Recent developments in the fatigue design rules
in Japan"
INTERNATIONAL SYMPOSIUM ON THE OCCASION
OF THE RETIREMENT OF PROF. J. DE BACK
p.173-187
Delft University Press
Delft, The Netherlands, September 1989.
- [73] Lange, J.F. de "The application of the line spring method to the
prediction of fatigue crack growth in tubular
joints"
Master Thesis, Delft University of Technology
Delft, The Netherlands, September 1990.
- [74] Mang, F. "Zeit und Dauerfestigkeit von geschweissten
Hohlprofilverbindungen. Zwischenberichte und
Übersichtstabellen mit Versuchsergebnisse über
K-Knoten durchgeführt in Karlsruhe"
Universität Karlsruhe.
(in German)
- [75] Mang, F.
Herion, S.
Bucak, Ö.
Dutta, D. "Fatigue behaviour of K- with gap and with overlap
made of rectangular hollow sections"
3rd INTERNATIONAL SYMPOSIUM ON TUBULAR
STRUCTURES, p.297-309
Elsevier applied science publishers ltd.
Amsterdam/London/New York/Tokio
Lappeenranta, Finland, September 1989.

- [76] Marshall, P.W. "Houdremont lecture: Connections for tubular structures"
2nd INTERNATIONAL CONFERENCE ON WELDING OF TUBULAR STRUCTURES
IIW, p.1-54 (in English)/p.57-115 (in French)
Boston, U.S.A., July, 1984.
- [77] Marshall, P.W. "State of the art in the U.S.A"
STEEL IN MARINE STRUCTURES (SIMS '87), p.39-48
Elsevier applied science publishers ltd.
Amsterdam/London/New York/Tokio
Delft, the Netherlands, June 1987.
- [78] Marshall, P.W. "Recent developments in the fatigue design rules in the USA"
INTERNATIONAL SYMPOSIUM ON THE OCCASION OF THE RETIREMENT OF PROF. J. DE BACK
p.153-171
Delft University Press
Delft, The Netherlands, September 1989.
- [79] Marshall, P.W. "Design of welded tubular connections: Basis and use of AWS code provisions"
Shell Oil Company, Houston, U.S.A.
Developments in Civil Engineering, Volume 37
Elsevier applied science publishers ltd.
Amsterdam/London/New York/Tokio
(Ph.D. thesis)
- [80] Marshall, P.W.
Wingerde, A.M. van Personal correspondence regarding the interpretation of the Rice test fatigue results.
Houston/Delft, 1992.
- [81] Niemi, E. "Recommendations concerning stress calculation for fatigue analysis of welded components"
IIW doc. XV-763-91
the Hague, the Netherlands, 1991.
- [82] Noordhoek, C.
Wardenier, J.
Dutta, D. "The fatigue behaviour of welded joints in square hollow sections"
Part 1: "Test results and S-N curves"
Stevin report 6-79-11
TNO-IBBC report BI-80-9/0063.4.3821.
- [83] Noordhoek, C.
Wardenier, J.
Dutta, D. "The fatigue behaviour of welded joints in square hollow sections"
Part 2: "Analysis"
Stevin report 6-80-4
TNO-IBBC report BI-80-10/0063.4.3821.

- [84] Packer, J.A.
Davies, G. "On the use and calibration of design standards for SHS joints"
THE STRUCTURAL ENGINEER, Volume 67, No. 21
Institution of Structural Engineers
U.K., November 1989.
- [85] Packer, J.A
Frater, G.S.
Wingerde, A.M. van Personal correspondence regarding the interpretation of the fatigue results of the Ph.D. study of G.S.Frater.
Toronto/Delft, 1989-1990.
- [86] Packer, J.A.
Henderson, J.E.
Wardenier, J. "Load and resistance factor design of welded box section trusses"
American Institute of Steel Construction (AISC)
NATIONAL STEEL CONFERENCE (NSC)
Washington D.C., June 1991.
- [87] Petershagen, H.
Fricke, W.
Massel, T. "Application of the local approach to the fatigue strength assessment of welded structures in ships"
IIW doc. XIII-1409-91.
- [88] Puthli, R.S. "Geometrical non-linearity in collapse analysis of thick walled shells, with application to tubular steel joints"
HERON, TU Delft, TNO-IBBC, Volume 26, No. 2, 1981.
- [89] Puthli, R.S.
Wardenier, J.
Koning, C.H.M. de
Wingerde, A.M. van
Dooren, F.J. van "Numerical and experimental determination of strain (stress) concentration factors of welded joints between square hollow sections"
HERON, TU Delft, TNO-IBBC, Volume 33 No. 2, 1988.
- [90] Puthli, R.S.
Koning, C.H.M. de
Panjeh Shahi, E.
Wingerde, A.M. van "Spanningsconcentratiefactoren (SCF) in verbindingen van ronde of vierkante buisprofielen"
RESEARCHDAG 1989, Delft
Staalbouwkundig Genootschap
Rotterdam, The Netherlands, 1989.
(in Dutch)
- [91] Reusink, J.H.
Wardenier, J. "Simplified design charts for axially loaded joints of square hollow sections"
3rd INTERNATIONAL SYMPOSIUM ON TUBULAR STRUCTURES, p.54-61
Elsevier applied science publishers ltd.
Amsterdam/London/New York/Tokio
Lappeenranta, Finland, September 1989.

- [92] Reusink, J.H.
Wardenier, J. "Simplified design charts for axially loaded joints of circular hollow sections"
3rd INTERNATIONAL SYMPOSIUM ON TUBULAR STRUCTURES, p.154-161
Elsevier applied science publishers ltd.
Amsterdam/London/New York/Tokio
Lappeenranta, Finland, September 1989.
- [93] Reynolds, A.G. "The fatigue performance of tubular joints
- An overview of recent work to revise Department of Energy guidance"
4th INTERNATIONAL SYMPOSIUM ON INTEGRITY OF OFFSHORE STRUCTURES, p.261-277
Elsevier applied science publishers ltd.
Amsterdam/London/New York/Tokio
Glasgow, U.K., July 1990.
- [94] Romeijn, A.
Puthli, R.S.
Koning, C.H.M. de
Wardenier, J. "Stress and strain concentration factors of multiplanar joints made of circular hollow sections"
INTERNATIONAL OFFSHORE AND POLAR ENGINEERING CONFERENCE (ISOPE '92)
paper ISOPE-92-C5-17
International Society of Offshore and Polar Engineers, P.O. Box 1107 Golden, Colorado, U.S.A.
San Francisco, U.S.A., June 1992.
- [95] Romeijn, A.
Puthli, R.S.
Wardenier, J. "Finite element modelling of multiplanar joints flexibility in tubular structures"
INTERNATIONAL OFFSHORE AND POLAR ENGINEERING CONFERENCE (ISOPE '92)
paper ISOPE-92-C5-134
International Society of Offshore and Polar Engineers, P.O. Box 1107 Golden, Colorado, U.S.A.
San Francisco, U.S.A., June 1992.
- [96] Sablok, A.K.
Hartt, W.H. "The influence of weld profile upon the thickness dependence of fatigue strength for steel in seawater"
9th INTERNATIONAL OFFSHORE MECHANICS AND ARCTIC ENGINEERING SYMPOSIUM (OMAE '91)
Volume III-B, p.347-362
American Society of Mechanical Engineers (ASME)
1991.

- [97] Sedlacek, G.
Wardenier, J.
Dutta, D.
Grotmann, D. "Hollow section construction under predominantly static loading in Eurocode 3"
4th INTERNATIONAL SYMPOSIUM ON TUBULAR STRUCTURES, p.514-526
Delft University Press
Delft, the Netherlands, June 1991.
- [98] Smedley, P.
Fisher, P. "Stress concentration factors for simple tubular joints"
9th INTERNATIONAL OFFSHORE AND POLAR ENGINEERING CONFERENCE (ISOPE '91, Volume IV, p.475-483
International Society of Offshore and Polar Engineers, P.O. Box 1107 Golden, Colorado, U.S.A.
Edinburgh, U.K, August 1991.
- [99] Society of Automotive Engineers "SAE fatigue design handbook" AE-4
Warrendale, PA, 1968.
- [100] Soh, A.K.
Too, H.K.
Wong, C.F. "SCF equations for T and K square tubular welded joints"
6th INTERNATIONAL OFFSHORE MECHANICS AND ARCTIC ENGINEERING SYMPOSIUM (OMAE '87) Volume III, p.247-254
American Society of Mechanical Engineers (ASME) 1987.
- [101] Soh, A.K.
Soh, C.K. "SCF equations for T/Y and K square-to-round tubular joints"
JOURNAL OF PETROLEUM TECHNOLOGY (JPT) p.289-296
American Institute of Mining and Metallurgical Engineers, March 1989.
- [102] Soh, A.K.
Soh, C.K. "A parametric stress analysis of T/Y and K square-to-square tubular joints"
JOURNAL OF CONSTRUCTIONAL STEEL RESEARCH number 15, p.173-190, 0143/974X/90/13-50
Elsevier applied science publishers ltd.
Amsterdam/London/New York/Tokio, 1990.

- [103] Soh, A.K.
Soh, C.K. "Stress analysis of DT/X square-to-round tubular joints"
INTERNATIONAL CONFERENCE ON STEEL & ALUMINIUM STRUCTURES (ICSAS '91), p.573-581
Elsevier applied science publishers ltd.
Amsterdam/London/New York/Tokio
Singapore, May 1991.
- [104] Soh, A.K.
Soh, C.K. "SCF equations for DT/X square-to-round tubular joints"
JOURNAL OF CONSTRUCTIONAL STEEL RESEARCH
no. 19, p.81-95
Elsevier applied science publishers ltd.
Amsterdam/London/New York/Tokio, 1991.
- [105] van Straalen, I.J.J.
Dijkstra, O.D. "Application of the fracture mechanics approach to the fatigue behaviour of welded tubular steel structures"
4th INTERNATIONAL SYMPOSIUM ON TUBULAR STRUCTURES, p.259-268
Delft University Press
Delft, the Netherlands, June 1991.
- [106] Strating, J. "Fatigue and stochastic loading"
Stevin Laboratory, paper 6,73,04
Delft University of Technology
Delft, the Netherlands, 1973.
- [107] Thorpe, T.W.
Sharp, J.V. "The fatigue performance of tubular joints in air and seawater"
MaTSU, Harwell Laboratory, Oxfordshire, U.K.
1989.
(presented during the OMAE '89, but not included in the proceedings)
- [108] UEG's TUBULAR JOINTS GROUP "Design of tubular joints for offshore structures"
UEG Publication UR33, London, U.K., 1985.
- [109] UEG's TUBULAR JOINTS GROUP "Review of current methods for determining 'hot-spot' stresses and stress concentration factors"
NEWSLETTER SUPPLEMENT NUMBER FIVE
London, U.K., 1987.

- [110] Wardenier, J.
Dutta, D. "The fatigue behaviour of lattice girder joints in square hollow sections"
CONFERENCE ON JOINTS IN STRUCTURAL STEELWORK
IIW doc. XV-493-81/ XIII-1005-81
Teesside , U.S.A., April 1981.
- [111] Wardenier, J. "Hollow and open sections"
JOURNAL OF THE AUSTRALIAN INSTITUTE OF STEEL CONSTRUCTION
Volume 15 No.2. 1981.
- [112] Wardenier, J. "Hollow section joints"
Delft University Press
Delft, The Netherlands, 1982.
- [113] Wardenier, J. "Buisconstructies: Ontwerp en Berekening - Vermoeiing"
STAALBOUWKUNDIG GENOOTSCHAP RESEARCHDAG 1989
Stevin laboratory, paper 6,89,07
Delft, The Netherlands, 1989.
(in Dutch)
- [114] Wardenier, J. "Static and fatigue design of hollow section joints"
CIDECT SEMINAR: LATEST DEVELOPMENTS IN THE DESIGN AND USE OF HOLLOW SECTION JOINTS
Stevin report 25-06-90-22
Turku, Finland, September 1990.
- [115] Wardenier, J.
Kurobane, Y.
Packer, J.A.
Dutta, D.
Yeomans, N. "Design guide for circular hollow section (CHS) joints under predominantly static loading"
CIDECT
ISBN 3885859750
Köln, Germany, 1991.
- [116] Wingerde, A.M van
Verheul, A.
Puthli, R.S.
Wardenier, J.
Dutta, D. "The fatigue behaviour of T joints made from square hollow sections"
WELDTECH 88 - INTERNATIONAL CONFERENCE ON WELD FAILURES, paper 4
The Welding Institute, London, U.K.
London, U.K., November 1988.

- [117] Wingerde, A.M van
Puthli, R.S.
Wardenier, J.
Dutta, D. "The fatigue behaviour of X- and T- joints made of square hollow sections"
3rd INTERNATIONAL SYMPOSIUM ON TUBULAR STRUCTURES, p.288-296
Elsevier applied science publishers ltd.
Amsterdam/London/New York/Tokio
Lappeenranta, Finland, September 1989.
- [118] Wingerde, A.M van
Puthli, R.S.
Wardenier, J.
Dutta, D. "Parametric formulae for the stress concentration factors of T- and X- joints made with square hollow sections"
INTERNATIONAL CONFERENCE ON STEEL & ALUMINIUM STRUCTURES (ICSAS '91), p.632-642
Elsevier applied science publishers ltd.
Amsterdam/London/New York/Tokio
Singapore, May 1991.
- [119] Wingerde, A.M van
Yu Y.
Puthli, R.S.
Wardenier, J.
Dutta, D. "Influence of corner radius and weld dimensions on the stress concentration factors of SHS T- and X-joints"
4th INTERNATIONAL SYMPOSIUM ON TUBULAR STRUCTURES, p.281-293
Delft University Press
Delft, the Netherlands, June 1991.
- [120] Wingerde, A.M van
Puthli, R.S.
Wardenier, J.
Dutta, D. "Evaluation of recent research on the fatigue behaviour of T- and X-joints made with square hollow sections"
INTERNATIONAL OFFSHORE AND POLAR ENGINEERING CONFERENCE (ISOPE '91), Volume IV, p. 492-500
International Society of Offshore and Polar Engineers, P.O. Box 1107 Golden, Colorado, U.S.A.
Edinburgh, U.K., August 1991.
- [121] Wingerde, A.M van
Puthli, R.S.
Wardenier, J.
Dutta, D. "The fatigue design of welded joints made of square hollow sections"
INTERNATIONAL SYMPOSIUM ON FATIGUE AND FRACTURE IN STEEL AND CONCRETE STRUCTURES (ISFF '91), p. 1213-1227
Oxford&IBH Publishing Co.Pvt.Ltd., New Delhi, India
Madras, India, December 1991.

- [122] Wingerde, A.M van
Puthli, R.S.
Wardenier, J.
Dutta, D.
Packer, J.A.
"Design recommendations and commentary regarding the fatigue behaviour of hollow section joints"
INTERNATIONAL OFFSHORE AND POLAR
ENGINEERING CONFERENCE (ISOPE '92)
paper ISOPE-92-C5-55
International Society of Offshore and Polar
Engineers, P.O. Box 1107 Golden, Colorado, U.S.A.
San Francisco, U.S.A., June 1992.
- [123] Yoshida, T.
Inui, T.
Takazawa, M.
Iida, K.
"A detailed analysis of strain distribution and a prediction of crack initiation life for tubular T-connections"
JOURNAL OF SOCIETY OF NAVAL ARCHITECTS OF JAPAN
No. 144, 1978.
(in Japanese)

HET VERMOEIINGSGEDRAG VAN T- EN X-VERBINDINGEN GEMAAKT VAN VIERKANTE BUISPROFIELEN

A.M. van Wingerde
Technische Universiteit Delft

SAMENVATTING

In dit proefschrift worden de resultaten van experimenteel en numeriek onderzoek naar het vermoeiingsgedrag van T- en X-verbindingen gemaakt van vierkante buizen waarvan de wandstaaf gelast is op het vlak van de randstaaf, zonder gebruikmaking van extra schotten. Het onderzoek is uitgevoerd in het kader van het CIDECT onderzoekprogramma 7K "Fatigue behaviour of uniplanar joints", en een hieraan voorafgaand ECSC (EGKS) onderzoekprogramma "Fatigue strength of welded unstiffened RHS joints in latticed structures and Vierendeel girders" (CECA 7210-SA/111). Hiernaast is gebruik gemaakt van experimentele resultaten van het CIDECT programma 7H "The low cycle fatigue behaviour of axially loaded T-joints between rectangular hollow sections".

Het doel van de onderzoekprogramma's is het opstellen van een ontwerpmethode voor op vermoeiing belaste verbindingen van vierkante buizen, welke gebaseerd is op de zogeheten 'hot spot' spanning methode. De resultaten kunnen worden opgenomen in Eurocode 3.

In het experimentele onderzoek worden de rek concentratie factoren gemeten op diverse plaatsen in de verbinding, ter vergelijking met de numerieke resultaten en voor de bepaling van de S-N lijnen.

Het numerieke onderzoek levert SCF waarden op aan de lasteen voor een variatie in verbindingsafmetingen. Deze resultaten vormen de basis voor formules die het mogelijk maken de SCF waarden aan de las van wandstaaf en randstaaf te bepalen, afhankelijk van de dimensieloze parameters β , 2γ and τ , die de geometrie van de verbinding beschrijven.

De resultaten van de experimenten en numerieke berekeningen zijn gebruikt om de uiteindelijk afgeleide formules te controleren in relatie tot de voorgestelde S-N lijnen.

TREFWOORDEN

vermoeiing, vierkante buisprofielen, hot spot spanning, spannings (rek) concentratie factor.

Personal data:

Name: Arno (Arnoldus Martinus) van Wingerde
Birth date: February 18, 1961
place: the Hague
Nationality: Dutch

Study: August 1979 - August 1987
Ph.D.: December 1987 - June 1992

Institute: Mechanics & Structures
Stevin Laboratory
Civil Engineering
Delft University of Technology
the Netherlands

Promotor: Prof. dr. ir. J. Wardenier

Master thesis: -

Development for a computer program and manual for the analysis of profiled sheeting, to be distributed with the new design recommendations by the Staalbouwkundig Genootschap. This subject was awarded a prize in steel related master thesis subjects.

ECSC study on the fatigue behaviour of T- and X-joints between square hollow sections, consisting of experiments carried out at the Stevin Laboratory and numerical (Finite Element) work carried out at TNO-IBBC. For this work a special purpose finite element mesh generator has been developed.

Ph.D.:

"Fatigue behaviour of joints between rectangular hollow sections". The research programme forms part of an ECSC/CIDECT investigation, carried out in the Netherlands and the Federal Republic of Germany, which aims to provide a basis for future design guidelines from EC3 and the IIW concerning the fatigue behaviour of joints between rectangular hollow sections.